Chapter 4
The Hydrothermal Minerals

Abstract Over 2200 chemical analyses of hydrothermal minerals collected at depth in different active geothermal systems were compiled and processed in this work. In agreement with the outcomes of previous studies, it turned out that hydrothermal quartz, calcite, adularia, albite, anorthite, and laumontite are virtually pure solid phases. Therefore, their activities can be assumed to be equal to one. In contrast, the other hydrothermal minerals of interest, i.e., white mica, chlorite, epidote, prehnite, wairakite, and garnet, are solid solutions of variable composition. Therefore, the activities of pertinent endmembers (i.e., muscovite, 7Å-clinochlore, clinozoisite, prehnite, wairakite, and grossular) were computed, under the assumption of random mixing of atoms on energetically equivalent sites. Then, following the approach delineated in Sect. 2.2.1, the Gibbs free energy and the thermodynamic equilibrium constant of the dissolution reaction of the solid solutions with average activity of these pertinent endmembers were computed. These log K values are points of reference more representative than the log K of the dissolution reactions of the corresponding pure minerals.

4.1 The Hydrothermal Alteration Suites and Their Zones

A general relationship between the occurrence of hydrothermal alteration minerals and temperature was recognized long ago, although the formation of these secondary solid phases is controlled also by fluid chemistry, permeability, and duration of hydrothermal activity (e.g., Browne and Ellis 1970; Kristmannsdóttir 1979; Browne 1978; Bird et al. 1984). As pointed out by Reyes (1990), two distinct hydrothermal alteration suites occur in the high-temperature geothermal systems of the Philippines, namely (a) the neutral-pH suite, associated with the neutral-pH, alkali chloride liquids and (b) the acidic alteration suite, related with sulfur-rich aqueous solutions of low pH.

Based on the key phyllosilicate minerals, the neutral-pH suite is divided in the following four zones:

R. Cioni and L. Marini, *A Thermodynamic Approach to Water Geothermometry*, Springer Geochemistry, https://doi.org/10.1007/978-3-030-54318-1_4

(1) Smectite zone, extending up to temperatures of 180 °C. Smectite is accompanied by chlorite, above 120 °C, and low-temperature zeolites, such as heulandite, stilbite, and ptilolite, although laumontite occurs above 120 °C.
(2) Transition zone, corresponding to temperatures of 180–220 °C. It is characterized by the increase in chlorite, the appearance of illite-smectite, and the persistence of laumontite, which is the typical Ca–Al-silicate of this zone. Albite, adularia, and sphene appear in this zone.
(3) Illite zone, corresponding to temperatures of 220 to 270–280 °C, although illite is stable at higher temperatures as well. Wairakite, epidote, and prehnite are the representative Ca–Al-silicates of this zone. They are accompanied by chlorite, adularia, albite, sphene, and sulfide minerals.
(4) Biotite zone, extending at temperatures higher than 270–280 °C. It is characterized by the appearance of high-temperature minerals, such as garnet (e.g., andradite and grossular), amphibole (e.g., actinolite and tremolite), and pyroxene (e.g., diopside), as well as by the persistence of illite, chlorite, albite, adularia, wairakite, epidote, sphene, and sulfide minerals.

Some minerals, such as quartz, calcite, and pyrite, occur at any temperature.

Based on the key hydroxy silicate of aluminum, the acidic alteration suite is divided in the following four zones: (i) The kaolinite zone, extending up to temperatures of 120 °C. (ii) The dickite ± kaolinite zone, corresponding to temperatures of 120–200 °C. (iii) The dickite ± phyrophyllite zone, corresponding to temperatures of 200–260 °C. (iv) The phyrophyllite ± illite zone, corresponding to temperatures of 230–320 °C. These hydroxy silicates of aluminum are typically accompanied by sulfur, alunite, anhydrite, diaspore, and pyrite as well as by other less common solid phases.

The same hydrothermal alteration zones present in active geothermal systems are also recognizable in hydrothermal ore deposits, which are fossil geothermal systems (Pirajino 2009). This homogeneity in the sequence of alteration minerals is not surprising considering that rocks act as suppliers of chemical elements during water-rock interaction and there are relatively limited differences in the concentrations of major (rock-forming) elements in different lithotypes (e.g., Turekian and Wedepohl 1961), apart from the extreme case of monomineralic rocks such as limestones, dolomites, and quartzites.

As pointed out by Giggenbach (1980, 1984, 1988), the non-conservative elements transferred to the aqueous solution by CO_2-driven rock dissolution remain in part in the fluid and are partly incorporated in hydrothermal alteration minerals. Under favorable conditions (e.g., constant temperature, low fluid/rock ratio), the aqueous solution is expected to approach and possibly attain the condition of chemical equilibrium with the hydrothermal alteration minerals, after a lapse of time largely depending on the kinetics of relevant dissolution-precipitation reactions.

Focusing on the felsic rocks prevailing in the continental crust, the thermodynamically stable hydrothermal paragenesis is expected to comprise quartz, muscovite (or illite), albite, adularia, clinochlore (or chlorite), and either a Ca–Al-silicate, if CO_2 fugacity is relatively low, or calcite, if CO_2 fugacity is comparatively high, in

accordance with mineralogical evidence (e.g., Ellis 1970; Ellis and Mahon 1977; Giggenbach 1984, 1988; Arnórsson et al. 1983a, b; Arnórsson and Gunnlaugsson 1985). If so, the activities of undissociated SiO_2 and Al^{3+}, Na^+, K^+, Mg^{2+}, and Ca^{2+} ions are fixed. In addition to the solid phases listed above, anhydrite, fluorite, and calcite may also be part of the hydrothermal mineral assemblage, thus fixing the activities of SO_4^{2-}, F^-, and HCO_3^- ions, respectively (Guidi et al. 1990; Chiodini et al. 1991 and references therein).

Therefore, the activity of all these compatible[1] aqueous species can be involved in geothermometers and f_{CO_2}-indicators, referring to suitable mineral-solution reactions. For performing correctly this task, it is necessary to know the main characteristics of these minerals and if they occur in active geothermal systems either as pure (or nearly pure) solid phases or as components of solid solutions. In fact, in the first case their activity can be assumed to be equal to one (based on the standard state convention for solids, see Sect. 2.1.2), whereas in the second case their activity must be properly calculated and involved in some way in geothermometers and f_{CO_2}-indicators (see Sect. 2.2.1). Therefore, the next sections of this chapter are devoted to summarize the main characteristics of relevant hydrothermal alteration minerals, especially their chemical composition, which is used to compute the activity of solid solution components of interest.

4.2 Feldspars

4.2.1 Main Characteristics of Feldspars

There is a number of books completely dedicated to feldspar minerals, such as Ribbe (1983), Smith and Brown (1988), and Deer et al. (2001).

Feldspars have either monoclinic or triclinic symmetry. The crystal structure of feldspars consists of a three dimensional framework of (Si, Al)–O or T–O tetrahedra, with each oxygen atom constituting the vertex of two adjacent tetrahedra. Each Si atom balances half charges of the four oxygen atoms in its Si–O tetrahedron, but one negative charge is unbalanced in each Al–O tetrahedron. Therefore, large monovalent and bivalent cations (collectively denoted M) occupy the interstices to maintain the charge balance. Because there is one interstice for every four tetrahedra and the interstices are completely filled up, the general crystallochemical formula of feldspars is MT_4O_8, where M is commonly Na^+, K^+ or Ca^{2+} and T is usually Al^{3+} or Si^{4+}, with $1 \leq Al \leq 2$ and $2 \leq Si \leq 3$.

Most feldspars are ternary solid solutions of albite [Ab, $NaAlSi_3O_8$], orthoclase [Or, $KAlSi_3O_8$], and anorthite [An, $CaAl_2Si_2O_8$]. The solid solutions predominantly

[1]Following Arnórsson et al. (1983b), the term "compatible" is utilized to indicate the chemical components whose activity is limited by incorporation in the lattice of hydrothermal alteration minerals.

composed of albite and orthoclase form the alkali feldspar series, whereas the solid solutions primarily made up of albite and anorthite form the plagioclase series.

At high temperatures (>1000 °C), feldspars exhibit remarkable solid solution. Accordingly, the plagioclase series comprises high-anorthite, with An > 90%; high-bytownite, with 70 < An < 90%; high-labradorite, with 50 < An < 70%; high-andesine with 30 < An < 50%; high-oligoclase, with 10 < An < 30%; and high-albite, with An < 10%. According to Parsons (2010), the alkali feldspar series comprises K-sanidine, with Or >80%; sanidine, with 50 < Or < 80%; Na-sanidine with 35 < Or < 50%; and anorthoclase, with Or < 35%, although different nomenclatures are adopted by other authors. High-albite and anorthoclase are triclinic at room temperature but they assume monoclinic symmetry when observed at elevated temperatures due to shearing transformation. Sanidine has monoclinic symmetry at all temperatures.

At low temperatures (<300 °C) feldspars exhibit very limited solid solution and the stable phases are triclinic low-microcline, low-albite and anorthite, all with nearly stoichiometric composition. In fact, low-temperature natural feldspars are frequently made up of intergrowths of two or more phases. Ideally, low-microcline, low-albite and anorthite are expected to exhibit Al–Si order. Nevertheless, disordered structures are frequent because of metastable crystallization.

There are two mechanisms for the transition from monoclinic to triclinic symmetry. In alkali feldspars with Ab > 60% it occurs by a quick shearing phase transformation brought about by twisting of (Si, Al)–O tetrahedra. In contrast, a slow 'diffusive' order-disorder transformation occurs in the Or-rich alkali feldspars, in which the Al ions, distributed randomly between four equivalent sites at high temperatures, become ordered on one of these sites during cooling.

For what concerns the substitutions, the M-site can be occupied by Rb^+, Tl^+, and NH_4^+ and in part by Li^+ and Cs^+ in alkali feldspars and by Sr^{2+}, Ba^{2+}, Pb^{2+}, and Eu^{2+}, as well as by (La^{3+}, Na^+) in alkali-earth feldspars. The ammonium alkali feldspar is buddingtonite, $NH_4AlSi_3O_8 \cdot ½\ H_2O$, whereas the barium plagioclase is celsian, Cls, $BaAl_2Si_2O_8$. The main substitutions in T-sites of natural feldspars are B and Fe. The boron analog of albite is reedmergnerite, $NaBSi_3O_8$.

4.2.2 The Chemistry of Hydrothermal Feldspars

Both adularia (i.e., hydrothermal orthoclase) and hydrothermal albite are widespread in active geothermal systems where they usually occur at temperatures higher than 120–150 °C, in spite of some notable exceptions (e.g., Browne 1970, 1978; Reyes 1990). For instance, only adularia occurs in the Cerro Prieto geothermal field, whereas hydrothermal albite is absent although primary plagioclase usually represents up to 10% of the sandstone mineral constituents at all depths (Bird et al. 1984; Schiffman et al. 1985). Conversely, hydrothermal albite replaces primary plagioclase at temperatures higher than 120 °C in the geothermal system of Onikobe, whereas adularia is absent (Seki et al. 1983). Hydrothermal anorthite and plagioclases of intermediate composition are uncommon.

In this work, several chemical analyses of hydrothermal feldspars obtained from deep boreholes drilled in active geothermal systems were compiled. 480 chemical analyses were considered of acceptable quality, having sum of oxides from 98 to 102 wt%, and processed to compute the percentages of albite, orthoclase, and anorthite.

The Ab–Or–An triangular plot of Fig. 4.1 displays the composition of 119 hydrothermal feldspars from the geothermal fields of Roosevelt Hot Springs, Utah (Ballantyne 1978), Salton Sea, California (Shearer et al. 1988), Heber, California (Browne 1977), Cerro Prieto, Mexico (Schiffman et al. 1985), Miravalles, Costa Rica (Milodowski et al. 1989), Berlin, El Salvador (Ruggieri et al. 2006), Kilauea, Hawaii (Bargar et al. 1996), Onikobe, Japan (Seki et al. 1983), Broadlands-Ohaaki, New Zealand (Lonker et al. 1990), Waiotapu, New Zealand (Hedenquist and Browne 1989) Milos, Greece (Liakopoulos 1987), as well as Latera (Cavarretta et al. 1985), Larderello (Cavarretta et al. 1982), and Pantelleria (Fulignati et al. 1997), Italy. Among these 119 hydrothermal feldspars, there are 60 adularias with Ab < 15 mol%,

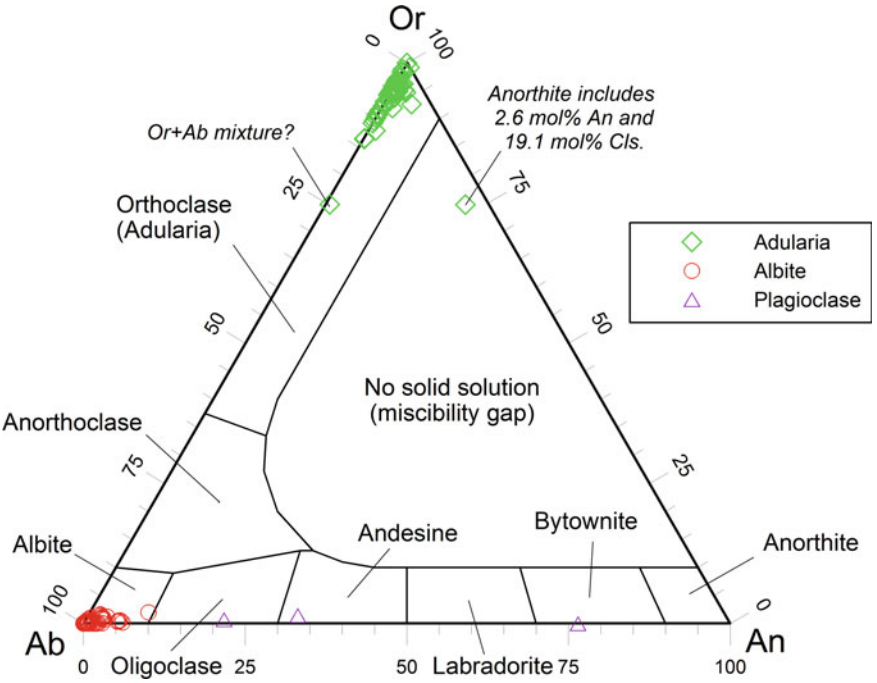

Fig. 4.1 Ab-Or-An triangular plot showing the composition of 119 hydrothermal feldspars from different active geothermal fields, including Roosevelt Hot Springs (Ballantyne 1978), Salton Sea (Shearer et al. 1988), Heber (Browne 1977), Cerro Prieto (Schiffman et al. 1985), Miravalles (Milodowski et al. 1989), Berlin (Ruggieri et al. 2006), Kilauea (Bargar et al. 1996), Onikobe (Seki et al. 1983), Broadlands-Ohaaki (Lonker et al. 1990), Waiotapu (Hedenquist and Browne 1989), Milos (Liakopoulos 1987), Latera (Cavarretta et al. 1985), Larderello (Cavarretta et al. 1982), and Pantelleria (Fulignati et al. 1997)

54 albites, and 5 anomalous samples, namely 1 probable mixture (intergrowth) of adularia and albite (with ~25 mol% Ab), 3 plagioclases of variable composition (1 oligoclase, 1 andesine, and 1 bytownite), and 1 celsian-rich adularia from Berlin, formally constituted by 74.7 mol% Or, 19.1 mol% Cls, 3.6 mol% Ab, and 2.6 mol% An.

Neglecting the 5 anomalous samples, the composition of adularias and hydrothermal albites from these different geothermal systems is described by the following statistical parameters:

(i) X_{Or} in adularia (N = 60): Min = 0.864, Max = 1.000, Mean = 0.946, Median = 0.951, Std. Dev. = 0.030.
(ii) X_{Ab} in albite (N = 54): Min = 0.889, Max = 1.000, Mean = 0.981, Median = 0.989, Std. Dev. = 0.022.

The composition of adularia shows limited variations in well State 2-14 at Salton Sea, with X_{Or} from 0.90 to 0.98 (Shearer et al. 1988). The composition of hydrothermal plagioclase is close to end-member albite at depths <1828.8 m, whereas the hydrothermal plagioclase is richer in An at depths >1828.8 m. Three hydrothermal feldspars coexists in samples below 3017.5 m depth, K-feldspar with X_{Or} ~ 0.91, albite-oligoclase with X_{Ab} 0.95–0.86, and oligoclase-andesine with X_{Ab} 0.75–0.63.

Both hydrothermal albite and oligoclase, with X_{Ab} from 0.883 to 0.850, occur in an altered diabase dike or sill at Heber (Browne 1977). Textural relations suggest that oligoclase is an early mineral, probably not in equilibrium with present-day geothermal fluids.

At Cerro Prieto, adularia has X_{Or} varying from 0.91 to 0.97, with a mean close to 0.95, whereas hydrothermal albite is absent (Schiffman et al. 1985), as already mentioned above.

In most of the Miravalles reservoir, hydrothermal plagioclase is almost pure albite (Milodowski et al. 1989). Uncommon hydrothermal oligoclase (with X_{Ab} close to 0.85) might be explained by the presence of primary plagioclase relicts in albite. Rare hydrothermal bytownite (with X_{An} of 0.77) occurs at 1453 m depth in association with grandite garnet (60–65 mol% andradite) and magnetite. Adularia shows small concentrations of Na and variable concentrations of Ba, which are higher in the cores of crystals.

At Berlin, hydrothermal albite has X_{Ab} from 0.90 to 0.98, whereas a Ba-bearing feldspar with X_{Cls} up to 0.191 occurs in well TR-2 at about 1500 m depth (Ruggieri et al. 2006).

At Onikobe (Seki et al. 1983), the replacement of primary plagioclase by hydrothermal albite (with $X_{Ab} > 0.95$) begins at 120–180 °C and the process comes to completion at temperatures higher than 230–240 °C. Adularia is absent as already mentioned above.

Adularia and hydrothermal albite span small compositional intervals at Broadlands-Ohaaki, with X_{Or} in adularia from 0.94 to 0.995 and X_{Ab} in hydrothermal albite from 0.96 to 0.99, irrespective of primary plagioclase composition (Lonker

et al. 1990). The intermediate compositions of adularia in well BR8 at 774–781 m depth cannot be explained involving primary sanidine because it is absent at Broadlands-Ohaaki (Browne and Ellis 1970). They are likely due to fine intergrowths of hydrothermal albite with adularia (Lonker et al. 1990).

At Waiotapu, hydrothermal albite and adularia are common as alteration products of primary andesine at temperatures higher than ~180 °C (Hedenquist and Browne 1989). Adularia is later than albite as indicated by textural evidence. Most hydrothermal plagioclase has X_{Ab} from 0.90 to 0.99, but some samples range from albite to andesine. The X_{Or} in adularia varies from 0.94 to 0.995.

At Milos, albite is practically pure, with X_{Ab} ranging from from 0.999 to 1.000, whereas X_{Or} in adularia varies from 0.926 to 0.974 (Liakopoulos 1987).

At Larderello, adularia has X_{Or} ranging from 0.950 to 0.959 in the Sasso-22 well at depths of 1600–2263 m based on microprobe analyses, whereas plagioclase compositions (as X_{Ab}) determined by optical microscopy are: (i) from 0.97 to 0.95 in the San Ippolito 122 well at 783 m depth; (ii) from 0.87 to 0.86 in the Sasso 22 well at 2770 m depth; (iii) from 0.66 to 0.60 in the Anqua well at 2635 m depth (Cavarretta et al. 1982).

At Pantelleria, hydrothermal albite has X_{Ab} varying from 0.982 to 0.992 and adularia has X_{Or} ranging from 0.946 to 1.000 (Fulignati et al. 1997).

As shown in the Ab–Or–An triangular plot of Fig. 4.2, the 361 hydrothermal feldspars from Reykjanes, Iceland (mostly from Libbey and Williams-Jones 2016 and subordinately from Marks et al. 2010; Fowler et al. 2015) comprise 150 adularias with Or >85 mol%, 182 albite-oligoclase samples, and 18 anorthites as well as 14 anomalous samples which are probable mixtures (i.e., intergrowths of two or more phases, possibly including relicts of primary phases), 8 rich in adularia and 6 rich in oligoclase.

Neglecting these 14 anomalous samples, the composition of the hydrothermal feldspars from Reykjanes is defined by the following statistical parameters:

(i) X_{Or} in adularia (N = 150): Min = 0.870, Max = 0.992, Mean = 0.954, Median = 0.963, Std. Dev. = 0.025.
(ii) X_{Ab} in albite-oligoclase (N = 179): Min = 0.697, Max = 0.977, Mean = 0.889, Median = 0.910, Std. Dev. = 0.060.
(iii) X_{An} in anorthite (N = 18): Min = 0.900, Max = 0.991, Mean = 0.955, Median = 0.963, Std. Dev. = 0.030.

Reykjanes is unique among the considered geothermal systems for the presence of hydrothermal anorthite, which occurs only in the deepest parts of the geothermal system, where temperature is >300 °C. Hydrothermal anorthite is distinguishable from its igneous counterpart being more An-rich and having much lower concentrations of K and Mg (Libbey and Williams-Jones 2016).

In contrast, hydrothermal albite and oligoclase are abundant throughout the Reykjanes geothermal system, where they mainly occur as replacement of primary plagioclase, although they are also present as subhedral crystals in veins and vugs (Libbey and Williams-Jones 2016). Therefore, most oligoclase might actually represent the product of incomplete replacement of a more calcic primary plagioclase, which could

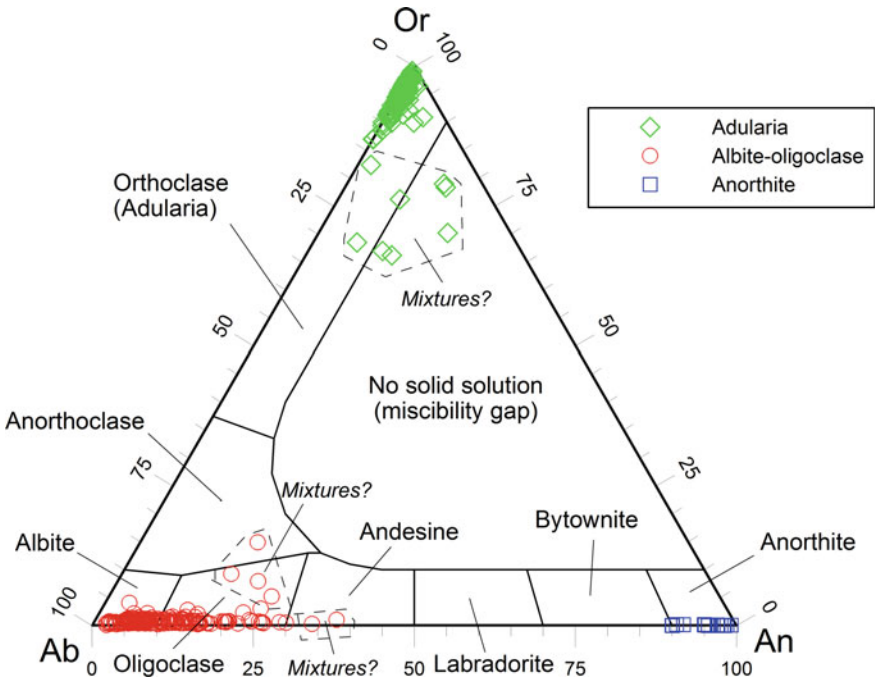

Fig. 4.2 Ab-Or-An triangular plot showing the composition of 361 hydrothermal feldspars from the Reykjanes geothermal field (data mainly from Libbey and Williams-Jones 2016 and subordinately from Marks et al. 2010 and Fowler et al. 2015)

be still present as relict. If so, oligoclase would be less frequent then evaluated above for Reykjanes, consistent with what is generally observed in active geothermal fields (Browne 1977).

Summing up, accepting that oligoclase compositions are due to the possible presence of relicts of primary plagioclase in hydrothermal albite and that mixed compositions are due to intergrowths of different endmember feldspars, it can be concluded that both adularia and albite are the most abundant hydrothermal feldspars in active geothermal systems, where they occur as pure or nearly pure solid phases. Based on this evidence, the activities of Or in adularia and Ab in albite can be reasonably assumed equal to one.

4.2.3 The Structural State and Degree of Ordering of Hydrothermal Alkali Feldspars

Only few investigations were performed so far to characterize the structural state and Al–Si order-disorder on the tetrahedral sites of authigenic K- and Na-feldspars from active geothermal systems.

The occurrence of almost pure adularia as hydrothermal mineral at temperature ≤265 °C in the Wairakei geothermal system was shown long ago by Steiner and coworkers (Steiner 1970 and references therein). Optical data indicate that hydrothermal K-feldspar is partly monoclinic and partly triclinic although X-ray diffractograms indicate only monoclinic lattice. According to Steiner (1970) either monoclinic and triclinic adularia are precipitated almost concomitantly, or triclinic K-feldspar alone is formed and the associated monoclinic structure is only apparent, being simulated by very fine twinning that is optically not detectable. If so, hydrothermal, pure potassium feldspar may have any degree of Si–Al ordering on crystallization.

McDowell (1986) investigated the structural state and Al–Si order on the tetrahedral sites of the authigenic and re-equilibrated detrital K- and Na-feldspars coexisting at temperatures of 250–360 °C in the Salton Sea geothermal reservoir and recovered from the Elmore 1 borehole. The ordering parameter Z (as defined by Thompson 1969) is 0.79 ± 0.09 at ~335 °C and 0.70 ± 0.07 at ~360 °C for albite (N = 6), whereas Z is 0.81 at ~335 °C for K-feldspar (N = 1).

Shearer et al. (1988) noted a systematic increase with depth of Al–Si disorder in K-feldspar from Salton Sea, but this information refers to allogenic-authigenic mixtures of this mineral because the XRD analyses do not distinguish allogenic and authigenic solid phases. Therefore, Shearer et al. (1988) concluded that the systematic increase in Al–Si disorder with depth probably suggests the presence of higher fractions of disordered authigenic (sanidine-like) K-feldspar in the hydrothermal assemblage.

Hedenquist and Browne (1989) studied the hydrothermal minerals at Waiotapu, concluding that (i) the albite structure is partially ordered, based on the position of the d_{204} reflection whereas (ii) adularia is almost completely ordered (maximum microcline) as indicated by the position of d_{060} and d_{204} reflections.

Adularias from low-temperature hydrothermal veins are remarkable for the extensive differences in structural state, from totally disordered monoclinic sanidine (or the highly disordered triclinic form) to highly ordered microcline, chiefly depending on nucleation and crystallization rates and temperature (Černý and Chapman 1986). To be noted that hydrothermal alkali feldspars probably formed under supersaturation conditions rather than at equilibrium. Consequently, their degree of ordering is expected to be a function of the extent of supersaturation, with the Al–Si distribution on the tetrahedral sites becoming more and more disordered with increasing supersaturation. In fact, at conditions of sufficient supersaturation, the disordered phase is kinetically favored over its ordered equivalent, irrespective of their relative thermodynamic stabilities (Carpenter and Putnis 1985).

The post-crystallization thermal regime can also affect the Al–Si distribution on the tetrahedral sites of alkali feldspar. For instance, initially disordered phases kept at high temperature could re-organize their lattice acquiring a more ordered Al–Si distribution. Owing to these potential thermal effects on the hydrothermal feldspars, it is advisable to take into consideration the authigenic alkali feldspars present in sedimentary rocks, which formed at low temperatures and were certainly not affected by annealing and, therefore, are expected to give reliable indications on the degree of ordering of adularia and albite.

According to Morad (1978), diagenetic K-feldspar crystals are monoclinic and, less commonly, triclinic with various degrees of Al–Si ordering, whereas diagenetic albite is well-ordered, triclinic. Kastner and Siever (1979) recognized that authigenic feldspars may have almost any state of Al–Si ordering, from completely ordered, triclinic microclines and albites to highly disordered monoclinic sanidines. Albites tend to be ordered (e.g., Kastner and Waldbaum 1968; Fishman et al. 1995) whereas the structural state of K-feldspar depends on rock type, probably due to kinetic factors. K-feldspars are fully ordered in carbonate rocks, are highly disordered in ash beds, whereas a wide range of ordering degree is found in sandstones and shales.

Further indications are given by the experiments performed by Flehmig (1977), who synthesized highly pure K-feldspar and albite crystals by means of hydroxide gels, mainly at 20 °C apart from a few runs at 3 and 60 °C. Strictly speaking, the factors controlling crystal growth in gels are the free solute concentrations and pH in the gel pores. However, since these parameters cannot be measured, the corresponding parameters in the supernatant solution were reported and discussed by Flehmig (1977). He found that the structural state and the degree of ordering of the synthesized feldspars depends on pH and Na and K concentrations. The growth of K-feldspar crystals took place in the pH range 5–10, with more ordered triclinic K-feldspar (microcline) at higher pH and alkali concentrations and less ordered monoclinic K-feldspar at lower pH and alkali concentrations. Albite crystals were obtained only at pH $\geq$8 and high Na concentrations and showed high degrees of ordering. Similar influences of pH and alkali concentration on the formation of low albite had previously been recognized by Martin (1969).

On the basis of the evidence summarized above, the hydrothermal alkali feldspars occurring in active geothermal systems are expected to be triclinic, fully ordered, albite and variably ordered adularia, from fully ordered microcline to completely disordered sanidine, with either triclinic or monoclinic symmetry.

These expectations are at variance with the findings of Stefánsson and Arnórsson (2000), who underscored that primary disordered plagioclases and alkali-feldspars of compositions typically found in volcanic rocks tend to dissolve in geothermal waters with simultaneous precipitation of ordered alkali-feldspars with near pure endmember compositions. However, Stefánsson and Arnórsson (2000) used the solubility constants of feldspars of Arnórsson and Stefánsson (1999) whose reliability is questionable, at least as far as the alkali feldspars are concerned, as shown in the next section.

4.2.4 The Thermodynamic Properties of Endmember Alkali Feldspars

As already underscored in Sect. 2.2, in the geochemical literature there is a lack of consensus on the thermodynamic data of several minerals, including the alkali feldspars. The reproduction of the monoclinic/triclinic transition temperature of alkali feldspars, which is close to 500 °C in K-feldspar and close to 660 °C in Na-feldspar at low pressures (Deer et al. 2001), represents a good way to prove the reliability of the thermodynamic data of alkali feldspars, because of the simplicity of the solid-solid reactions of interest (see below).

First, the thermodynamic data of high-albite, low-albite, sanidine, and microcline from Holland and Powell (1998) and Arnórsson and Stefánsson (1999), see Table 4.1, were inserted into SUPCRT92.

The heat capacity coefficients of Holland and Powell (1998) refer to the polynomial equation:

$$C_P^\circ = a + b \cdot T + c \cdot T^{-2} + d \cdot T^{-1/2}, \tag{4.1}$$

whereas the heat capacity coefficients of Arnórsson and Stefánsson (1999) are consistent with the polynomial relation:

$$C_P^\circ = a + 2b \cdot T + c \cdot T^{-2} + f \cdot T^2 + g \cdot T^{-1/2}. \tag{4.2}$$

Therefore, heat capacity coefficients were recalculated to make them consistent with the Maier-Kelley relation, Eq. (2.17). The thermodynamic data of Holland and Powell (2011) were not considered because these authors give the same entropy (214.3 J K^{-1} mol^{-1}) for sanidine and microcline probably due to a typo. In fact, Holland and Powell (1998) give different entropies for sanidine (230 J mol^{-1} K^{-1}) and microcline (216 J mol^{-1} K^{-1}), as expected from configurational entropy considerations (Openshaw et al. 1976).

Second, the standard Gibbs free energy, ΔG°_r, of the solid-solid reaction;

$$\text{Microcline} = \text{Sanidine} \tag{4.3}$$

was calculated by means of SUPCRT92 as a function of temperature, at both 1 bar and 1 kbar, considering alternatively the thermodynamic data of Helgeson et al. (1978), Holland and Powell (1998), and Arnórsson and Stefánsson (1999).

Results are displayed in the diagram of ΔG°_r versus temperature (Fig. 4.3) which shows that:

(a) the thermodynamic data of Helgeson et al. (1978) are consistent with a sanidine/microcline transition temperature close to 500 °C, in agreement with the available experimental evidence (see above),

Table 4.1 Standard state molal thermodynamic properties, at 25 °C, 1 bar, of maximum-microcline, high-sanidine, low-albite, and high-albite from H78 = Helgeson et al. (1978), HP98 = Holland and Powell (1998), and AS99 = Arnórsson and Stefánsson (1999)[a]

Mineral	ΔG_f^o	ΔH_f^o	S°	V°	a	b ($\times 10^3$)	c ($\times 10^{-5}$)	References
	cal mol^{-1}	cal mol^{-1}	cal K^{-1} mol^{-1}	cm^3 mol^{-1}	cal K^{-1} mol^{-1}	cal K^{-2} mol^{-1}	cal K mol^{-1}	
Max-microcline	−895,374	−949,188	51.13	108.74	63.83	12.9	−17.05	H78
Microcline	−896,317	−950,060	51.63	108.92	56.29	22.76	−12.79	HP98
Microcline	−896,163	−950,022	51.20	108.74	49.41	32.66	−9.49	AS99
High-sanidine	−893,738	−946,538	54.53	109.01	63.83	12.9	−17.05	H78
Sanidine	−894,888	−947,634	54.97	109.00	56.29	22.76	−12.79	HP98
Sanidine	−895,305	−947,832	55.66	109.01	51.09	30.86	−10.04	AS99
Low-albite	−886,308	−939,680	49.51	100.07	61.7	13.9	−15.01	H78
Low-Albite	−887,168	−940,392	50.22	100.06	57.30	21.85	−13.38	HP98
Low-albite	−887,437	−940,771	49.76	100.07	52.09	29.41	−10.42	AS99
High-albite	−884,509	−937,050	52.30	100.43	61.7	13.9	−15.01	H78
High-albite	−885,784	−938,059	53.39	101.09	57.30	21.85	−13.38	HP98
High-albite	−885,531	−937,710	53.63	100.43	51.30	31.07	−10.23	AS99

Following Helgeson et al. (1978), the names high-sanidine and high-albite connote complete disorder, whereas maximum-microcline and low-albite refer to the completely ordered phases

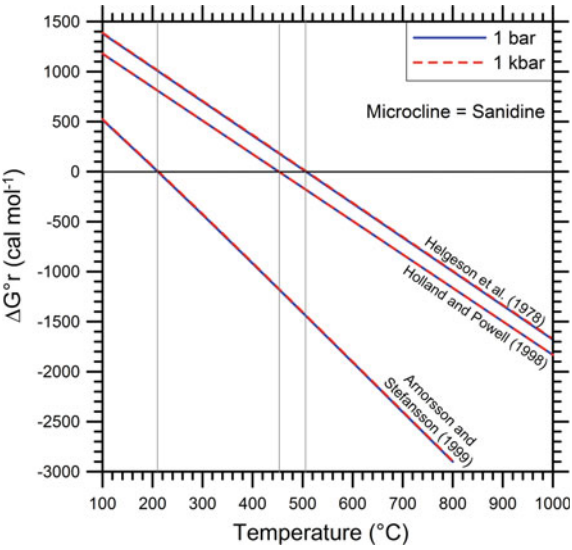

Fig. 4.3 Diagram of the standard Gibbs free energy of sanidine/microcline transition as a function of temperature, at a pressure of 1 bar and 1 kbar, based on the thermodynamic data of Helgeson et al. (1978), Holland and Powell (1998), and Arnórsson and Stefánsson (1999)

(b) as explicitly stated in the paper of Holland and Powell (1998), their thermodynamic data are consistent with a sanidine/microcline transition temperature of 452°C, which is ~50 °C lower than the experimental datum;
(c) the thermodynamic data of Arnórsson and Stefánsson (1999) are consistent with a sanidine/microcline transition temperature of 210 °C, which is ~290 °C lower than the experimental value.

Third, the ΔG°_r of the solid-solid reaction;

$$\text{High-albite} = \text{Low-albite} \tag{4.4}$$

was computed as a function of temperature, at both 1 bar and 1 kbar, taking into account alternatively the thermodynamic data of Helgeson et al. (1978), Holland and Powell (1998), and Arnórsson and Stefánsson (1999).

Results are presented in the plot of ΔG°_r versus temperature (Fig. 4.4) which shows that:

(a) the thermodynamic data of Helgeson et al. (1978) are consistent with a high-albite/low-albite transition temperature close to 660 °C, in accordance with the available experimental evidence (see above),
(b) the thermodynamic data of Holland and Powell (1998) are consistent with a high-albite/low-albite transition temperature of 460–465 °C, which is ~200 °C lower than the experimental datum;
(c) the thermodynamic data of Arnórsson and Stefánsson (1999) are consistent with a high-albite/low-albite transition temperature of 515 °C, which is ~145 °C lower than the experimental value.

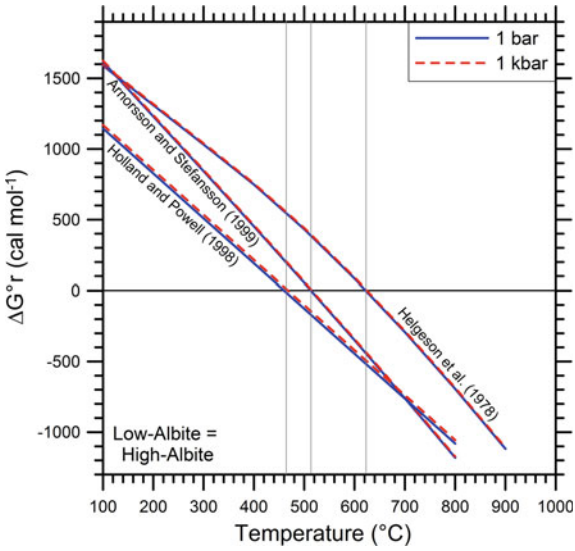

Fig. 4.4 Diagram of the standard Gibbs free energy of high-albite/low-albite transition as a function of temperature, at a pressure of 1 bar and 1 kbar, based on the thermodynamic data of Helgeson et al. (1978), Holland and Powell (1998), and Arnórsson and Stefánsson (1999)

Summing up, only the thermodynamic data of Helgeson et al. (1978) are consistent with the monoclinic/triclinic transition temperatures of alkali feldspars whereas the thermodynamic data of Holland and Powell (1998) and Arnórsson and Stefánsson (1999) are not. Consequently, the thermodynamic data of Helgeson et al. (1978) can be used to compute the log K values of the exchange reactions involving alkali feldspars and other Al-bearing minerals of interest for geothermometry and f_{CO_2} evaluation, as discussed in Chaps. 6–9, whereas the thermodynamic data of Holland and Powell (1998) and Arnórsson and Stefánsson (1999) cannot be used to this aim. In addition to these general implications, the monoclinic/triclinic transition temperatures of alkali feldspars have other specific implications on Na–K geothermometry, whose discussion is postponed to Sect. 6.1.

4.2.5 The Thermodynamic Properties of Variably Ordered Alkali Feldspars

Since the conversion between the monoclinic and triclinic crystal structures in K-feldspar has little or no effect on its thermodynamic behavior, the different thermodynamic properties of ordered microcline and disordered sanidine are entirely due to substitutional Al–Si order-disorder or nearly so (Helgeson et al. 1978). In contrast, the displacive transformation in albite from monoclinic to triclinic symmetry is accompanied by a relatively large heat of transition and, therefore, albite experiences two superimposed lambda transitions with increasing temperature, one caused

by exchange of Al and Si atoms on its tetrahedral sites, and the other produced by displacive changes in its symmetry (Helgeson et al. 1978).

Accepting that variably ordered adularia occurs in active geothermal systems (see Sect. 4.2.3), the thermodynamic properties of adularia with ordering parameter Z varying from 0.9 to 0.1, at steps of 0.1 units, were calculated in this work and added to the SUPCRT92 thermodynamic database. In these calculations, maximum-microcline and high-sanidine were assumed to be representative of adularia with ordering parameter Z of 1 and 0, respectively. Following Helgeson et al. (1978), the standard molal enthalpy and the standard molal entropy of substitutional disorder for variably ordered adularia, $\Delta H^{\circ}_{ds,Adl}$ (in cal mol^{-1}) and $\Delta S^{\circ}_{ds,Adl}$ (in cal K^{-1} mol^{-1}), respectively, at 25 °C, 1 bar, were computed using the simple relations:

$$\Delta H^{\circ}_{ds,Adl} = 2650 \cdot (1 - Z) \tag{4.5}$$

$$\Delta S^{\circ}_{ds,Ad1} = 3.4 \cdot (1 - Z). \tag{4.6}$$

The standard molal Gibbs free energy of substitutional disorder for variably ordered adularia, $\Delta G^{\circ}_{ds,Adl}$ (in cal mol^{-1}), at 25 °C, 1 bar, was then obtained by means of the fundamental Eq. (2.1), rewritten as:

$$\Delta G^{\circ}_{ds,Adl} = \Delta H^{\circ}_{ds,Adl} - T \cdot \Delta S^{\circ}_{ds,Adl}. \tag{4.7}$$

Helgeson et al. (1978) assumed the same heat capacity power function coefficients for high-sanidine and maximum-microcline, because the difference in the heat capacity of the two K-feldspars, at 25 °C and 1 bar, is only 0.07 cal K^{-1} mol^{-1} (Openshaw et al. 1976). Here, this hypothesis was adopted for adularia, irrespective of its ordering parameter Z.

Accepting that hydrothermal albite occurring in active geothermal systems is fully ordered (see Sect. 4.2.3), there is no need to calculate the thermodynamic properties of variably ordered albite. Nevertheless, the thermodynamic properties of albite with ordering parameter Z varying from 0.9 to 0.1, at steps of 0.1 units, were also computed in this work and added to the SUPCRT92 thermodynamic database. In these calculations, low-albite and high-albite were assumed to be representative of albite with ordering parameter Z of 1 and 0, respectively. Following Helgeson et al. (1978), the standard molal enthalpy and the standard molal entropy of substitutional disorder for variably ordered albite, $\Delta H^{\circ}_{ds,Ab}$ (in cal mol^{-1}) and $\Delta S^{\circ}_{ds,Ab}$ (in cal K^{-1} mol^{-1}), respectively, at 25 °C, 1 bar, were calculated utilizing the equations:

$$\Delta H^{\circ}_{ds,Ab} = 2630 \cdot (1 - Z). \tag{4.8}$$

$$\Delta S^{\circ}_{ds,Ab} = 2.79 \cdot (1 - Z). \tag{4.9}$$

The standard molal Gibbs free energy of substitutional disorder for variably ordered albite, $\Delta G^{\circ}_{ds,Ab}$ (in cal mol^{-1}), at 25 °C, 1 bar, was then be computed by

means of the fundamental relation (2.1) rewritten as:

$$\Delta G^{\circ}_{ds,Ab} = \Delta H^{\circ}_{ds,Ab} - T \cdot \Delta S^{\circ}_{ds,Ab}. \quad (4.10)$$

The same heat capacity power function coefficients were adopted for any variably ordered albite because those of high-albite are equal to those of low-albite, at least below 350 °C (Helgeson et al. 1978).

The molar volumes of variably ordered adularia were computed through linear interpolation of the values of maximum-microcline and high-sanidine reported by Helgeson et al. (1978). Similarly, the molar volumes of variably ordered albite were calculated through linear interpolation of the values of low-albite and high-albite given by Helgeson et al. (1978). The standard state molal thermodynamic properties, at 25 °C, 1 bar, of variably ordered adularia and albite are listed in Table 4.2 together with those of maximum-microcline, high-sanidine, low-albite, and high-albite reported by Helgeson et al. (1978).

4.3 White Micas

4.3.1 Main Characteristics of White Micas

The three rock-forming white micas are muscovite $[KAl_2^{VI}(AlSi_3)^{IV}O_{10}(OH)_2]$, paragonite $[NaAl_2^{VI}(AlSi_3)^{IV}O_{10}(OH)_2]$, and margarite $[CaAl_2^{VI}(AlSi_2)^{IV}O_{10}(OH)_2]$. As pointed out by Guidotti and Sassi (2002): (i) muscovite may contain up to 38 mol% of paragonite in solution, (ii) paragonite may contain up to 15 mol% of muscovite in solution, and (iii) practically no solution occurs between muscovite and margarite.

In spite of these possible mixing relations, muscovite prevails by far over paragonite and margarite in white micas (or sericites) from active geothermal systems, including phengites and illites. Phengites may be described as binary solid solutions of muscovite and celadonites $[K(M^{3+})^{VI}(M^{2+})^{VI}Si_4^{IV}O_{10}(OH)_2]$ (Ernst 1963; Velde 1977). In the chemical formula of celadonite, M^{3+} generally represents Al^{3+} or Fe^{3+}, whereas M^{2+} usually stands for Fe^{2+} or Mg^{2+}, thus leading to four limiting compositions called celadonite $[K(Fe^{3+})^{VI}(Mg^{2+})^{VI}Si_4^{IV}O_{10}(OH)_2]$, Fe-celadonite $[K(Fe^{3+})^{VI}(Fe^{2+})^{VI}Si_4^{IV}O_{10}(OH)_2]$, Fe–Al-celadonite $[KAl^{VI}(Fe^{2+})^{VI}Si_4^{IV}O_{10}(OH)_2]$ and Mg–Al-celadonite $[KAl^{VI}(Mg^{2+})^{VI}Si_4^{IV}O_{10}(OH)_2]$ (Li et al. 1997). Illites are solid solutions of muscovite, celadonites and pyrophyllite $[Al_2Si_4O_{10}(OH)_2]$ (Weaver and Pollard 1973).

Following Brigatti and Guggenheim (2002) and references therein, we recall that the 2:1 mica structure is constituted by two opposing tetrahedral (T) sheets with an octahedral (M) sheet between them to produce a TMT layer. The general chemical formula of micas is:

$$A^{XII}M^{VI}_{2-3}\,\square^{VI}_{1-0}T^{IV}_4O_{10}(X)_2,$$

Table 4.2 Standard state molal thermodynamic properties, at 25 °C, 1 bar, of maximum-microcline, high-sanidine, low-albite, and high-albite (from Helgeson et al. 1978) as well as of variably ordered adularia and albite (this work)

Mineral	ΔG°_f	ΔH°_f	S°	V°	a	b ($\times 10^3$)	c ($\times 10^{-5}$)
	cal mol^{-1}	cal mol^{-1}	cal K^{-1} mol^{-1}	cm^3 mol^{-1}	cal K^{-1} mol^{-1}	cal K^{-2} mol^{-1}	cal K mol^{-1}
Max-microcline, Z = 1	−895,374	−949,188	51.13	108.74	63.83	12.9	−17.05
Adularia, Z = 0.9	−895,210	−948,923	51.47	108.88	63.83	12.9	−17.05
Adularia, Z = 0.8	−895,047	−948,658	51.81	108.90	63.83	12.9	−17.05
Adularia, Z = 0.7	−894,883	−948,393	52.15	108.91	63.83	12.9	−17.05
Adularia, Z = 0.6	−894,720	−948,128	52.49	108.93	63.83	12.9	−17.05
Adularia, Z = 0.5	−894,556	−947,863	52.83	108.94	63.83	12.9	−17.05
Adularia, Z = 0.4	−894,392	−947,598	53.17	108.95	63.83	12.9	−17.05
Adularia, Z = 0.3	−894,229	−947,333	53.51	108.97	63.83	12.9	−17.05
Adularia, Z = 0.2	−894,065	−947,068	53.85	108.98	63.83	12.9	−17.05
Adularia, Z = 0.1	−893,902	−946,803	54.19	108.99	63.83	12.9	−17.05
High-sanidine, Z = 0	−893,738	−946,538	54.53	109.01	63.83	12.9	−17.05
Low-albite, Z = 1	−886,308	−939,680	49.51	100.07	61.7	13.9	−15.01
Albite, Z = 0.9	−886,128	−939,417	49.79	100.11	61.7	13.9	−15.01
Albite, Z = 0.8	−885,948	−939,154	50.07	100.14	61.7	13.9	−15.01
Albite, Z = 0.7	−885,768	−938,891	50.35	100.18	61.7	13.9	−15.01

(continued)

Table 4.2 (continued)

Mineral	$\Delta G°_f$	$\Delta H°_f$	S°	V°	a	b ($\times 10^3$)	c ($\times 10^{-5}$)
	cal mol^{-1}	cal mol^{-1}	cal K^{-1} mol^{-1}	cm^3 mol^{-1}	cal K^{-1} mol^{-1}	cal K^{-2} mol^{-1}	cal K mol^{-1}
Albite, Z = 0.6	−885,588	−938,628	50.63	100.21	61.7	13.9	−15.01
Albite, Z = 0.5	−885,408	−938,365	50.91	100.25	61.7	13.9	−15.01
Albite, Z = 0.4	−885,229	−938,102	51.18	100.29	61.7	13.9	−15.01
Albite, Z = 0.3	−885,049	−937,839	51.46	100.32	61.7	13.9	−15.01
Albite, Z = 0.2	−884,869	−937,576	51.74	100.36	61.7	13.9	−15.01
Albite, Z = 0.1	−884,689	−937,313	52.02	100.39	61.7	13.9	−15.01
High-albite, Z = 0	−884,509	−937,050	52.30	100.43	61.7	13.9	−15.01

in which:

- A^{XII} refers to the twelve-coordinated interlayer sites, which are generally occupied by K, Na, Ca, Ba, and rarely by Rb, Cs, Sr, NH_4, and H_3O;
- M^{VI} indicates the six-coordinated octahedral sites, which are usually occupied by Mg, Fe^{2+}, Al, and Fe^{3+}, although Li, Ti, V, Cr, Mn, Co, Ni, Cu, and Zn may also be present in peculiar micas;
- $\square^{VI}$ indicates a vacant six-coordinated octahedral site;
- T^{IV} denotes the four-coordinated tetrahedral sites, which are generally occupied by Si, Al and Fe^{3+} and infrequently by B and Be;
- X refers to (OH), F, Cl, O, S.

The smallest structural unit of micas contains three octahedral sites. All the three octahedral sites are occupied in the so-called trioctahedral micas, such as biotite and phlogopite, whereas only two octahedral sites [usually M(2)] are occupied and one is vacant [generally M(1)], in the micas known as dioctahedral, such as muscovite, paragonite, margarite, celadonite, and illite, which are those of interest to us.

4.3.2 *The Activities of Muscovite, Celadonites, and Pyrophyllite in Hydrothermal White Micas*

Following Helgeson et al. (1978), Aagaard and Helgeson (1983), Helgeson and Aagaard (1985), and Aagaard and Jahren (1992), the activities of muscovite, a_{Ms}, pyrophyllite, a_{Prl}, celadonite, a_{Cel}, Fe-celadonite, a_{Fe-Cel}, Fe–Al-celadonite, $a_{Fe-Al-Cel}$, and Mg–Al-celadonite, $a_{Mg-Al-Cel}$, in white micas are computed using the following equations:

$$a_{Ms} = k_{Ms} \cdot X_{K,A} \cdot X^2_{Al,M(2)} \cdot X_{Al,T} \cdot X^3_{Si,T} \tag{4.11}$$

$$a_{Prl} = k_{Prl} \cdot X_{\square,A} \cdot X^2_{Al,M(2)} \cdot X^4_{Si,T} \tag{4.12}$$

$$a_{Cel} = k_{Cel} \cdot X_{K,A} \cdot X_{Mg,M(2)} \cdot X_{Fe^{3+},M(2)} \cdot X^4_{Si,T} \tag{4.13}$$

$$a_{Fe-Cel} = k_{Fe-Cel} \cdot X_{K,A} \cdot X_{Fe^{2+},M(2)} \cdot X_{Fe^{3+},M(2)} \cdot X^4_{Si,T} \tag{4.14}$$

$$a_{Fe-Al-Cel} = k_{Fe-Al-Cel} \cdot X_{K,A} \cdot X_{Fe^{2+},M(2)} \cdot X_{Al,M(2)} \cdot X^4_{Si,T} \tag{4.15}$$

$$a_{Mg\text{ - }Al\text{ - }Cel} = k_{Mg\text{ - }Al\text{ - }Cel} \cdot X_{K,A} \cdot X_{Mg,M(2)} \cdot X_{Al,M(2)} \cdot X^4_{Si,T} \tag{4.16}$$

which are based on the assumption of random mixing of atoms on energetically equivalent sites. In Eqs. (4.11)–(4.16):

$k_{Ms} = 9.4815$, $k_{Prl} = 1$, $k_{Cel} = k_{Fe-Cel} = k_{Fe-Al-Cel} = k_{Mg-Al-Cel} = 4$ are constants relating the inter- and intra-crystalline standard states;

$X_{K,A}$ and $X_{\square,A}$ are the mole fractions of potassium and vacancies on the interlayer A site;

$X_{Al,M(2)}$, $X_{Fe^{3+},M(2)}$, $X_{Mg,M(2)}$, $X_{Fe^{2+},M(2)}$ are the mole fractions of aluminum, trivalent iron, magnesium, and divalent iron on the M(2) octahedral sites;

$X_{Al,T}$ and $X_{Si,T}$ are the mole fractions of aluminum and silicon on the T tetrahedral sites.

Chemical analyses of white micas are available for several active geothermal systems, including Salton Sea, California, for the temperature range 190–322 °C McDowell and Elders (1980, 1983); Coso, California, for the temperature interval 190–250 °C (Bishop and Bird 1987); Roosevelt Hot Springs, Utah, for temperatures varying from 212 to 255 °C (Ballantyne 1978; Capuano and Cole 1982); Los Azufres, Mexico, for temperatures ranging from 190 to 270 °C (Cathelineau 1988; Cathelineau and Izquierdo 1988); Bouillante, Guadeloupe, for the temperature range 204–260 °C (Mas et al. 2006); Larderello, Italy, for the temperature interval 248–315 °C (Boyce et al. 2003); Pantelleria, Italy, at temperatures of 170 and 275 °C (Fulignati et al. 1997); Aluto-Langano, Ethiopia, for the temperature range 215–300 °C (Teklemariam et al. 1996); Waiotapu, New Zealand, for the temperature interval 170–282 °C (Hedenquist and Browne 1989); Broadlands-Ohaaki, New Zealand, for temperatures varying from 222 to 300 °C (Lonker and Gerald 1990; Lonker et al. 1990); Kakkonda, Japan, at temperatures of 205 and 300 °C (Inoue et al. 2004).

These 94 chemical analyses of white mica samples were compiled. Since the FeO and Fe_2O_3 contents are not reported and only the total Fe content is available, it is necessary to adopt some hypotheses concerning the redox state of iron to compute, first, site occupancies and, second, the activities of muscovite, pyrophyllite, and celadonite components using Eqs. (4.11)–(4.16). The adopted hypotheses are that 86.5% of total Fe is present as Fe^{3+}, which is the average value for illites according to Weaver and Pollard (1973), and that Fe^{3+} is present only in the octahedral sites. The exclusive occurrence of Fe^{3+} in the octahedral sites is a reasonable assumption considering both that Fe^{3+} occupies the octahedral sites in the ferric endmembers of celadonite (e.g., Li et al. 1997), pyrophyllite (e.g., Badaut et al. 1992 and references therein), and muscovite (e.g., Guidotti and Sassi 2002), and that Fe^{3+} tetrahedral substitution does not take place in dioctahedral micas, whereas it occurs in trioctahedral micas, such as tetra-ferriphlogopite, tetra-ferri-annite and anandite (Brigatti and Guggenheim 2002). To be noted that the alternative assumption of Fe completely present as Fe^{2+} (which was adopted by Cathelineau and Izquierdo (1988) determines changes (i) in the mole fractions of Fe^{2+} and Fe^{3+} on the M(2) octahedral sites, whereas other mole fractions are unaffected by the hypotheses on the Fe redox state and (ii) in the activities of celadonite, Fe-celadonite, and Fe–Al-celadonite, whereas the activities of Mg–Al-celadonite, muscovite, and pyrophyllite are not influenced by the assumptions on the Fe redox state.

The correlation plot of the activity of muscovite in the white mica samples versus the mole fraction of Al on the tetrahedral site (Fig. 4.5), is a good starting point to analyze the data of geothermal white micas. Since illites and white micas in general

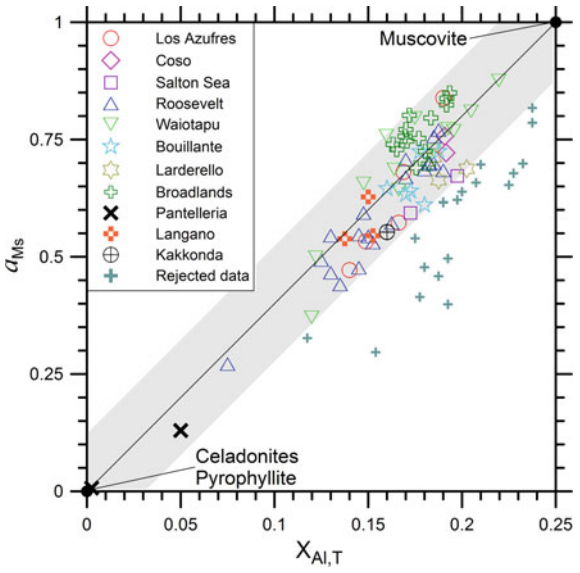

Fig. 4.5 Diagram of the activity of muscovite versus the mole fraction of Al on the T tetrahedral sites for the 94 white mica samples from different geothermal fields (see legend), also showing the idealized stoichiometry of the components of white micas, that is muscovite, pyrophyllite and celadonites

are solid solutions of muscovite, celadonites and pyrophyllite (see above), they are expected to be found along the tie line joining the muscovite point and the point representative of both celadonites and pyrophyllite or at least close to this Ms − (Prl + Cel) tie line. Allowing for a maximum deviation of ±0.12 a_{Ms} units, 75 chemical analyses were considered representative of white micas, whereas the remaining 19 were rejected. All these rejected samples show negative deviations from the Ms − (Prl + Cel) tie line, possibly because they are white micas mixed with other clay minerals or other phyllosilicates. Alternatively, assuming that all Fe is present as Fe^{3+} and occupies the tetrahedral sites, 11 samples would deviate from the Ms − (Prl + Cel) tie line by more than 0.12 a_{Ms} units, although the other 8 would exhibit smaller deviations.

Aagaard and Helgeson (1983) underscored that the distribution of Al^{3+} ion among the tetrahedral and octahedral sites of clay minerals allows one to distinguish illites from montmorillonites and mixed-layer clays. In fact, these minerals occupy different fields in the plot of Fig. 4.6, which was slightly modified adding the idealized stoichiometry of the components of white micas, that is muscovite, pyrophyllite and celadonites.

As expected: (i) the 75 accepted samples of geothermal white micas are situated inside the compositional space delimited by these three endmembers, and most of these samples are found in the field of illites or close to it, whereas (ii) the 19 rejected samples are positioned to the right of the Ms–Prl–Cel triangle. However, assuming that all Fe is present as Fe^{3+} and occupies the tetrahedral sites, also the 19 rejected samples would be found inside the Ms–Prl–Cel triangle or close to it. Since the ambiguity concerning these 19 rejected samples cannot be resolved, it is advisable to rely only on the other 75 samples.

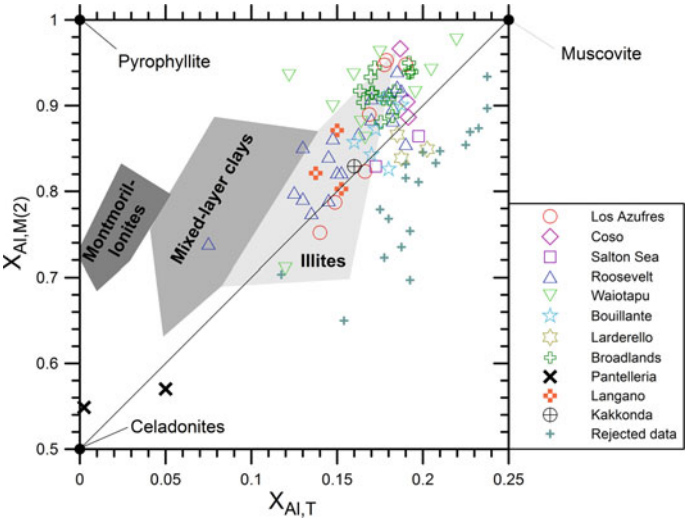

Fig. 4.6 Diagram of the mole fraction of Al on the M(2) octahedral sites versus the mole fraction of Al on the T tetrahedral sites for the 94 white mica samples from different geothermal fields (see legend). The grey fields of illites, mixed-layer clays, and montmorillonites (smectites) are from Aagaard and Helgeson (1983). The idealized stoichiometry of the components of white micas, that is muscovite, pyrophyllite and celadonites, are also shown

The activity of the muscovite endmember in the considered 75 white mica samples varies between 0.007 and 0.875, with an average of 0.654, a median of 0.688 and a standard deviation of 0.156. The sum of the activities of the celadonite components ranges from 0.033 to 0.677, with an average of 0.228, a median of 0.202 and a standard deviation of 0.130. The activity of the pyrophyllite component spans the range 0.000 to 0.156, with an average of 0.060, a median of 0.056 and a standard deviation of 0.035.

The muscovite endmember prevails in 70 of the 75 white mica samples, the celadonite components dominates the remaining 5 samples, whereas the pyrophyllite endmember is always subordinate, as shown by the triangular diagram of Fig. 4.7.

The two diagrams of Fig. 4.8 show that:

(i) the activities of the muscovite and pyrophyllite endmembers in the white mica samples of interest are not correlated, as also indicated by the very low value of the squared linear regression coefficient, $R^2 = 0.027$, whereas

(ii) there is a significant negative correlation between the activity of the muscovite component and the sum of the activities of the celadonite components, as also pointed out by the squared linear regression coefficient, $R^2 = 0.748$.

The activity of the muscovite endmember, the sum of the activities of the celadonite components and the activity of the pyrophyllite endmember have no significant relation with temperature for the 75 accepted white mica samples as pointed out by the very small R^2 values of 0.0004, 0.0191, and 0.174, respectively.

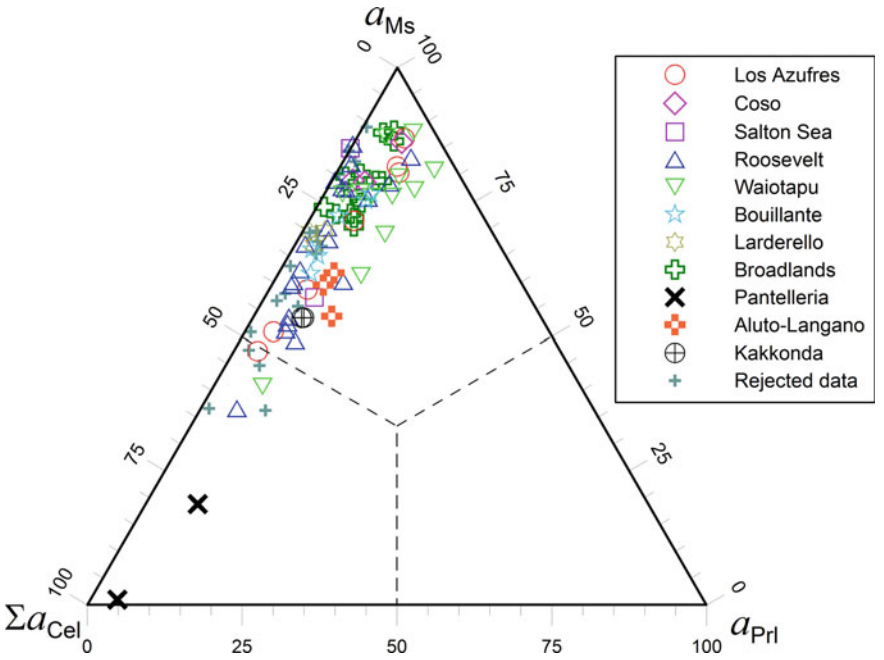

Fig. 4.7 Triangular diagram comparing the activities of muscovite, celadonites and pyrophyllite for the 75 accepted white mica samples from different geothermal fields (see legend)

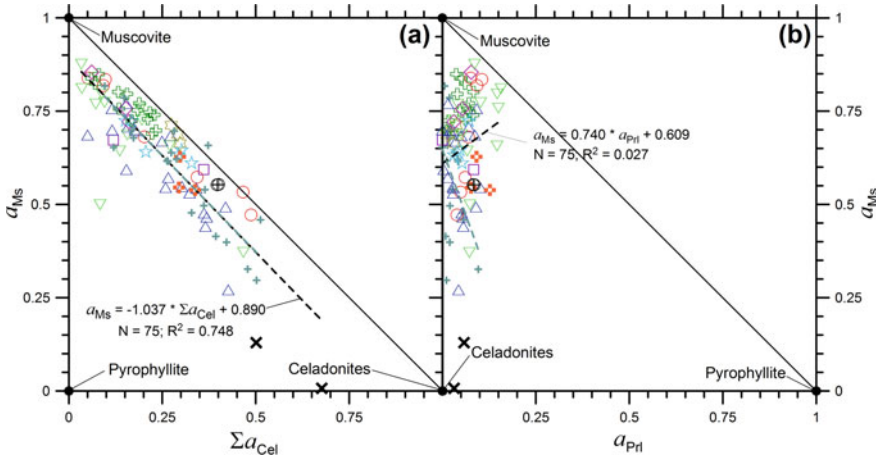

Fig. 4.8 Diagrams of the activity of the muscovite component versus **a** the sum of the activities of the celadonite components and **b** the activity of the pyrophyllite component for the 75 accepted white mica samples from different geothermal fields (symbols as in Figs. 4.5, 4.6 and 4.7). The idealized stoichiometry of muscovite, pyrophyllite and celadonites are also shown

In contrast, a_{Ms}, $a_{\Sigma Cel}$, and a_{Prl} exhibit a meaningful temperature dependence for the 19 rejected samples, with R^2 values of 0.686, 0.705, and 0.266, respectively. Again, this evidence suggests that white micas are mixed with other clay minerals or other phyllosilicates in these 19 rejected samples.

4.3.3 The Thermodynamic Properties of Muscovite

The values of the $\Delta G°_f$ and $\Delta H°_f$ of muscovite at 25 °C, 1 bar given in the first row of Table 4.3 were calculated by Helgeson et al. (1978) from the equilibrium constants derived from high pressure, high temperature experimental data for the following equilibria:

$$2 \text{ muscovite} + 6 \text{ quartz} + 2 \text{ H}^+ = 3 \text{ pyrophyllite} + 2 \text{ K}^+ \tag{4.17}$$

$$\text{muscovite} + \text{quartz} = \text{K-feldspar} + \text{andalusite} + \text{H}_2\text{O}. \tag{4.18}$$

Sverjensky et al. (1991) adopted a similar approach and considered the following equilibria:

$$1.5 \text{ K-feldspar} + \text{H}^+ = 0.5 \text{ muscovite} + 3 \text{ quartz} + \text{K}^+ \tag{4.19}$$

$$\text{muscovite} + \text{H}^+ + 1.5 \text{ H}_2\text{O} = 1.5 \text{ kaolinite} + \text{K}^+ \tag{4.20}$$

$$\text{muscovite} + \text{H}^+ + 3 \text{ quartz} = 1.5 \text{ pyrophyllite} + \text{K}^+ \tag{4.21}$$

$$\text{muscovite} + \text{H}^+ = 1.5 \text{ andalusite} + 1.5 \text{ quartz} + 1.5 \text{ H}_2\text{O} + \text{K}^+. \tag{4.22}$$

However, Sverjensky et al. (1991) used more recent thermodynamic data for the relevant aqueous species, obtaining the $\Delta G°_f$, $\Delta H°_f$, and $S°$ values at 25 °C, 1 bar listed in the second row of Table 4.3. These $\Delta G°_f$, $\Delta H°_f$, and $S°$ values differ from those of Helgeson et al. (1978) by 634 cal mol^{-1}, 992 cal mol^{-1}, and 1.20 cal K^{-1} mol^{-1}, respectively. Sverjensky et al. (1991) proposed also to adjust the free energies and enthalpies at 25 °C, 1 bar of all the K-bearing silicates by adding −236 cal mol^{-1} to preserve the consistency with phase equilibria at high pressures and temperatures. In principle, the thermodynamic data of muscovite of Sverjensky et al. (1991) are probably more representative than those of Helgeson et al. (1978), but their adoption and the addition of −236 cal mol^{-1} to the free energies and enthalpies at 25 °C, 1 bar of all the K-bearing silicates are not sufficient for maintaining the internal consistency of the thermodynamic database of Helgeson and coworkers unless a thorough revision is performed.

Table 4.3 Standard state molal thermodynamic properties, at 25 °C, 1 bar, of muscovite [$KAl_2(AlSi_3)O_{10}(OH)_2$] from H78 = Helgeson et al. (1978), S91 = Sverjensky et al. (1991), HP98 = Holland and Powell (1998), and HP11 = Holland and Powell (2011) as well as of pyrophyllite [$Al_2Si_4O_{10}(OH)_2$] from H78 = Helgeson et al. (1978)

Mineral	$\Delta G°_f$	$\Delta H°_f$	S°	V°	a	b ($\times 10^3$)	c ($\times 10^{-5}$)	d	References
	cal mol^{-1}	cal mol^{-1}	cal K^{-1} mol^{-1}	cm^3 mol^{-1}	cal K^{-1} mol^{-1}	cal K^{-2} mol^{-1}	cal K mol^{-1}	cal $K^{-0.5}$ mol^{-1}	
Muscovite	−1,336,301	−1,427,408	68.8	140.71	97.56	26.38	-25.44	–	H78
Muscovite	−1,335,667	−1,426,416	70.0	–	–	–	–	–	S91
Muscovite	−1,339,319	−1,430,239	69.8	140.83	180.8	−4.7419	−5.186	−1668.1	HP98
Muscovite	−1,337,512	−1,428,432	69.8	140.83	180.8	−4.7419	−5.186	−1668.1	HP11
Pyrophyllite	−1,255,997	−1,345,313	57.2	126.6	79.432	39.214	−17.282	–	H78

The suggestion of Sverjensky et al. (1991) was questioned by Holland and Powell (1998), who proposed the $\Delta G°_f$, $\Delta H°_f$, and $S°$ values at 25 °C, 1 bar given in the third row of Table 4.3 which differ from those of Helgeson et al. (1978) by 3018 cal mol^{-1}, 2813 cal mol^{-1}, and 1 cal K^{-1} mol^{-1}, respectively. Holland and Powell (2011) suggested the $\Delta G°_f$ and $\Delta H°_f$ at 25 °C, 1 bar listed in the fourth row of Table 4.3. These $\Delta G°_f$ and $\Delta H°_f$ are more similar to those of Helgeson et al. (1978) than the free energy and enthalpy proposed Holland and Powell (1998), with deviations of 1211 cal mol^{-1} and 1024 cal mol^{-1}, respectively. Because of the remarkable differences in the thermodynamic data stored for muscovite in these different thermodynamic databases, it is meaningless to pick up the data from distinct databases because it would be like mixing apples and oranges.

As shown in Sect. 4.3.2, muscovite is the main component of white mica solid solutions, whereas pyrophyllite and celadonites play a subordinate role. Among the different components of white mica solid solutions, Helgeson et al. (1978) report the thermodynamic properties of muscovite and pyrophyllite (seventh row of Table 4.3) but not of celadonites.

Following the approach delineated in Sect. 2.2.1, it is advantageous to consider the white mica solid solution with average activity of muscovite, $a_{Ms} = 0.654$, and to compute the Gibbs free energy and the thermodynamic equilibrium constant of its dissolution reaction. The results obtained taking into account the muscovite thermodynamic data of Helgeson et al. (1978) are listed in Table 4.4 as a function of temperature together with the standard molal Gibbs free energies and the natural and decimal logarithms of the thermodynamic equilibrium constant of the dissolution reaction of pure muscovite:

$$KAl_3Si_3O_{10}(OH)_2 + 10\ H^+ = K^+ + 3\ Al^{3+} + 3\ SiO_{2(aq)} + 6\ H_2O. \qquad (4.23)$$

Table 4.4 Standard molal Gibbs free energies and natural and decimal logarithms of the thermodynamic equilibrium constant of the dissolution reactions of both pure muscovite and the white mica solid solution with average activity of muscovite as a function of temperature

T	$\Delta_r G°_{Ms}$	$\Delta_r G°_{Ms,aa}$	ln K_{Ms}	ln $K_{Ms,aa}$	log K_{Ms}	log $K_{Ms,aa}$
°C	cal mol^{-1}	cal mol^{-1}				
0	−18,378	−18,147	33.8574	33.4328	14.7041	14.5197
25	−15,732	−15,480	26.5525	26.1279	11.5316	11.3472
60	−11,004	−10,723	16.6214	16.1968	7.2186	7.0342
100	−5084	−4769	6.8561	6.4315	2.9776	2.7932
150	2711	3068	−3.2240	−3.6486	−1.4002	−1.5846
200	10,976	11,375	−11.6735	−12.0982	−5.0698	−5.2542
250	19,962	20,403	−19.2015	−19.6261	−8.3391	−8.5235
300	30,064	30,548	−26.3958	−26.8205	−11.4636	−11.6480

4.4 Chlorites

4.4.1 Main Characteristics of Chlorites

The structure of chlorites consists in the regularly alternating (i) octahedral, brucite-like layers, also known as the hydroxide or O sheets, and (ii) tetrahedral-octahedral-tetrahedral, talc-like layers, also known as T–O–T or 2:1 sheets (e.g., Bailey 1988). Chlorites are, therefore, defined as T–O–T + O or 2:1 + 1 phyllosilicates.

Wiewiora and Weiss (1990) proposed a crystallochemical classification involving six octahedral positions and four tetrahedral positions, corresponding to half unit cell. The six octahedral sites are occupied by both (i) trivalent (and tetravalent) cations, such as Al^{3+}, Fe^{3+}, Cr^{3+}, (and Ti^{4+}), whose sum is indicated by R^{3+} and (ii) divalent cations, such as Mg^{2+}, Fe^{2+}, Mn^{2+}, and Ni^{2+}, whose sum is represented by R^{2+}. Vacancies are indicated by the symbol □. The four tetrahedral sites are occupied by Si and Al. Therefore, the chemistry of chlorites is described by the general crystallochemical formula (from Wiewiora and Weiss 1990, modified by De Caritat et al. 1993):

$$(R^{2+}_u R^{3+}_y \square_z)^{VI}(Si_{(4-x)}Al_x)^{IV}O_{10+w}(OH)_{8-w}$$

where $u + y + z = 6$, $z = (y - x - w)/2$, and w is usually zero or a small number. Octahedral occupancy is the sum of all cations in the octahedral sites and is given by $\Sigma^{VI} = u + y$. Based on the general crystallochemical formula of chlorites, the charge balance is expressed by the following relation:

$$2u + 3y - x - w - 12 = 0. \tag{4.24}$$

Foster (1962) compiled 150 chemical analyses of chlorites and found that: (i) Si^{IV} values range between 2.34 and 3.45 and 99% of these values are in the 2.40–3.40 interval, corresponding to $0.60 < x < 1.60$; (ii) octahedral vacancies range from −0.05 to +0.55 but are usually in the 0.0 to +0.3 interval; (iii) all the data have charge balance within the range −0.05 to +0.05, with 94% of those data falling within the smaller interval −0.03 to +0.03. The last point implies that the charge balance assumption is reasonable for the chlorite structure.

4.4.2 Crystal Chemistry of Hydrothermal and Diagenetic Chlorites

Referring to the general crystallochemical formula of chlorites, the chemical composition of chlorites with Mg or Fe^{2+}, Al, and □ in the octahedral positions is limited by the following four nodes:

(1) $u = 6, y = 0, z = 0, x = 0$, corresponding to the stoichiometry of either serpentine, $Mg_6Si_4O_{10}(OH)_8$, or greenalite, $Fe^{2+}_6Si_4O_{10}(OH)_8$;
(2) $u = 4, y = 2, z = 0, x = 2$, which is consistent with the formulae of either amesite, $(Mg_4Al_2)(Si_2Al_2)O_{10}(OH)_8$, or Fe^{2+}-amesite, $\left(Fe^{2+}_4Al_2\right)(Si_2Al_2)O_{10}(OH)_8$;
(3) $u = 0, y = 4.67, z = 1.33, x = 2$ or $(Al_{4.67}\square_{1.33})(Si_2Al_2)O_{10}(OH)_8$; this composition exceptionally rich in Al has no equivalent among the chlorites found in nature.
(4) $u = 0, y = 4, z = 2, x = 0$ or $(Al_4\square_2)Si_4O_{10}(OH)_8$; this chemical composition is relatively similar to that of some natural dioctahedral chlorites.

These four nodes and some intermediate compositions are shown in the chlorite classification diagram of Wiewiora and Weiss (1990) of Fig. 4.9, in which octahedral R^{2+} and tetrahedral Si are reported on the abscissa and ordinate axes, respectively, whereas octahedral Al and vacancies are represented in the grid. Both 181 chemical analyses of hydrothermal chlorites from different active geothermal systems and 54 chemical analyses of diagenetic chlorites are shown in this plot.

Chlorites, especially those from low-temperature environments, are often interstratified with smectite, vermiculite, saponite, and/or illite. Since the resolution of the scanning electron microscope is insufficient to establish the possible presence of

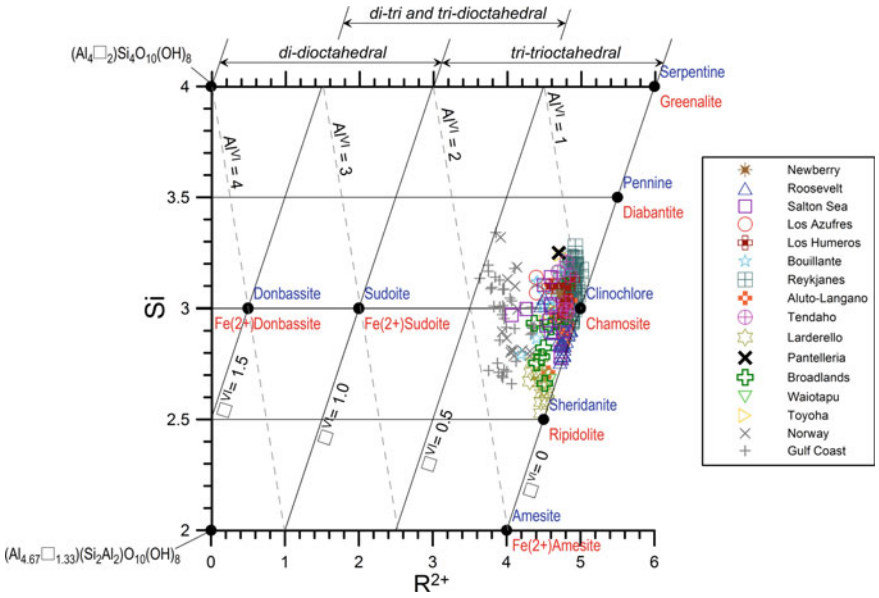

Fig. 4.9 Projection of chlorite structural formulae in the plot of tetrahedral Si versus the sum of octahedral divalent cations, R^{2+}, both expressed in atoms per half unit cell (from Wiewióra and Weiss 1990). Names of Mg-bearing chlorites are in blue whereas names of Fe^{2+}-bearing chlorites are in red. Structural formulae refer to 181 hydrothermal chlorites from different geothermal systems (see legend) and 54 diagenetic chlorites occurring in deeply buried sandstones from the Gulf Coast and the Norwegian Continental Shelf (see legend)

these minerals in the analyzed chlorites, the chemical analyses with ($CaO + Na_2O + K_2O$) > 0.5 wt% were rejected. This procedure was adopted by previous authors (e.g., Foster 1962), based on the assumption that these elements are not hosted in the chlorite lattice.

The considered diagenetic chlorites were obtained from deeply buried sandstones of both (i) the Gulf Coast area, Texas, where pressure is in the 300–1200 bar interval and temperature is in the 102–232 °C range (Bourdelle et al. 2013) and (ii) the Norwegian Continental Shelf at depths of 2393–4967 m, where temperature varies from 90 to 180 °C (Jahren and Aagaard 1992).

The considered hydrothermal chlorites were sampled from the following active geothermal systems: Newberry Caldera, Oregon, at 287 °C (Keith and Bargar 1988); Roosevelt Hot Springs, Utah, in the temperature range 228–253 °C (Ballantyne 1978; Capuano and Cole 1982); Salton Sea, California, in the temperature interval 190–322 °C (McDowell and Elders 1980, 1983); Los Azufres, Mexico, for temperatures ranging from 210 to 310 °C (Cathelineau and Nieva 1985; Cathelineau 1988); Los Humeros, Mexico, for temperatures varying from 145 to 315 °C (Martinez-Serrano and Dubois 1998; Martinez-Serrano 2002); Bouillante, Guadeloupe, in the temperature range 182–260 °C (Mas et al. 2006); Reykjanes, Iceland, in the temperature interval 170–331 °C (Libbey and Williams-Jones 2016); Aluto-Langano, Ethiopia, for temperatures ranging from 180 to 300 °C (Teklemariam et al. 1996); Tendaho, Ethiopia, for temperatures varying from 165 to 270 °C (Gianelli et al. 1998); Larderello, Italy, in the temperature range 248–315 °C (Boyce et al. 2003); Pantelleria, Italy, at 256 °C (Fulignati et al. 1997); Broadlands-Ohaaki, New Zealand, in the temperature interval 267–300 °C (Lonker et al. 1990); Waiotapu, New Zealand, at temperatures of 285–290 °C (Hedenquist and Browne 1989); Toyoha, Japan, for temperatures varying from 209 to 298 °C (Inoue et al. 2010).

All these literature data were compiled and their structural formulae were calculated on the basis of 10 oxygen atoms and 8 hydroxyl groups for a total of 28 negative charge units. Iron was distributed between Fe^{2+} and Fe^{3+} assuming that negative charges are balanced by the same number of positive charges, which is a reasonable hypothesis (see above). In this way, Fe^{2+} resulted to range between 1.08 and 4.33 atoms per half unit cell, whereas Fe^{3+} turned out to be strongly subordinated, with a maximum value of 0.39.

The diagram of Fig. 4.9 shows that:

(a) 90% of the hydrothermal chlorites have tetrahedral Si values ranging from 2.7 and 3.2, R^{2+} varying between 4.4 and 4.9, octahedral Al oscillating from 1.0 to 1.6, and octahedral occupancy of 5.8–6.0;
(b) the diagenetic chlorites have Si^{IV} values generally varying from 2.7 and 3.2, which compares with the range of the hydrothermal chlorites, but other parameters are different, with R^{2+} usually oscillating between 3.8 and 4.4, octahedral Al generally ranging from 1.5 to 1.8 and octahedral occupancy of 5.5–5.8.

These differences between the diagenetic and hydrothermal chlorites considered here (apart from the similarity in tetrahedral Si values) were already underscored by previous authors (e.g., De Caritat et al. 1993 and references therein).

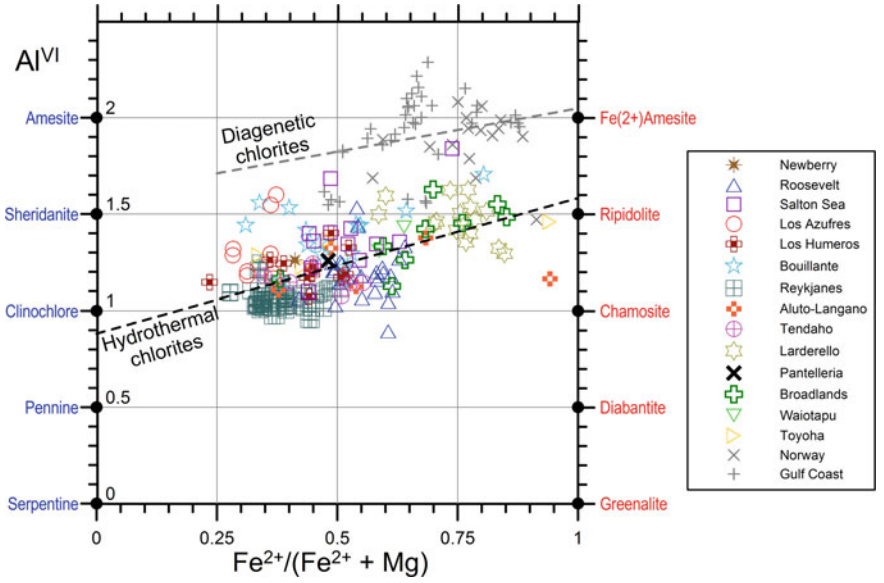

Fig. 4.10 Diagram of the $Fe^{2+}/(Fe^{2+} + Mg)$ atomic ratio versus the octahedral Al value, in atoms per half unit cell for 181 hydrothermal chlorites from different geothermal systems (see legend) and 54 diagenetic chlorites occurring in deeply buried sandstones from the Gulf Coast and the Norwegian Continental Shelf (see legend). Names of Mg-bearing chlorites are in blue whereas names of Fe^{2+}-bearing chlorites are in red

In the diagram of Fig. 4.9, the Mg-bearing chlorites (whose names are in blue) cannot be distinguished from the Fe^{2+}-bearing chlorites (whose names are in red) having the same R^{2+} value. This distinction is conveniently performed by means of the plot of Fig. 4.10, in which the $Fe^{2+}/(Fe^{2+} + Mg)$ ratio is contrasted with the octahedral Al value.

This diagram highlights that:

(i) The diagenetic chlorites are richer in ferrous iron, with the $Fe^{2+}/(Fe^{2+} + Mg)$ ratio ranging from 0.47 to 0.91 and can be considered mixtures of Fe^{2+}-amesite, amesite, and sheridanite, with the ferrous endmember generally prevailing over the magnesian components.

(ii) The hydrothermal chlorites have highly variable $Fe^{2+}/(Fe^{2+} + Mg)$ ratio, from 0.23 to 0.94, that is from Fe^{2+}-rich compositions, close to ripidolite, to Mg-rich compositions, relatively similar to clinochlore or sheridanite.

Considering separately each geothermal system which is represented by at least 4 chlorite samples ($N \geq 4$), usually the $Fe^{2+}/(Fe^{2+} + Mg)$ ratio distributes in a relatively small range, in the order of 0.21–0.30 units, as is the case of Tendaho (range = 0.21, N = 6), Roosevelt (range = 0.22, N = 29), Reykjanes (range = 0.23, N = 61), Larderello (range = 0.26, N = 15), Los Humeros (range = 0.29, N = 11), and Salton Sea (range = 0.30, N = 12). The 9 chlorite samples from Los Azufres span an

even smaller $Fe^{2+}/(Fe^{2+} + Mg)$ range, of 0.09 units only, whereas a relatively large $Fe^{2+}/(Fe^{2+} + Mg)$ range characterizes the chlorites from Broadlands (range = 0.47, N = 9), Bouillante (range = 0.49, N = 15), Aluto-Langano (range = 0.56, N = 6), and Toyoha (range = 0.60, N = 4).

The relatively small $Fe^{2+}/(Fe^{2+} + Mg)$ range of most geothermal systems suggests that they are hosted in rocks of relatively uniform mineralogical and chemical composition. In particular, the hydrothermal chlorites from geothermal systems hosted in silica-rich rocks, such as granite at Larderello (Boyce et al. 2003), have Fe^{2+}-rich compositions, whereas the hydrothermal chlorites from geothermal systems associated to silica-poor rocks, such as basalt at Reykjanes (Libbey and Williams-Jones 2016) have Mg-rich compositions.

In contrast, the relatively large $Fe^{2+}/(Fe^{2+} + Mg)$ range of Broadlands, Bouillante, Aluto-Langano, and Toyoha calls for either (i) the occurrence of rocks of different mineralogical and chemical composition, for instance basalts and silicic ignimbrites at Aluto-Langano (Teklemariam et al. 1996) or (ii) the local presence of mineralized zones bearing sulfide minerals, as is the case of Broadlands (Weissberg et al. 1979) and Toyoha (Inoue et al. 2010), or (iii) the occurrence of successive alteration stages during the thermal history of the geothermal system, as is the case of Bouillante (Mas et al. 2006).

These findings agree with what was recognized long ago by Albee (1962), who pointed out that chlorite chemistry depends upon the composition of both the rock and the minerals associated with it. This matter was thoroughly discussed by De Caritat et al. (1993).

Also fluids can control to some extents the composition of chlorites. For instance, the Mg-rich chlorites of Reykjanes and Bouillante might be due to the inflow of Mg-rich seawater into these geothermal systems, as suggested by Arnórsson for Reykjanes and Sanjuan et al. (2001) for Bouillante.

4.4.3 The Activities of Clinochlore and Chamosite in Hydrothermal and Diagenetic Chlorites

Following Helgeson et al. (1978), Aagaard and Helgeson (1983), Helgeson and Aagaard (1985), and Aagaard and Jahren (1992), the activity of clinochlore, a_{Clc}, and the activity of chamosite, a_{Chm}, in the chlorite solid solutions of interest were calculated by means of the following relations:

$$a_{Clc} = k_{Clc} \cdot X_{Mg,O}^{5} \cdot X_{Al,O} \cdot X_{Al,T} \cdot X_{Si,T}^{3} \tag{4.25}$$

$$a_{Chm} = k_{Chm} \cdot X_{Fe^{2+},O}^{5} \cdot X_{Al,O} \cdot X_{Al,T} \cdot X_{Si,T}^{3} \tag{4.26}$$

which are based on the hypothesis of random mixing of atoms on energetically equivalent sites. In Eqs. (4.25) and (4.26):

$k_{Clc} = k_{Chm} = 141.55776$ are constants relating the inter- and intra-crystalline standard states;

$X_{Mg,O}$, $X_{Fe^{2+},O}$, and $X_{Al,O}$ are the mole fractions of magnesium, divalent iron, and aluminum, on the octahedral sites;

$X_{Al,T}$ and $X_{Si,T}$ are the mole fractions of aluminum and silicon on the tetrahedral sites.

The selected 181 hydrothermal chlorites have:

(i) activity of the clinochlore endmember varying from 4.39×10^{-7} to 0.250, with an average of 0.0553, a median of 0.0451 and a standard deviation of 0.0484, and
(ii) activity of the chamosite endmember ranging from 6.77×10^{-4} to 0.589, with an average of 0.0480, a median of 0.0173 and a standard deviation of 0.0794.

The 54 diagenetic chlorites considered in this work have:

(i) activity of the clinochlore endmember ranging from 4.04×10^{-6} to 0.0333, with an average of 0.00513, a median of 0.00216 and a standard deviation of 0.00832, and
(ii) activity of the chamosite endmember varying from 0.0194 to 0.539, with an average of 0.135, a median of 0.0875 and a standard deviation of 0.110.

As shown in the diagram of Fig. 4.11a, the activities of both endmembers in the considered chlorite solid solutions are linked by a hyperbolic relationship, which reflects the tight inverse correlation between $X_{Mg,O}$ and $X_{Fe^{2+},O}$ (Fig. 4.11b; R-squared = 0.891, N = 235).

The activities of both clinochlore and chamosite are poorly correlated with the temperature measured at the depth of provenance of the chlorite samples, as shown

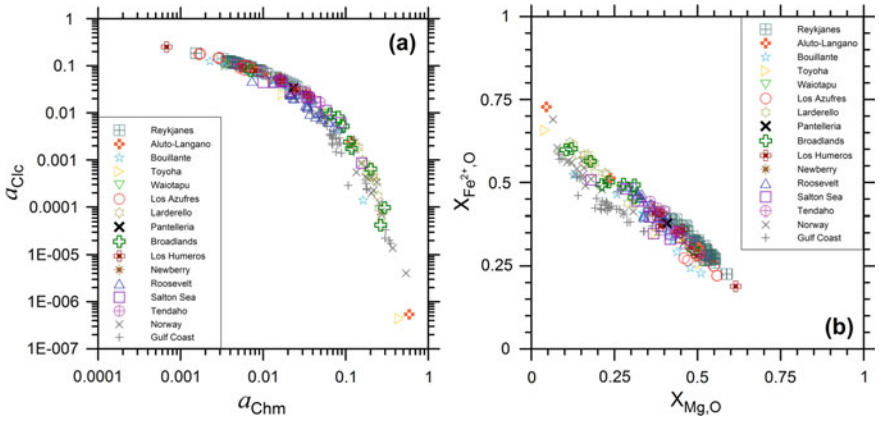

Fig. 4.11 Plots of **a** the activity of clinochlore, a_{Clc}, versus the activity of chamosite, a_{Chm}, and **b** the mole fraction of octahedral Fe^{2+} versus the mole fraction of octahedral Mg for 181 hydrothermal chlorites from different geothermal systems (see legend) and 54 diagenetic chlorites occurring in deeply buried sandstones from the Gulf Coast and the Norwegian Continental Shelf (see legend)

Table 4.5 Squared linear regression coefficients of the pairs a_{Clc}–temperature and a_{Chm}–temperature for the entire chlorite dataset as well as for each geothermal system which is represented by at least 4 chlorite samples

System	N	R^2 [a_{Clc}-T]	R^2 [a_{Chm}-T]
Reykjanes	59	0.321	0.162
Gulf Coast	38	0.046	0.003
Roosevelt	29	0.00007	0.003
Norway	16	0.157	0.488
Larderello	15	0.147	0.121
Bouillante	15	0.112	0.037
Salton Sea	12	0.203	0.491
Los Humeros	11	0.073	0.494
Broadlands	9	0.024	0.354
Los Azufres	9	0.006	0.021
Tendaho	6	0.0002	0.042
Aluto-Langano	6	0.003	0.353
Toyoha	4	0.831	0.854
All dataset	237	0.133	0.112

by the squared linear regression coefficients of the pairs a_{Clc}–temperature and a_{Chm}–temperature for the entire dataset as well as for each geothermal system which is represented by at least 4 chlorite samples (Table 4.5). The only exception is the Toyoha geothermal field, but the relatively high R^2 values are probably fortuitous, also taking into account the low number of available samples.

The lack of correlation between temperature and the activities of both clinochlore and chamosite in the chlorite solid solution is not surprising considering that, according to De Caritat et al. (1993) and other authors, there is a lack of confidence in applying the chlorite geothermometers which have been designed by several workers to obtain indications of palaeo-temperature from chlorite composition and structure.

4.4.4 The Thermodynamic Properties of Chlorites

The only minerals of the chlorite group considered by Helgeson et al. (1978) are 7Å-clinochlore and 14Å-clinochlore, both of stoichiometry $Mg_5Al_2Si_3O_{10}(OH)_8$. The clinochlore with 7Å basal spacing is metastable with respect to its 14Å counterpart at all temperatures and pressure. According to Helgeson et al. (1978), the reason for this is probably the relatively high activation energy required for the conversion of 7Å-clinochlore to the 14Å variety. This hypothesis could explain the persistence of 7Å-clinochlore in weathering profiles, sedimentary environments, hydrothermal alteration zones, and laboratory experiments at temperatures lower than 400–500 °C. Accepting this explanation, 7Å-clinochlore is the clinochlore variety of interest for this work.

As shown by Table 4.6, the thermodynamic data of seven chlorite minerals are

Table 4.6 Standard state molal thermodynamic properties, at 25 °C, 1 bar, of different chlorite minerals from H78 = Helgeson et al. (1978), HP98 = Holland and Powell (1998), and HP11 = Holland and Powell (2011)

Name	$\Delta G°_f$	$\Delta H°_f$	S°	V°	a	b ($\times 10^3$)	c ($\times 10^{-5}$)	d	References
	cal mol^{-1}	cal mol^{-1}	cal K^{-1} mol^{-1}	cm^3 mol^{-1}	cal K^{-1} mol^{-1}	cal K^{-2} mol^{-1}	cal K mol^{-1}	cal $K^{-0.5}$ mol^{-1}	
7Å-Clinochlore	−1,957,101	−2,113,197	106.5	211.5	162.82	50.62	−40.88	–	H78
14Å-Clinochlore	−1,961,703	−2,116,964	111.2	207.11	166.50	42.10	−37.47	–	H78
Ord-Clinochlore	−1,974,988	−2,134,288	98.1	210.9	277.68	2.4218	−18.301	−2316.2	HP98
Ord-Clinochlore	−1,971,946	−2,129,357	104	211.4	279.83	−0.3604	−9.144	−2465.3	HP11
Al-free chlorite	−1,930,801	−2,089,914	97.5	216.6	274.04	2.6828	−18.776	−2229.6	HP98
Al-free chlorite	−1,929,293	−2,086,197	105	215.7	276.05	−0.0997	−9.619	−2378.8	HP11
14Å-Amesite	−2,002,481	−2,163,607	93.2	205.2	281.31	2.1609	−17.827	−2402.7	HP98
14Å-Amesite	−2,001,077	−2,160,564	98.7	207.1	283.46	−0.6212	−8.669	−2551.9	HP11
Daphnite (chamosite)	−1,562,036	−1,709,845	130	213.4	295.75	3.2490	−8.946	−2688.8	HP98
Daphnite (chamosite)	−1,555,905	−1,700,935	140	216.2	284.89	−1.4197	−11.535	−2334.7	HP11
Mn-chlorite	−1,688,695	−1,835,681	139	225.9	293.45	−6.4508	−15.057	−2502.2	HP98
Mn-chlorite	−1,694,993	−1,840,911	142	225.9	271.63	−1.2531	−13.260	−2129.9	HP11
Sudoite	−1,906,494	−2,063,662	95.4	203.0	343.24	−11.6513	−6.569	−3289.7	HP98
Sudoite	−1,904,428	−2,061,881	94.4	203.0	343.24	−11.6513	−6.569	−3289.7	HP11
Fe-Sudoite	−1,738,924	−1,891,197	109	204.0	350.45	−11.3205	−2.827	−3438.8	HP98
Fe-Sudoite	−1,735,827	−1,888,172	109	204.0	350.45	−11.3205	−2.827	−3438.8	HP11

listed by both Holland and Powell (1998) and Holland and Powell (2011), namely Ordered Clinochlore [$Mg_5Al_2Si_3O_{10}(OH)_8$], Al-free chlorite [$Mg_6Si_4O_{10}(OH)_8$], 14Å-Amesite [$Mg_4Al_4Si_2O_{10}(OH)_8$], Daphnite [$Fe_5Al_2Si_3O_{10}(OH)_8$], Mn-chlorite [$Mn_5Al_2Si_3O_{10}(OH)_8$], Sudoite [$Mg_2Al_4Si_3O_{10}(OH)_8$], and Fe-Sudoite [$Fe_2Al_4Si_3O_{10}(OH)_8$]. Incidentally, the term chamosite should be used instead of daphnite, for consistency with the chlorite classification of Wiewiora and Weiss (1990).

Since the 14Å basal spacing is specified only for amesite, we assume that all the other compositions have 7Å basal spacing. If so, the $\Delta G°_f$ and $\Delta H°_f$ values reported by Holland and Powell (1998) for clinochlore differ from those of Helgeson et al. (1978) by 17887 cal mol^{-1} and 21091 cal mol^{-1}, respectively, whereas the $\Delta G°_f$ and $\Delta H°_f$ values given by Holland and Powell (2011) deviate from those of Helgeson et al. (1978) by 14845 cal mol^{-1} and 16160 cal mol^{-1}, respectively. Moreover, for the same mineral, there are differences from 1404 to 6298 cal mol^{-1} in $\Delta G°_f$ and from 1781 to 8910 cal mol^{-1} in $\Delta H°_f$ between the database of Holland and Powell (1998) and that of Holland and Powell (2011). Again, due to these considerable differences in the thermodynamic data stored for clinochlore in the different thermodynamic databases, it is not possible to put together the data from distinct databases because it would be equivalent to mix apples and oranges.

Following the approach outlined in Sect. 2.2.1, it is advisable to consider the chlorite solid solution with average activity of clinochlore, $a_{Clc} = 0.0553$, and to compute the Gibbs free energy and the thermodynamic equilibrium constant of its dissolution reaction. The results obtained considering the 7Å-clinochlore thermodynamic data of Helgeson et al. (1978) are listed in Table 4.7 as a function of temperature together with the standard molal Gibbs free energies and the natural and decimal logarithms of the thermodynamic equilibrium constant of the dissolution reaction of pure 7Å-clinochlore:

Table 4.7 Standard molal Gibbs free energies and natural and decimal logarithms of the thermodynamic equilibrium constant of the dissolution reactions of both pure 7Å-clinochlore and the chlorite solid solution with average activity of clinochlore as a function of temperature

T	$\Delta_r G°_{Clc}$	$\Delta_r G°_{Clc,aa}$	ln K_{Clc}	ln $K_{Clc,aa}$	log K_{Clc}	log $K_{Clc,aa}$
°C	cal mol^{-1}	cal mol^{-1}				
0	−98,377	−96,806	181.2380	178.3431	78.7107	77.4534
25	−94,465	−92,750	159.4385	156.5435	69.2432	67.9860
60	−88,148	−86,231	133.1465	130.2515	57.8248	56.5675
100	−80,703	−78,556	108.8337	105.9387	47.2659	46.0086
150	−71,323	−68,889	84.8188	81.9238	36.8363	35.5791
200	−61,652	−58,930	65.5700	62.6750	28.4767	27.2194
250	−51,199	−48,189	49.2484	46.3534	21.3883	20.1310
300	−39,258	−35,961	34.4681	31.5731	14.9693	13.7120

$$Mg_5Al_2Si_3O_{10}(OH)_8 + 16\ H^+ = 5\ Mg^{2+} + 2\ Al^{3+} + 3\ SiO_{2(aq)} + 12\ H_2O \quad (4.27)$$

4.5 Epidotes

4.5.1 Main Characteristics and Nomenclature of the Minerals of the Epidote Group

The following notes on the nomenclature and main features of the minerals of the epidote group are largely based on the review paper of Franz and Liebscher (2004). The minerals of the epidote group are monoclinic sorosilicates with the general formula $A_2M_3[Si_2O_7][SiO_4]O(OH)$ indicating the presence of both SiO_4 tetrahedra and Si_2O_7 groups, as well as the M cations in six-fold octahedral coordination and the A cations in eight-fold coordination (further details in the next section). Orthorhombic zoisite is a polymorph of clinozoisite and is structurally very similar to the monoclinic minerals of the epidote group.

According to the Commission on New Minerals, Nomenclature and Classification (CNMNC) of the International Mineralogical Association (IMA) on the nomenclature of epidote minerals:

(i) The term epidote refers to the mineral, the whole mineral group and the composition $Ca_2(Al_2Fe^{3+})[Si_2O_7][SiO_4]O(OH)$. To avoid confusion, the terms epidote and epidote component (or endmember) are used in this book to indicate the mineral/mineral group and the solid solution component (endmember), respectively.
(ii) The name clinozoisite identifies the stoichiometry $Ca_2Al_3[Si_2O_7][SiO_4]O(OH)$.
(iii) The term piemontite refers to the composition $Ca_2(Al_2Mn^{3+})[Si_2O_7][SiO_4]O(OH)$.
(iv) The name mukhinite identifies the stoichiometry $Ca_2(Al_2V^{3+})[Si_2O_7][SiO_4]O(OH)$.
(v) The terms allanite-Ce, allanite-La, allanite-Nd, and allanite-Y refer to the composition $[Ca(REE)](Al_2Fe^{2+})[Si_2O_7][SiO_4]O(OH)$, in which REE = Ce, La, Nd, and Y, respectively.

The name tawmawite was used for the Cr^{3+} endmember, $Ca_2(Al_2Cr^{3+})[Si_2O_7][SiO_4]O(OH)$, but is not approved by IMA. Also the term pistacite, which was utilized to describe either Fe^{3+}-rich epidotes of stoichiometry close to $Ca_2(Al_2Fe^{3+})[Si_2O_7][SiO_4]O(OH)$ or the hypothetical endmember $Ca_2Fe^{3+}_3[Si_2O_7][SiO_4]O(OH)$ should generally be avoided.

Most monoclinic epidote minerals occurring in geological systems belong to the clinozoisite-epidote solid solution series with epidote mole fractions, X_{Ep}, usually

lower than 0.4, whereas compositions with X_{Ep} as high as 0.4–0.5 were rarely found. Natural binary solid solutions along the clinozoisite-piemontite join are uncommon because most samples also contain Fe^{3+}. In addition, the octahedral M sites can be rarely occupied by Cr^{3+} and V^{3+}, whereas the concentration of the divalent cations Fe^{2+}, Mn^{2+}, and Mg^{2+} on these sites is usually very low. The A sites generally house Ca^{2+}, which can be substituted by Sr^{2+}, Ba^{2+}, Pb^{2+}, and REE^{3+}. Allanite minerals exhibit larger and more complex compositional variations, according to the formula $[(Ca,Ce,La,Y)_2(Al,Fe^{3+},Fe^{2+},Mn^{2+})_3[Si_2O_7][SiO_4]O(OH)]$.

Orthorhombic zoisite exhibits composition closer to the endmember stoichiometry $Ca_2Al_3Si_3O_{12}(OH)$ than the monoclinic minerals of the epidote group. Similar to what occurs in monoclinic epidotes, Fe^{3+}, Mn^{3+}, Cr^{3+}, and V^{3+} substitute for Al^{3+} in the octahedral M sites (although the mole fraction of Fe^{3+} is usually ≤ 0.15), whereas Sr^{2+} and Pb^{2+} substitute for Ca^{2+} in the A sites of zoisite.

Usually, hydrothermal epidote from active geothermal systems shows a wide interval in octahedral substitution of Al^{3+} for Fe^{3+}, with important oscillatory or irregular compositional zoning. These variable characteristics of hydrothermal epidote are due to the variations, in time and space, of temperature, permeability, and fluid parameters such as flux, pH, CO_2 partial pressure, redox potential, and the aqueous speciation of Al and Fe (Bird and Spieler 2004).

4.5.2 The Crystal Chemistry of Epidote Solid Solutions

This section is mainly focused on the equilibrium mixing model of Bird and Helgeson (1980) and, therefore, it is largely derived from their article. Epidote solid solutions can be represented by the following crystallochemical formula:

$$A_2^{VIII}M(1)^{VI}\ M(2)^{VI}\ M(3)^{VI}T_3^{IV}O_{12}(OH),$$

in which:

- A^{VIII} refers to the two large eight-fold coordinated sites, which are predominantly occupied by Ca^{2+} ions;
- $M(1)^{VI}$, $M(2)^{VI}$, and $M(3)^{VI}$ indicate the three six-fold coordinated octahedral sites, which are energetically different and are occupied by Al^{3+} and Fe^{3+} ions;
- T stands for the three tetrahedral sites, which are almost completely occupied by Si^{4+} ions.

Crystal structure site refinements and Mössbauer spectral data indicate that the Fe^{3+} ions are mainly housed by the largest and most distorted $M(3)^{VI}$ octahedral sites, although minor quantities of Fe^{3+} occur also in the $M(1)^{VI}$ sites. In contrast, the $M(2)^{VI}$ sites contain only Al^{3+} ions. According to Bird and Helgeson (1980), Fe^{3+} ions are only present in the M(3) octahedral sites if epidote is completely ordered, whereas octahedral disordering of epidote can be represented by the following reaction:

$$Ca_2Al_{M(1)}Al_{M(2)}Fe_{M(3)}Si_3O_{12}(OH) \rightarrow Ca_2(Al_{1-x}Fe_x)_{M(1)}Al_{M(2)}(Al_xFe_{1-x})_{M(3)}Si_3O_{12}(OH)$$

where x represents the mole fraction of Fe^{3+} ion on the M(1) sites. Bird and Helgeson (1980) defined an ordering parameter for epidote, $\sigma = 1 - 2x$, which assumes the value 1 if the mineral is fully ordered and becomes equal to 0 if it is entirely disordered. The intracrystalline exchange reaction of Al^{3+} and Fe^{3+} ions among the M(1) and M(3) sites:

$$Fe^{3+}_{M(3)} + Al^{3+}_{M(1)} \leftrightarrow Fe^{3+}_{M(1)} + Al^{3+}_{M(3)} \tag{4.28}$$

is regulated by the intracrystalline standard state equilibrium constant:

$$K = \frac{a_{Fe^{3+}_{M(1)}} \cdot a_{Al^{3+}_{M(3)}}}{a_{Fe^{3+}_{M(3)}} \cdot a_{Al^{3+}_{M(1)}}}, \tag{4.29}$$

which is a temperature function as expressed by the relation:

$$\log\ K = -1523.4 \cdot \left(\frac{1}{T} - \frac{1}{Tr}\right) - 5.0, \tag{4.30}$$

with Tr = 298.15. Assuming that the ratios between the activity coefficients of Al^{3+} and Fe^{3+} ions on the M(1) and M(3) sites are equal to 1, it follows that the ordering parameter σ is related to K by the relation:

$$\text{arctanh}\ \sigma = -(\ln\ K)/4. \tag{4.31}$$

Therefore, it is possible to compute σ, knowing or assuming a suitable temperature value. Following Bird and Helgeson (1980), the next step is the calculation of the mole fraction of Fe^{3+} ions on the M(3) sites using the relation:

$$X_{Fe^{3+}_{M(3)}} = -\left[\frac{X_{Ep}}{K-1} + \left(\frac{K \cdot (1 - X_{Ep}) + X_{Ep} + 1}{2 \cdot (K-1)}\right)^2\right]^{0.5} - \frac{K \cdot (1 - X_{Ep}) + X_{Ep} + 1}{2 \cdot (K-1)} \tag{4.32}$$

which is written in a simplified form, that is assuming absence of ions other than Al^{3+} and Fe^{3+} on the M(3) sites. Then, the mole fractions of Fe^{3+} and Al^{3+} ions on the M(1) sites and the mole fraction of Al^{3+} ions on the M(3) sites are computed by means of the equations:

$$X_{Fe^{3+}_{M(1)}} = X_{Ep} - X_{Fe^{3+}_{M(3)}} \tag{4.33}$$

$$X_{Al^{3+}_{M(1)}} = 1 - X_{Fe^{3+}_{M(1)}} \tag{4.34}$$

$$X_{Al^{3+}_{M(3)}} = 2 - X_{Ep} - X_{Al^{3+}_{M(1)}}. \tag{4.35}$$

The mole fractions computed by means of Eqs. (4.32) through (4.35) are then used to calculate the activities of the clinozoisite and epidote endmembers based on the hypothesis of random mixing of atoms on energetically equivalent sites (Helgeson et al. 1978; Bird and Helgeson 1980; Bird and Norton 1981; Helgeson and Aagaard 1985):

$$a_{Czo} = X^2_{Ca^{2+}_A} \cdot X_{Al^{3+}_{M(1)}} \cdot X_{Al^{3+}_{M(3)}} \cdot X^3_{Si^{4+}_T} \tag{4.36}$$

$$a_{Ep} = k_{Ep} \cdot X^2_{Ca^{2+}_A} \cdot \left(X_{Al^{3+}_{M(1)}} \cdot X_{Fe^{3+}_{M(3)}}\right)^{\frac{1+\sigma}{2}} \cdot \left(X_{Al^{3+}_{M(3)}} \cdot X_{Fe^{3+}_{M(1)}}\right)^{\frac{1-\sigma}{2}} \cdot X^3_{Si^{4+}_T} \tag{4.37}$$

where k_{Ep} is the constant relating the inter- and intra-crystalline standard states, which is given by:

$$k_{Ep} = \left(\frac{1+\sigma}{2}\right)^{-(1+\sigma)} \cdot \left(\frac{1-\sigma}{2}\right)^{-(1-\sigma)}. \tag{4.38}$$

The equilibrium model of Bird and Helgeson (1980) for partitioning of Al^{3+} and Fe^{3+} ions among the M(1) and M(3) sites in epidote was based on the data available at that time. In subsequent researches, the order-disorder degree was found either higher than theoretically predicted by the equilibrium model or in good agreement with model's predictions or lower than theoretically predicted by the model (Franz and Liebscher 2004). In spite of possible limitations, the model of Bird and Helgeson (1980) is used in the next section, first, to calculate the equilibrium distribution of Al^{3+} and Fe^{3+} ions among the M(1) and M(3) sites in epidote solid solutions coming from active geothermal systems, starting from the analytical data, and second, to compute the activities of the epidote and clinozoisite components of the epidote solid solutions of interest.

4.5.3 The Activities of Clinozoisite and Epidote Endmembers in Hydrothermal Epidote Solid Solutions

A total of 436 chemical analyses of epidote solid solutions collected in deep geothermal wells at variable depths and temperatures were compiled. Most samples, for a total of 259, come from the geothermal system of Reykjanes, Iceland, at temperatures of 176–345 °C (mainly from Libbey and William-Jones 2016 and subordinately

from Fowler et al. 2015 and Ottolini et al. 2012). Of the remaining 177 chemical analyses, 57 are from Larderello, Italy, at temperatures of 250–368 °C (Cavarretta et al. 1980, 1982), 40 are from Milos, Greece, at temperatures of 305–323 °C (Liakopoulos 1987), 23 are from Salton Sea, California, at temperatures of 250–353 °C (Keith et al. 1968; Bird et al. 1988; Cho et al. 1988; Shearer et al. 1988), 14 are from Los Humeros, Mexico, at temperatures of 235–350 °C (Martinez-Serrano 2002), 9 are from Waiotapu, New Zealand, at temperatures of 220–285 °C (Hedenquist and Browne 1989), 8 are from Cerro Prieto, Mexico, at temperatures of 325–350 °C (Schiffman et al. 1985), 8 are from Kakkonda, Japan, at temperatures of 225–285 °C (Muramatsu and Doi 2000; Sawaki et al. 2001), 8 are from Onikobe, Japan, at temperatures of 125–173 °C (Seki et al. 1983), 4 are from Broadlands, New Zealand, at temperatures of 260–300 °C (Lonker et al. 1990), 2 are from Hachimantai, Japan, at temperatures of 200–230 °C (Shimazu and Yajima 1973), 2 are from Newberry Caldera, Oregon, at temperature of 260 °C (Keith and Bargar 1988), and 2 are from Miravalles, Costa Rica, at temperature of 240 °C (Milodowski et al. 1989).

Clinozoisite is the main component of these hydrothermal epidote solid solutions, with mole fraction varying between 0.527 and 0.893, both average and median equal to 0.728, and standard deviation of 0.061. Being the complement to 1 of the clinozoisite mole fraction, the epidote component mole fraction ranges from 0.107 to 0.463, both average and median are equal to 0.272, and standard deviation is the same of clinozoisite, 0.061. Consequently, available data are positioned along a line of slope-1 in the correlation plot of the clinozoisite mole fraction versus the epidote component mole fraction (Fig. 4.12a). The composition of the considered hydrothermal epidote solid solutions compares with that of most monoclinic epidote minerals occurring in different geological systems.

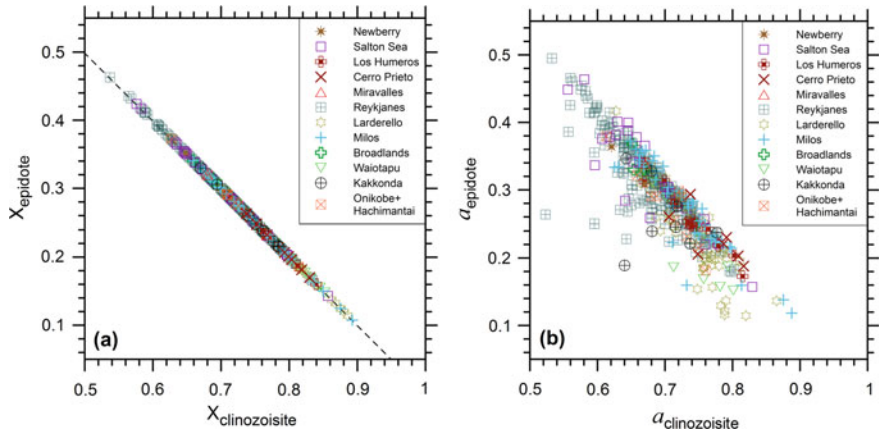

Fig. 4.12 Plots of **a** the clinozoisite mole fraction versus the epidote component mole fraction and **b** the activity of clinozoisite versus the activity of the epidote component for 436 hydrothermal epidote solid solutions from different geothermal systems (see legend)

The activity of clinozoisite varies between 0.523 and 0.888, with a mean of 0.703, a median of 0.706, and a standard deviation of 0.057, whereas the activity of the epidote component ranges from 0.115 to 0.495, with an average of 0.288, a median of 0.287 and a standard deviation of 0.066. Also in the correlation diagram of the activity of clinozoisite versus the activity of the epidote component (Fig. 4.12b), sample points are distributed along a line of slope-1, because activities of both clinozoisite and epidote endmembers are not very different from the corresponding mole fractions. Nevertheless, in Fig. 4.12b there is a considerable scatter, which is evidently due to varying deviations from ideality.

Such deviations are described by the activity coefficients of both clinozoisite and epidote endmembers which were computed by means of Eq. (2.3) solved with respect to λ. Interestingly, the activity coefficient of clinozoisite is usually <1, with minimum of 0.763 and maximum of 1.001, whereas the activity coefficient of epidote is generally >1, up to a maximum of 1.129, even though its minimum value is 0.839 (Fig. 4.13a). However, average and median are close to unity, being 0.966 and 0.973, respectively, for clinozoisite and 1.060 and 1.066, respectively, for the epidote component. The standard deviation is small in both case, with 0.028 for clinozoisite and 0.035 for the epidote component.

These deviations from ideality are ascribable to the varying degree of substitutional order/disorder which is a temperature function, as defined by Eq. (4.30) and shown in Fig. 4.13b, according to the equilibrium model of Bird and Helgeson (1980).

The temperature measured at the depth of collection of hydrothermal epidote was considered in calculations, although observed mineral alteration may have formed under thermal conditions different from contemporary temperatures. In addition, Arnórsson (1995) noted that the number of hydrothermal minerals reported in a

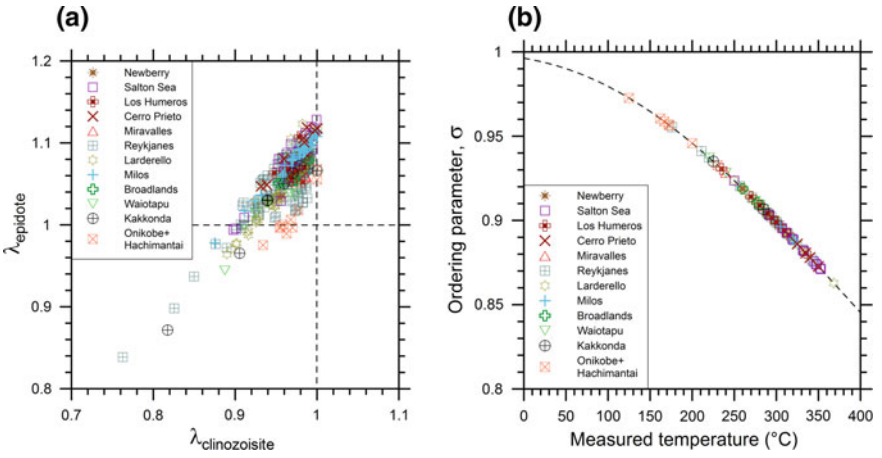

Fig. 4.13 Plots of **a** the activity coefficient of clinozoisite versus the activity coefficient of the epidote component and **b** the ordering parameter σ versus the measured temperature, for 436 hydrothermal epidote solid solutions from different geothermal systems (see legend)

single drill hole sample is commonly greater than permitted by consideration of the phase rule, indicating that secondary mineral assemblages may form over a range of temperatures and fluid compositions, and that metastable phase relations are not uncommon.

The hydrothermal epidote samples appear to be relatively ordered, as indicated by the range of the ordering parameter σ, from 0.863 to 0.973, with a mean of 0.905, a median of 0.904, and a standard deviation of 0.018. However, deviations from the equilibrium distribution predicted by the model of Bird and Helgeson (1980) are possible, due to occurrence of metastable states of substitutional order/disorder on the octahedral sites. For instance, this condition was ascertained by means of ^{57}Fe Mössbauer spectroscopy for four epidote samples from the State 2–14 drill hole, Salton Sea (Bird et al. 1988) and for the epidotes from the fossil geothermal system of Saint Martin (Patrier et al. 1991), see also Liebscher (2004).

4.5.4 The Thermodynamic Properties of Epidotes

The thermodynamic properties of four minerals of the epidote group are reported by Helgeson et al. (1978), namely clinozoisite and zoisite, both of chemical formula $Ca_2Al_3Si_3O_{12}(OH)$, as well as epidote (which refers to the stable state of substitutional order/disorder at any pressure and temperature) and ordered epidote, both of stoichiometry $Ca_2FeAl_2Si_3O_{12}(OH)$. Holland and Powell (1998) estimated the thermodynamic properties of four minerals of the epidote group, again clinozoisite and zoisite, both of chemical formula $Ca_2Al_3Si_3O_{12}(OH)$, and ordered epidote of stoichiometry $Ca_2FeAl_2Si_3O_{12}(OH)$, as well as a solid phase richer in Fe^{3+}, called Fe-epidote, of chemical composition $Ca_2Fe_2AlSi_3O_{12}(OH)$. Monoclinic epidote minerals were treated as regular solid solutions of clinozoisite, ordered epidote, and Fe-epidote extending the model of Bird and Helgeson (1980) through incorporation of non-ideal mixing. Holland and Powell (2011) revised the thermodynamic properties of the four minerals of the epidote group considered by Holland and Powell (1998) and estimated also the thermodynamic properties of ordered piemontite, of chemical formula $Ca_2MnAl_2Si_3O_{12}(OH)$. All these data are reported in Table 4.8.

The $\Delta G°_f$ and $\Delta H°_f$ reported by Holland and Powell (1998) differ from those of Helgeson et al. (1978) by 4570 and 4467 cal mol^{-1} for clinozoisite, 951 and 286 cal mol^{-1} for ordered epidote, and 4456 and 4667 cal mol^{-1} for zoisite. The $\Delta G°_f$ and $\Delta H°_f$ listed by Holland and Powell (2011) differ from those of Helgeson et al. (1978) by 3927 and 3824 cal mol^{-1} for clinozoisite, 2582 and 2843 cal mol^{-1} for ordered epidote, and 3963 and 4103 cal mol^{-1} for zoisite. Besides, for the same mineral, there are differences from 493 to 4071 cal mol^{-1} in $\Delta G°_f$ and from 564 to 6066 cal mol^{-1} in $\Delta H°_f$ between the database of Holland and Powell (1998) and that of Holland and Powell (2011).

A very detailed analysis of the thermodynamic properties of zoisite, orthoepidote, clinozoisite, and epidote was performed by Gottschalk (2004), who examined *inter alias* the experimental measurements carried out by several authors, as well as

Table 4.8 Standard state molal thermodynamic properties, at 25 °C, 1 bar, of different epidote minerals from H78 = Helgeson et al. (1978), HP98 = Holland and Powell (1998), and HP11 = Holland and Powell (2011)

Name	$\Delta G°_f$	$\Delta H°_f$	S°	V°	a	b ($\times 10^3$)	c ($\times 10^{-5}$)	d	References
	cal mol^{-1}	cal mol^{-1}	cal K^{-1} mol^{-1}	cm^3 mol^{-1}	cal K^{-1} mol^{-1}	cal K^{-2} mol^{-1}	cal K mol^{-1}	cal $K^{-0.5}$ mol^{-1}	
Clinozoisite	−1,549,680	−1,644,221	70.64	136.2	106.118	25.214	−27.145	–	H78
Clinozoisite	−1,554,250	−1,648,688	71.9	136.30	135.5	4.3172	−16.812	−622.1	HP98
Clinozoisite	−1,553,607	−1,648,045	71.9	136.30	150.8	3.2727	−15.884	−891.8	HP11
Epidote	−1,451,346	−1,544,432	75.28	139.2	117.622	12.816	−31.864	–	H78
Epidote (ord)	−1,451,346	−1,544,456	75.2	139.2	113.78	14.69	−28.92	–	H78
Epidote (ord)	−1,452,297	−1,544,742	78.4	139.10	130.2	5.9228	−26.840	−284.9	HP98
Epidote (ord)	−1,453,928	−1,547,299	75.3	139.20	146.6	5.2749	−17.113	−714.1	HP11
Fe-epidote	−1,344,250	−1,434,558	85.3	141.90	124.3	7.5284	−36.869	52.3	HP98
Fe-epidote	−1,348,320	−1,440,624	78.6	142.10	139.7	7.2770	−18.342	−536.4	HP11
Piemontite (ord)	−1,470,118	−1,563,824	81.3	138.20	136.2	6.6420	−13.009	−672.2	HP11
Zoisite	−1,549,619	−1,644,131	70.74	135.90	106.118	25.214	−27.145	–	H78
Zoisite	−1,554,075	−1,648,798	71.0	135.75	142.4	14.8893	−14.152	−811.4	HP98
Zoisite	−1,553,582	−1,648,234	71.2	135.75	158.2	2.4895	−14.356	−1018.3	HP11

Table 4.9 Standard molal Gibbs free energies and natural and decimal logarithms of the thermodynamic equilibrium constant of the dissolution reactions of both pure clinozoisite and the epidote solid solution with average activity of clinozoisite as a function of temperature

T	$\Delta_r G^\circ_{Czo}$	$\Delta_r G^\circ_{Czo,aa}$	ln K_{Czo}	ln $K_{Czo,aa}$	log K_{Czo}	log $K_{Czo,aa}$
°C	cal mol^{-1}	cal mol^{-1}				
0	−59,755	−59,564	110.0855	109.7331	47.8095	47.6565
25	−56,211	−56,002	94.8732	94.5208	41.2029	41.0499
60	−50,204	−49,971	75.8325	75.4801	32.9336	32.7806
100	−42,797	−42,536	57.7148	57.3624	25.0652	24.9122
150	−33,067	−32,771	39.3240	38.9716	17.0782	16.9251
200	−22,723	−22,392	24.1671	23.8147	10.4956	10.3426
250	−11,420	−11,054	10.9849	10.6325	4.7707	4.6176
300	1379	1780	−1.2107	−1.5631	−0.5258	−0.6789

the values reported in internally consistent datasets, underscoring the discrepancies between different sources and the missing pieces of information.

Finally, the recommended values of the thermodynamic parameters are listed by Gottschalk (2004), but no supporting motivation is given. The concluding statement of Gottschalk (2004) "*However, the specific choice of a value might be somewhat subjective and reflects the opinion of the author*" might seem disappointing at the end of such a thorough review. However, it is a further example of the impossibility to select reliable values of thermodynamic properties by focusing the attention on a single group of minerals only. A much wider analysis is needed to establish the internal consistency of the whole thermodynamic database.

Adopting the approach described in Sect. 2.2.1, it is advisable to consider the epidote solid solution with average activity of clinozoisite, $a_{Czo} = 0.703$, and to compute the Gibbs free energy and the thermodynamic equilibrium constant of its dissolution reaction. The results obtained taking into account the clinozoisite thermodynamic data of Helgeson et al. (1978) are listed in Table 4.9 as a function of temperature together with the standard molal Gibbs free energies and the natural and decimal logarithms of the thermodynamic equilibrium constant of the dissolution reaction of pure clinozoisite:

$$Ca_2Al_3Si_3O_{12}(OH) + 13\ H^+ = 2\ Ca^{2+} + 3\ Al^{3+} + 3\ SiO_{2(aq)} + 7\ H_2O. \quad (4.39)$$

4.6 Prehnite

As indicated by several authors (e.g., Papike and Zoltai 1967; Baur et al. 1990), there are two prehnite polymorphs, namely monoclinic clinoprehnite and orthorhombic orthoprehnite, which in turn have two distinct structures according to Akizuki

(1987). The two prehnite polymorphs have very similar unit cell volumes, 469.5(1) and 468.7(2) $Å^3$, respectively, and supposedly a tiny energetic difference, as also suggested by their close association in nature (Baur et al. 1990). Therefore, the two polymorphs of prehnite are not distinguished in the following discussion.

4.6.1 The Crystal Chemistry of Prehnite/Ferri-Prehnite Solid Solutions

Single crystal structure analyses (e.g., Preisinger 1965; Papike and Zoltai 1967; Zunić et al. 1990; Baur et al. 1990; Artioli et al. 1995; Akasaka et al. 2003) indicate that prehnite solid solutions have seven-coordinated sites A filled by Ca^{2+}, octahedral sites M(1) containing both Al^{3+} and Fe^{3+}, and two different types of tetrahedral sites T1 and T2. The T1 sites are entirely occupied by Si^{4+} or nearly so, whereas the T2 sites house Al^{3+} and Si^{4+} in variable degrees of order-disorder. The structural formula of prehnite solid solutions can thus be written as (Bird and Helgeson 1980, modified):

$$Ca_2\left[Al_{(1-y)}Fe_y\right]^{M(1)}(Si)_2^{T1}\left(Al_{(1-x)}Si_x\right)^{T2}O_{10}(OH)_2$$

where y is the mole fraction of Fe^{3+} on the octahedral sites M(1) and x is the mole fraction of Si^{4+} on the tetrahedral sites T2.

Prehnite solid solutions from natural systems show considerable octahedral substitution of Fe^{3+} for Al^{3+}, which may be as high as 60 mol percent based on the chemical analyses of this mineral from different metamorphic environments (Bird and Helgeson 1980, and references therein), whereas other compositional variations are very limited. In fact, sodium, potassium, magnesium, ferrous iron and manganese substitution for calcium on the seven-coordinated sites, as well as the substitution of Fe^{3+} or Al^{3+} for Si^{4+} on the tetrahedral sites are usually lower than 0.1 atoms per formula unit.

Under the hypotheses of random intrasite mixing and equal interaction of Al^{3+} and Fe^{3+} on the octahedral sites M(1) and Al^{3+} and Si^{4+} on the tetrahedral sites T2, the activity of the prehnite endmember $[Ca_2Al(AlSi_3)O_{10}(OH)_2]$ and the ferri-prehnite component $[Ca_2Fe(AlSi_3)O_{10}(OH)_2]$ in prehnite solid solutions are calculated by means of the relations (Helgeson et al. 1978; Helgeson and Aagaard 1985):

$$a_{Prh} = k_{Prh} \cdot X^2_{Ca^{2+}_A} \cdot X_{Al^{3+}_{M(1)}} \cdot \left(X_{Al^{3+}_{T2}} \cdot X_{Si^{4+}_{T2}}\right) \tag{4.40}$$

$$a_{Fe-Prh} = k_{Fe-Prh} \cdot X^2_{Ca^{2+}_A} \cdot X_{Fe^{3+}_{M(1)}} \cdot \left(X_{Al^{3+}_{T2}} \cdot X_{Si^{4+}_{T2}}\right) \tag{4.41}$$

where $k_{Prh} = k_{Fe\text{-}Prh} = 4$ are the constants relating the inter- and intra-crystalline standard states.

4.6.2 *The Endmember Activities in Hydrothermal Prehnite/Ferri-Prehnite Solid Solutions*

In this work, a total of 127 chemical analyses of prehnite solid solutions obtained from deep geothermal wells at different temperatures and depths were compiled. Most of these chemical analyses, namely 96, comes from the two geothermal systems of Darajat, Indonesia (N = 61, temperatures 225–350 °C; Herdianita 2012) and Reykjanes, Iceland (N = 35; temperatures 170–342 °C; Libbey and Williams-Jones 2016). Of the other 31 chemical analyses, 14 are from Onikobe, Japan (temperatures 112–173 °C; Seki et al. 1983), 7 are from Cerro Prieto, Mexico (temperatures 325–350 °C; Schiffman et al. 1985), 4 are from Heber (temperature 175 °C; Wheeler et al. 2001), 3 are from Kakkonda, Japan (temperature 225 °C; Muramatsu and Doi 2000), 1 is from Larderello, Italy (temperature 290 °C; Cavarretta et al. 1982), 1 is from Miravalles (temperature 240 °C; Milodowski et al. 1989), and 1 is from Krafla (temperature not specified; Kristmannsdóttir 1979).

The plots of Fig. 4.14a, b are very similar because the activities of the prehnite and ferri-prehnite endmembers computed by means of Eqs. (4.40) and (4.41) are nearly equal to the mole fractions of Al^{3+} and Fe^{3+} on the octahedral sites M(1), respectively. Since $X_{Al^{3+}_{M(1)}} + X_{Fe^{3+}_{M(1)}} \cong 1$ and $a_{Prh} + a_{Fe-Prh} \cong 1$, most prehnite solid solutions are situated close to the line of equation $X_{Fe^{3+}_{M(1)}} = 1 - X_{Al^{3+}_{M(1)}}$ in Fig. 4.14a and to the line of equation $a_{Fe\text{-}Prh} = 1 - a_{Prh}$ in Fig. 4.14b.

Prehnite is the main component of most hydrothermal prehnite solid solutions, with activities ranging between 0.373 and 0.998, average of 0.763, median of 0.779,

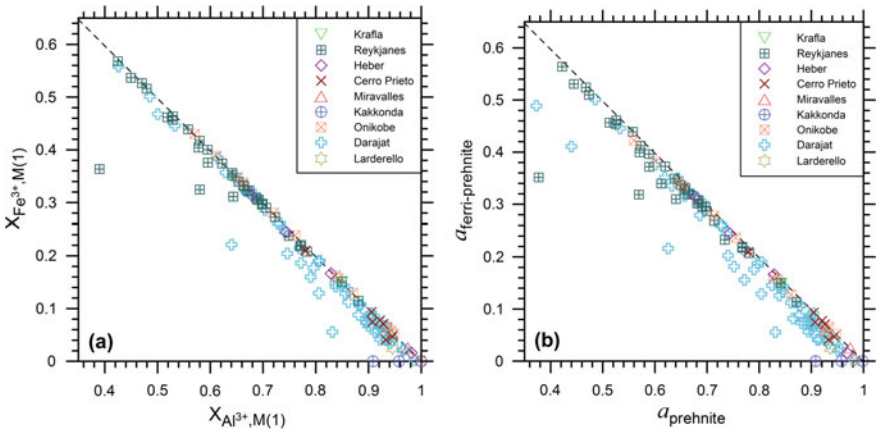

Fig. 4.14 Plots of **a** the mole fraction of Al^{3+} on the octahedral sites M(1) versus the mole fraction of Fe^{3+} on the octahedral sites M(1) and **b** the activity of prehnite versus the activity of ferri-prehnite for 127 prehnite solid solutions from different active geothermal systems (see legend). The dashed line corresponds to the equations $X_{Fe^{3+}_{M(1)}} = 1 - X_{Al^{3+}_{M(1)}}$ in **a** an $a_{Fe\text{-}Prh} = 1 - a_{Prh}$ in **b**

and standard deviation of 0.154. The activity of ferri-prehnite varies from 0.000 to 0.564, with average of 0.210, median of 0.190, and standard deviation of 0.148.

Interestingly, the prehnite solid solutions from the geothermal systems hosted in basaltic rocks, such as Reykjanes and Onikobe, are generally richer in ferri-prehnite than the prehnite samples from the geothermal systems housed in granites or clastic sedimentary rocks, such as Larderello, Cerro Prieto, and especially Kakkonda, where prehnite is Fe-free. The hydrothermal prehnite samples of Darajat distribute over the whole compositional range, although the solid solutions rich in prehnite are more abundant than those rich in ferri-prehnite.

4.6.3 The Thermodynamic Properties of Prehnite

Helgeson et al. (1978), Holland and Powell (1998), and Holland and Powell (2011) report the thermodynamic properties of prehnite of stoichiometry $Ca_2Al_2Si_3O_{10}(OH)_2$, but Holland and Powell (2011) give also the thermodynamic parameters of ferri-prehnite of composition $Ca_2FeAlSi_3O_{10}(OH)_2$ and describe deviation from ideality of prehnite solid solutions in terms of a regular solution model. According to Helgeson et al. (1978), the standard state molal ΔG°_f, ΔH°_f, and S° at 25 °C, 1 bar of prehnite should be regarded as provisional approximations. All these thermodynamic data of prehnite and ferri-prehnite are reported in Table 4.10, showing that the ΔG°_f and ΔH°_f of Holland and Powell (1998) differ from those of Helgeson et al. (1978) by 1702 and 502 cal mol^{-1}, respectively, whereas the ΔG°_f and ΔH°_f of Holland and Powell (2011) differ from those of Helgeson et al. (1978) by 1449 and 248 cal mol^{-1}, respectively.

Employing the approach described in Sect. 2.2.1, it is advisable to consider the prehnite/ferri-prehnite solid solution with average activity of prehnite, $a_{Prh} = 0.763$, and to compute the Gibbs free energy and the thermodynamic equilibrium constant of its dissolution reaction. The results obtained taking into account the prehnite thermodynamic data of Helgeson et al. (1978) are listed in Table 4.11 as a function of temperature together with the standard molal Gibbs free energies and the natural and decimal logarithms of the thermodynamic equilibrium constant of the dissolution reaction of pure prehnite:

$$Ca_2Al_2Si_3O_{10}(OH)_2 + 10\ H^+ = 2\ Al^{3+} + 2\ Ca^{2+} + 3\ SiO_{2(aq)} + 6\ H_2O. \quad (4.42)$$

Table 4.10 Standard state molal thermodynamic properties, at 25 °C, 1 bar of prehnite and ferri-prehnite from H78 = Helgeson et al. (1978), HP98 = Holland and Powell (1998), and HP11 = Holland and Powell (2011)

Name	$\Delta G°_f$	$\Delta H°_f$	S°	V°	a	b ($\times 10^3$)	c ($\times 10^{-5}$)	d	References
	cal mol^{-1}	cal mol^{-1}	cal K^{-1} mol^{-1}	cm^3 mol^{-1}	cal K^{-1} mol^{-1}	cal K^{-2} mol^{-1}	cal K mol^{-1}	cal $K^{-0.5}$ mol^{-1}	
Prehnite	−1,390,537	−1,482,089	65.0	140.33	91.60	37.82	−19.60	–	H78
Prehnite	−1,392,239	−1,482,591	69.98	140.26	173.3	−3.3138	−4.9211	−1511.4	HP98
Prehnite	−1,391,986	−1,482,337	69.98	140.26	173.3	−3.3138	−4.9211	−1511.4	HP11
Ferri-prehnite	−1,288,005	−1,378,286	76.48	148.00	176.2	−4.0177	−4.6781	−1519.6	HP11

Table 4.11 Standard molal Gibbs free energies and natural and decimal logarithms of the thermodynamic equilibrium constant of the dissolution reactions of both pure prehnite and the prehnite/ferri-prehnite solid solution with average activity of prehnite as a function of temperature

T(°C)	$\Delta_r G^\circ_{Prh}$	$\Delta_r G^\circ_{Prh,aa}$	ln K_{Prh}	ln $K_{Prh,aa}$	log K_{Prh}	log $K_{Prh,aa}$
	cal mol^{-1}	cal mol^{-1}				
0	−44,958	−44,811	82.8253	82.5548	35.9706	35.8531
25	−43,057	−42,897	72.6718	72.4013	31.5610	31.4435
60	−39,407	−39,228	59.5238	59.2533	25.8509	25.7334
100	−34,749	−34,548	46.8615	46.5910	20.3517	20.2342
150	−28,569	−28,342	33.9749	33.7044	14.7551	14.6376
200	−21,965	−21,711	23.3609	23.0904	10.1455	10.0280
250	−14,682	−14,401	14.1226	13.8521	6.1334	6.0159
300	−6292	−5984	5.5243	5.2538	2.3992	2.2817

4.7 Laumontite and Wairakite

4.7.1 Main Characteristics of Ca-Zeolites

Laumontite and wairakite are the two most common zeolites in active geothermal systems (e.g., Browne 1978; Kristmannsdóttir and Tomasson 1976), together with heulandite [$(Na,K,Ca_{0.5})_{10}(A1_{10}Si_{26}O_{72})\cdot 24H_2O$] – clinoptilolite [$(Na,K,Ca_{0.5})_{5.4}$ $(A1_{5.4}Si_{30.6}O_{72})$ · 20 H_2O], forming a continuous compositional series (Bish and Boak 2001). Less frequent zeolites comprise stilbite [$NaCa_4(Al_9Si_{27}O_{72})$ · 30 H_2O], chabazite [$(Ca_{0.5},Na,K)_4(A1_4Si_8O_{24})$ · 12 H_2O], thomsonite [$Ca_7Na_5(Al_{19}Si_{21}O_{80})\cdot 24\ H_2O$], scolecite [$Ca_8(Al_{16}Si_{24}O_{80})\cdot 24\ H_2O$], mordenite [$Na_3Ca_2K(Al_8Si_{40}O_{96})$ · 28 H_2O], yugawaralite [$Ca_2(Al_4Si_{12}O_{32})$ · 8 H_2O], levyne [$(Ca_{0.5},Na)_6(A1_6Si_{12}O_{36})$ · 18 H_2O], gismondine [$Ca_4(Al_8Si_8O_{32})$ · 16 H_2O], and gmelinite [$(Na,K,Ca_{0.5})_8(Al_8Si_{16}O_{48})$ · 22 H_2O].

Only laumontite and wairakite are considered in this work, because all their thermodynamic properties (and those of analcime) were retrieved by Helgeson et al. (1978). In contrast, Helgeson et al. (1978) estimated only the standard molal entropy and heat capacity power function coefficients for and other zeolites, including chabazite [$Ca(A1_2Si_4O_{12})$ · 6 H_2O], epilstilbite [$Ca(A1_2Si_6O_{16})$ · 5 H_2O], heulandite [$Ca(A1_2Si_7O_{18})$ · 6 H_2O], natrolite [$Na_2(A1_2Si_3O_{10})$ · 2 H_2O], Na-phillipsite [$Na_2(A1_2Si_5O_{14})$ · 5 H_2O], K-phillipsite [$K_2(A1_2Si_5O_{14})$ · 5 H_2O], Ca-phillipsite [$Ca(A1_2Si_5O_{14})$ · 5 H_2O], and stilbite [$NaCa_2(A1_5Si_{13}O_{36})$ · 14 H_2O].

The activity of aqueous silica and relevant cations, such as H^+, Na^+, K^+, Ca^{2+}, and Al^{3+} are essential fluid parameters determining which zeolites will form or whether zeolites will form at all. Temperature plays an important role in controlling zeolite stability, partly because of the high water content of zeolites, whereas pressure is less important (Chipera and Apps 2001).

Zeolites usually occur in the shallower parts of active geothermal systems, at temperatures <200 °C, although wairakite forms at temperatures >200 °C and is often associated with epidote (Bird et al. 1984). A peculiarity of laumontite is its occurrence also as precipitate from hot spring waters, at atmospheric pressure and temperatures from 43 to 89 °C (McCulloh et al. 1981). In contrast, wairakite occurs almost exclusively in geothermal systems, both active and fossil. Indeed, the name wairakite is after Wairakei, New Zealand, where this zeolite was first found during the study of hydrothermal alteration minerals in cores recovered from local boreholes (Steiner 1955; Coombs 1955).

4.7.2 Crystal Chemistry of Wairakite and Analcime

The identification of several samples with chemistry and physical properties (e.g., refractive indices and density) intermediate between those of wairakite [$CaAl_2Si_4O_{12} \cdot 2H_2O$] and those of analcime [$NaAlSi_2O_6 \cdot H_2O$] suggests the existence of a continuous isomorphous series between these two endmembers (Passaglia and Sheppard 2001 and references therein). These samples with intermediate properties are classified either as analcime if Na/(Na + Ca) > 0.5 or as wairakite if Na/(Na + Ca) < 0.5. The Si/(Si + Al + Be) ratio has average value of 0.67 in both analcime and wairakite and range 0.60 to 0.74 in analcime and 0.65 to 0.70 in wairakite. Subordinate extra-framework cations are Ca, K, Mg, and Cs in analcime and Na and Cs in wairakite.

Pure wairakite is monoclinic and has six tetrahedral sites, of which four are occupied by Si^{4+} and two by Al^{3+}, as well as an octahedral site housing one Ca^{2+} ion (Armbruster and Gunter 2001). Ca is coordinated by two H_2O molecules and four oxygen atoms, belonging to two AlO_4 tetrahedra. Allowing for the substitutions of Na^+ and K^+ for Ca^{2+} on the octahedral M2 sites, of Fe^{3+} for Al^{3+} on the tetrahedral T2 sites, and of Ti^{4+} for Si^{4+} on the tetrahedral T1 sites, the structural formula of wairakite/analcime solid solutions can be written as:

$$\left[Ca_{(1-x-y)}Na_xK_y\right]\left[Al_{(1-m)}Fe^{3+}_m\right]_2\left[Si_{(1-p)}Ti_p\right]_4O_{12} \cdot 2\ H_2O$$

where x and y are the mole fractions of Na^+ and K^+, respectively, on the octahedral M2 sites, m is the mole fraction of Fe^{3+} on the tetrahedral T2 sites, and p is the mole fraction of Ti^{4+} on the tetrahedral T1 sites. Under the hypothesis of random mixing of atoms on energetically equivalent sites, the activity of the wairakite endmember [$Ca(Al_2Si_4)O_{12} \cdot 2H_2O$] and the analcime component [$Na(AlSi_2)O_6 \cdot H_2O$] in the wairakite/analcime solid solutions can be calculated by means of the relations (Helgeson et al. 1978; Helgeson and Aagaard 1985):

$$a_{Wrk} = k_{Wrk} \cdot X_{Ca^{2+}_{M2}} \cdot X^2_{Al^{3+}_{T2}} \cdot X^4_{Si^{4+}_{T1}} \tag{4.43}$$

$$a_{\mathrm{Anl}} = \mathrm{k_{Anl}} \cdot \mathrm{X}_{\mathrm{Na}^{+}_{\mathrm{M2}}} \cdot \mathrm{X}_{\mathrm{Al}^{3+}_{\mathrm{T2}}} \cdot \mathrm{X}^{2}_{\mathrm{Si}^{4+}_{\mathrm{T1}}} \tag{4.44}$$

where $\mathrm{k_{Wrk}} = \mathrm{k_{Anl}} = 1$ are the constants relating the inter- and intra-crystalline standard states.

4.7.3 Crystal Chemistry of Laumontite

According to Armbruster and Gunter (2001) fully hydrated laumontite has stoichiometry $CaAl_2Si_4O_{12} \cdot 4.5\ H_2O$, but previous studies, including Helgeson et al. (1978), assumed that it contains $4H_2O$ molecules. Upon exposure to low humidity at room temperature, laumontite experiences partial dehydration with production of leonhardite, of stoichiometry $CaAl_2Si_4O_{12} \cdot 3.5\ H_2O$. The reaction is reversed by soaking leonhardite in H_2O at room temperature (Coombs 1952). The Si/(Si + Al + Be) ratio of laumontite has average value of 0.67 and range 0.65–0.69, similar to analcime and wairakite (see above). Subordinate extra-framework cations are Na and K (Passaglia and Sheppard 2001).

Similar to wairakite, the laumontite structure is monoclinic and has six tetrahedral sites, of which four house Si^{4+} and two house Al^{3+} ions, as well as an octahedral site occupied by a Ca^{2+} ion (Armbruster and Gunter 2001). Ca is coordinated by three H_2O molecules and four oxygen atoms, belonging to AlO_4 tetrahedra.

Again, as for wairakite/analcime solid solutions, permitting the vicariance of Na^+ and K^+ for Ca^{2+} on the octahedral M2 sites, of Fe^{3+} for Al^{3+} on the tetrahedral T2 sites, and of Ti^{4+} for Si^{4+} on the tetrahedral T1 sites, the structural formula of laumontite solid solutions can be written as:

$$\left[\mathrm{Ca}_{(1-\mathrm{x}-\mathrm{y})}\mathrm{Na}_{\mathrm{x}}\mathrm{K}_{\mathrm{y}}\right]\left[\mathrm{Al}_{(1-\mathrm{m})}\mathrm{Fe}^{3+}_{\mathrm{m}}\right]_2\left[\mathrm{Si}_{(1-\mathrm{p})}\mathrm{Ti}_{\mathrm{p}}\right]_4\mathrm{O}_{12} \cdot 4.5\ \mathrm{H_2O}$$

where x and y are the mole fractions of Na^+ and K^+, respectively, on the octahedral M2 sites, m is the mole fraction of Fe^{3+} on the tetrahedral T2 sites, and p is the mole fraction of Ti^{4+} on the tetrahedral T1 sites. Hence, the structural formula of laumontite solid solutions is equal to that of wairakite/analcime solid solutions (see above), apart from the different number of water molecules.

Assuming random mixing of atoms on energetically equivalent sites, the activity of the laumontite endmember $[Ca(Al_2Si_4)O_{12} \cdot 4.5\ H_2O]$ and the related hypothetical alkali component $[(Na,K)(Al_2Si_4)O_{12} \cdot 4.5\ H_2O]$ in the laumontite solid solutions can be computed using the relations (Helgeson et al. 1978; Helgeson and Aagaard 1985):

$$a_{\mathrm{Lmt}} = \mathrm{k_{Lmt}} \cdot \mathrm{X}_{\mathrm{Ca}^{2+}_{\mathrm{M2}}} \cdot \mathrm{X}^{2}_{\mathrm{Al}^{3+}_{\mathrm{T2}}} \cdot \mathrm{X}^{4}_{\mathrm{Si}^{4+}_{\mathrm{T1}}} \tag{4.45}$$

$$a_{\mathrm{Na,K-Lmt}} = \mathrm{k_{Na,K\text{-}Lmt}} \cdot (\mathrm{X}_{\mathrm{Na}^{+}_{\mathrm{M2}}} + \mathrm{X}_{\mathrm{K}^{+}_{\mathrm{M2}}}) \cdot \mathrm{X}^{2}_{\mathrm{Al}^{3+}_{\mathrm{T2}}} \cdot \mathrm{X}^{4}_{\mathrm{Si}^{4+}_{\mathrm{T1}}} \tag{4.46}$$

where $k_{Lmt} = k_{Na,K\text{-}Lmt} = 1$ are the constants relating the inter- and intra-crystalline standard states.

4.7.4 The Activity of Wairakite in Hydrothermal Wairakite/Analcime Solid Solutions

A total of 136 chemical analyses of wairakite/analcime solid solutions sampled in geothermal wells at different depths and temperatures were compiled in this work. Most of these chemical analyses, namely 119, come from the two geothermal systems of Onikobe, Japan (N = 60; temperature 110–240 °C; Seki et al. 1983) and Darajat, Indonesia (N = 59; temperature 220–267 °C; Herdianita 2012). The remaining 17 chemical analyses are from Hachimantai, Japan (N = 6; temperature 160–195 °C; Shimazu and Yajima 1973), Waiotapu, New Zealand (N = 3; temperature 220–285 °C; Hedenquist and Browne 1989), Cerro Prieto, Mexico (N = 2; temperature 320 °C; Schiffman et al. 1985), Krafla (N = 1, temperature not given; Kristmannsdottir, 1979), Reydarfjordur (N = 1; temperature not reported; Viereck et al. 1982), Yellowstone, Wyoming (N = 1; temperature 138 °C; Bargar and Beeson 1981), Kakkonda, Japan (N = 1; temperature not specified; Muramatsu and Doi 2000), Wairakei, New Zealand (N = 1; temperature not given; Steiner 1955), and Larderello, Italy (temperature 120 °C; Cavarretta et al. 1982).

The compiled wairakite/analcime solid solutions have wairakite activity ranging from 0.573 to 0.999, with average of 0.891, median of 0.920, and standard deviation of 0.090 and analcime activity varying from 0.000 to 0.427, with mean of 0.096, median of 0.068, and standard deviation of 0.091. As expected, in the diagram of Fig. 4.15a, most wairakite/analcime solid solutions are located close to the line of equation $a_{Anl} = 1 - a_{Wrk}$.

The wairakite/analcime samples coming from the two most studied geothermal systems show different characteristics, with those from Onikobe spanning a compositional range much larger than those from Darajat. In fact, at Onikobe, wairakite activity varies from 0.648 to 0.977, with average of 0.844, median of 0.846, and standard deviation of 0.083, whereas, at Darajat, wairakite activity ranges from 0.857 to 0.999, with average of 0.942, median of 0.946, and standard deviation of 0.037. The different activities of wairakite and analcime at Onikobe and Darajat might be due to differences in temperatures and in the lithological framework between the two geothermal fields.

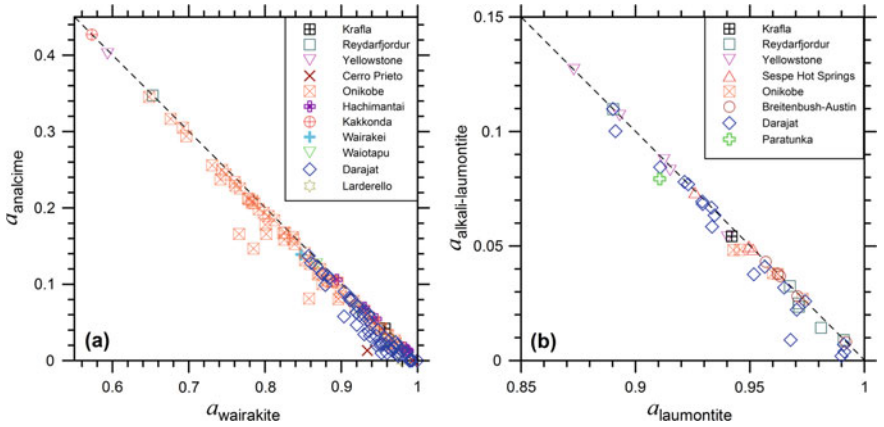

Fig. 4.15 Plots of **a** the activity of wairakite versus the activity of analcime for 136 wairakite/analcime solid solutions from different active geothermal systems (see legend) and **b** the activity of laumontite versus the activity of alkali-laumontite for 45 laumontite/alkali-laumontite solid solutions from various active geothermal systems (see legend). The dashed line corresponds to the equations $a_{\mathrm{Anl}} = 1 - a_{\mathrm{Wrk}}$ in **a** an $a_{\mathrm{Na,K\text{-}Lmt}} = 1 - a_{\mathrm{Lmt}}$ in **b**

4.7.5 The Activity of Laumontite in Hydrothermal Laumontite/Alkali-Laumontite Solid Solutions

In this work, it was possible to compile only 45 chemical analyses of laumontite/alkali-laumontite solid solutions, all obtained from geothermal wells at varying depths and temperatures, apart from those of Sespe Hot Springs which were collected at the surface.

Most of these chemical analyses, namely 19, come from the geothermal system of Darajat, Indonesia (temperature 220–231 °C; Herdianita 2012). The other 26 laumontite data are from Reydarfjordur (N = 6; temperature not reported; Mehegan et al. 1982; Viereck et al. 1982; Exley 1982), Yellowstone, Wyoming (N = 5; temperature 120–140 °C; Bargar and Beeson 1985), Breitenbush-Austin, Oregon (N = 5; temperature 110–140 °C; Oscarson and Bargar 1996), Onikobe, Japan (N = 5; temperature 118–175 °C; Seki et al. 1969, 1983), Sespe Hot Springs (N = 3, temperature 89 °C; McCulloh et al 1981), Paratunka, Kamchatka (N = 1, temperature not given, Petrova 1970), and Krafla (N = 1, temperature not given; Kristmannsdóttir 1979).

The considered laumontite/alkali-laumontite solid solutions exhibit laumontite activity varying from 0.873 to 0.992, with mean of 0.946, median of 0.951, and standard deviation of 0.031 whereas the activity of the alkali-component ranges from 0.002 to 0.127, with average of 0.051, median of 0.048, and standard deviation of 0.032. Not surprisingly, in the diagram of Fig. 4.15b, most laumontite/alkali-laumontite solid solutions are situated near the line of equation $a_{\mathrm{Na,K\text{-}Lmt}} = 1 - a_{\mathrm{Lmt}}$.

4.7.6 The Thermodynamic Properties of Wairakite and Laumontite

The thermodynamic properties of wairakite of stoichiometry $CaAl_2Si_4O_{12} \cdot 2\ H_2O$ and laumontite of composition $CaAl_2Si_4O_{12} \cdot 4\ H_2O$ given by Helgeson et al. (1978), Holland and Powell (1998), and Holland and Powell (2011) are shown in Table 4.12.

Helgeson et al. (1978) derived the thermodynamic properties of wairakite and laumontite from the experimental data of Liou (1970, 1971a), considering the following equilibria:

$$\text{wairakite} = \text{anorthite} + 2\ \text{quartz} + 2\ H_2O \tag{4.47}$$

$$\text{laumontite} = \text{wairakite} + 2\ H_2O. \tag{4.48}$$

However, the thermodynamic properties of laumontite are inconsistent with the experimental data of Thompson (1970) for the equilibrium reaction:

$$\text{laumontite} = \text{anorthite} + 2\ \text{quartz} + 4\ H_2O, \tag{4.49}$$

as pointed out by Helgeson et al. (1978).

Holland and Powell (1998) derived the enthalpy of both zeolites from the experimental results of Thompson (1970), Liou (1970, 1971a, b), and Cho et al. (1987) and estimated the entropy of laumontite and wairakite by means of the method of Holland (1989), considering an entropy contribution of zeolitic H_2O of 6.9 cal K^{-1} mol^{-1}. The differences between the thermodynamic properties reported by Helgeson et al. (1978) and those of Holland and Powell (1998) and Holland and Powell (2011) are probably due to the use of different experimental data to retrieve these thermodynamic data. To be noted also that:

(i) The ΔH°_f values of Helgeson et al. (1978), Holland and Powell (1998), and Holland and Powell (2011) differ from the calorimetric results of Kiseleva et al. (1996) by +4147, −4209, and −2782 cal mol^{-1}, respectively, for laumontite and by +9046, −4742, and −3752 cal mol^{-1}, respectively, for wairakite.

(ii) The S° values of Helgeson et al. (1978), Holland and Powell (1998), and Holland and Powell (2011) deviate from the calorimetric outcomes of Kiseleva et al. (1996) by +0.1, −6.8, and −4.9 cal K^{-1} mol^{-1}, respectively, for laumontite and by +9.3, −6.1, and −4.9 cal K^{-1} mol^{-1}, respectively, for wairakite.

A thorough discussion on the thermodynamic properties of several zeolites, including laumontite and wairakite, is provided by Chipera and Apps (2001).

Adopting the approach delineated in Sect. 2.2.1, it is advisable to take into consideration the wairakite/analcime solid solution with average activity of wairakite, $a_{Wrk} = 0.891$, and the laumontite/alkali-laumontite solid solution with mean activity of laumontite, $a_{Lmt} = 0.946$, and to calculate the Gibbs free energy and the thermodynamic equilibrium constant of their dissolution reactions. The results calculated

Table 4.12 Standard state molal thermodynamic properties, at 25 °C, 1 bar of wairakite and laumontite from H78 = Helgeson et al. (1978), HP98 = Holland and Powell (1998), HP11 = Holland and Powell (2011), and Ki96 = Kiseleva et al. (1996)

Name	$\Delta G°_f$	$\Delta H°_f$	S°	V°	a	b ($\times 10^3$)	c ($\times 10^{-5}$)	d	References
	cal mol^{-1}	cal mol^{-1}	cal K^{-1} mol^{-1}	cm^3 mol^{-1}	cal K^{-1} mol^{-1}	cal K^{-2} mol^{-1}	cal K mol^{-1}	cal $K^{-0.5}$ mol^{-1}	
Laumontite	−1,597,043	−1,728,884	116.1	207.55	123.2	44.47	−16.43	–	H78
Laumontite	−1,603,119	−1,737,239	109.2	203.70	242.2	−5.1178	−5.344	−2104.9	HP98
Laumontite	−1,602,262	−1,735,813	111.1	203.70	242.2	−5.1178	−5.344	−2104.9	HP11
Laumontite	–	−1,733,031 ± 2032	116.0 ± 5.0	–	–	–	–	–	Ki96
Wairakite	−1,477,652	−1,579,553	105.1	186.87	100.4	44.47	−16.43	0.0	H78
Wairakite	−1,486,628	−1,593,341	89.6	190.40	200.4	−5.1291	−5.430	−1742.9	HP98
Wairakite	−1,485,994	−1,592,352	90.8	190.40	200.4	−5.1291	−5.430	−1742.9	HP11
Wairakite	–	−1,588,599 ± 1506	95.8	–	–	–	–	–	Ki96

using the wairakite and laumontite thermodynamic data of Helgeson et al. (1978) are listed in Tables 4.13 and 4.14, respectively, as a function of temperature together with the standard molal Gibbs free energies and the natural and decimal logarithms of the thermodynamic equilibrium constant of the dissolution reactions of pure wairakite:

$$CaAl_2Si_4O_{12} \cdot 2\ H_2O + 8\ H^+ = Ca^{2+} + 2\ Al^{3+} + 4\ SiO_{2(aq)} + 6\ H_2O \quad (4.50)$$

and pure laumontite:

$$CaAl_2Si_4O_{12} \cdot 4\ H_2O + 8\ H^+ = Ca^{2+} + 2\ Al^{3+} + 4\ SiO_{2(aq)} + 8\ H_2O. \quad (4.51)$$

Table 4.13 Standard molal Gibbs free energies and natural and decimal logarithms of the thermodynamic equilibrium constant of the dissolution reactions of both pure wairakite and the wairakite/analcime solid solution with average activity of wairakite as a function of temperature

T(°C)	$\Delta_r G^\circ_{Wrk}$	$\Delta_r G^\circ_{Wrk,aa}$	ln K_{Wrk}	ln $K_{Wrk,aa}$	log K_{Wrk}	log $K_{Wrk,aa}$
	cal mol^{-1}	cal mol^{-1}				
0	−24,784	−24,721	45.6591	45.5437	19.8295	19.7794
25	−22,792	−22,724	38.4684	38.3530	16.7066	16.6565
60	−18,725	−18,649	28.2839	28.1685	12.2835	12.2334
100	−13,465	−13,379	18.1585	18.0431	7.8861	7.8360
150	−6529	−6432	7.7644	7.6490	3.3720	3.3219
200	736	845	−0.7828	−0.8982	−0.3400	−0.3901
250	8512	8632	−8.1877	−8.3031	−3.5559	−3.6060
300	17,160	17,291	−15.0663	−15.1817	−6.5432	−6.5933

Table 4.14 Standard molal Gibbs free energies and natural and decimal logarithms of the thermodynamic equilibrium constant of the dissolution reactions of both pure laumontite and the laumontite/alkali−laumontite solid solution with average activity of laumontite as a function of temperature

T(°C)	$\Delta_r G^\circ_{Lmt}$	$\Delta_r G^\circ_{Lmt,aa}$	ln K_{Lmt}	ln $K_{Lmt,aa}$	log K_{Lmt}	log $K_{Lmt,aa}$
	cal mol^{-1}	cal mol^{-1}				
0	−18,222	−18,192	33.5700	33.5145	14.5793	14.5552
25	−16,777	−16,744	28.3163	28.2608	12.2976	12.2735
60	−13,520	−13,483	20.4218	20.3663	8.8691	8.8450
100	−9247	−9206	12.4702	12.4147	5.4158	5.3916
150	−3623	−3576	4.3085	4.2530	1.8712	1.8471
200	2248	2300	−2.3909	−2.4464	−1.0383	−1.0624
250	8555	8613	−8.2291	−8.2846	−3.5738	−3.5979
300	15,662	15,725	−13.7511	−13.8066	−5.9720	−5.9961

For laumontite there is a difference of 0.024 units between the log K_{Lmt} and log $K_{Lmt,aa}$ values, corresponding to differences of 30–63 cal mol^{-1} in the Gibbs free energies of the dissolution reactions. Therefore, there is not much difference in using the thermodynamic data of pure laumontite or those of the laumontite/alkali-laumontite solid solution of average laumontite activity occurring in active geothermal systems.

4.8 Garnets

Winchell (1933) divided the silicate garnets in the following two series:

- the ugrandites, comprising the endmember garnets uvarovite [$Ca_3Cr_2Si_3O_{12}$], grossular [$Ca_3Al_2Si_3O_{12}$], and andradite [$Ca_3(Fe^{3+},Ti^{4+})_2Si_3O_{12}$], as well as intermediate compounds;
- the pyralspites, including the endmember garnets pyrope [$Mg_3Al_2Si_3O_{12}$], almandine $\left[Fe_3^{2+}Al_2Si_3O_{12}\right]$, and spessartine [$Mn_3Al_2Si_3O_{12}$], and also the intermediate compositions.

According to Deer et al. (1982), there is an almost complete and continuous variation in composition within each of these two series whereas the variation between ugrandites and pyralspites is less continuous.

4.8.1 Crystal Chemistry of Garnets

Garnet solid solutions are represented by the general crystallochemical formula (Novak and Gibbs 1971):

$$X_3^{VIII}Y_2^{VI}Z_3^{IV}O_{12},$$

in which, consistent with the endmembers recognized by Winchell (1933):

- X^{VIII} refers to the eight-fold dodecahedral coordinated sites, which are occupied by the divalent cations Ca^{2+}, Mg^{2+}, Mn^{2+}, and Fe^{2+}.
- Y^{VI} indicates the six-fold octahedral coordinated sites, housing the trivalent cations Al^{3+}, Fe^{3+}, and Cr^{3+} as well as Ti^{4+}.
- Z^{IV} designates the four-fold tetrahedral coordinated sites that are mainly occupied by Si^{4+} ions and subordinately by Al^{3+}.

According to Rickwood (1968), possible endmembers garnets could be of the following three types:

- Type 1: $\left\{R_3^{2+}\right\}$ $[R_2^{3+}](R_3^{4+})O_{12}$
- Type 2: $\left\{R_3^{2+}\right\}$ $[R^{3+}R^{4+}](R^{3+}R_2^{4+})O_{12}$
- Type 3: $\left\{R_3^{2+}\right\}$ $[R_2^{4+}](R_2^{3+}R^{4+})O_{12}$.

Accepting the presence of Fe^{3+} and Ti^{4+} in the tetrahedral sites in addition to Si^{4+} and Al^{3+}, but disregarding the endmembers with more Ti^{4+} in tetrahedral sites than in octahedral sites and with more than one element of any valence state, it is possible to obtain 12 endmember garnets of type (1), none of type (2), and 8 of type (3). Rickwood (1968) proposed also a procedure to recast garnet analyses into the mole fractions of 19 endmember garnets, which were suitably chosen to accommodate also Y on the dodecahedral sites, V and Zr on the octahedral sites, and H on the tetrahedral sites.

More recently, Locock (2008) suggested an alternative method, designed to recalculate garnet analyses into the mole fractions of 29 endmember garnets, including 15 natural minerals species and 14 hypothetical components. The Locock's method is consistent with the general crystallochemical formula given above, including 8 cations and 12 anions (O or F) with no vacancies in the dodecahedral and octahedral sites.

If ferric and ferrous iron are not measured separately, their proportions are computed from the total iron concentration given as FeO, using the relation of Droop (1987), which is based on the hypotheses that iron is the only multivalent element and that there are no vacant cation sites. Both assumptions are justified for most Al-silicate garnets. Based on their general crystallochemical formula (see above), the relation of Droop (1987) can be written as follows for garnets:

$$N_{Fe^{3+}} = 24 \cdot (1 - 8/S). \tag{4.52}$$

In Eq. (4.52), S is the total number of cations initially computed assuming all iron to be Fe^{2+}. If $S < 8$, then all iron is actually present as Fe^{2+}. Alternatively, if $S > 8$, Eq. (4.52) is used to calculate $N_{Fe^{3+}}$. Then, the number of Fe^{2+} ions per formula unit, $N_{Fe^{2+}}$, is computed by subtracting $N_{Fe^{3+}}$ from the number of Fe^{2+} ions per formula unit previously computed assuming all iron to be Fe^{2+}, $N_{Fe^{2+},in}$:

$$N_{Fe^{2+}} = N_{Fe^{2+},in} - N_{Fe^{3+}}. \tag{4.53}$$

If Eq. (4.53) gives a negative result, $N_{Fe^{2+}}$ is set equal to zero.

Mn^{3+} is calculated only for compositions that cannot charge balance with Fe^{3+} alone. Only fluorine and the following oxides (expressed in weight percent) are considered: SiO_2, TiO_2, ZrO_2, SnO_2, Y_2O_3, Al_2O_3, Sc_2O_3, Cr_2O_3, V_2O_3, FeO, MnO, MgO, CaO, Na_2O, H_2O. The following oxidation states are assumed: Ti^{4+}, Sn^{4+}, Cr^{3+}, V^{3+}. To be underscored that titanium occurs exclusively at the tetravalent oxidation state in garnet, as suggested by most experimental evidence (Locock 2008).

In the Locock's method cation and anion assignments are as follows: Mn^{3+} is assigned to the octahedral site. H is assumed to occur as $(H_4O_4)_3$ in substitution for $(SiO_4)_3$. H_4 is treated as one cation. Si is assigned to the tetrahedral site, but Si in excess of 3 *apfu* is assigned to the octahedral site. The tetrahedral site is filled, first with Si and H_4 and afterwards with Al and Fe^{3+}, if necessary and possible. F substitutes for O in a coupled substitution with vacancies on the tetrahedral site. Zr, Sn and Ti are assigned exclusively to the octahedral site. Any remaining Al and Fe^{3+}

as well as Sc, V and Cr are assigned to the octahedral site. The remainder of the octahedral site is filled with Fe^{2+} and Mg, if necessary and possible. Ca, Mn^{2+}, and Na are assigned to the dodecahedral site with the remaining Fe^{2+} and Mg, if any. Proportions are based on 8 cations, including F-related tetrahedral vacancies and H_4.

The proportions of the 29 endmembers are computed by the Locock's procedure in the order given in Table 4.15.

In other terms, the proportions of the Mn^{3+} endmembers henritermierite and blythite are computed first and are followed by katoite, F-garnets, and yttrogarnet. The proportions of the remaining endmembers are calculated based on the octahedral cations, in the order: Zr, Sn, Ti, Si, Sc, V, Cr, Al, Fe^{3+}. For a given octahedral cation, endmembers are usually considered in order of increasing rarity. The rigorous assignment of cations to particular sites may lead to non-ideal subtotals for that site, e.g., if (Ca + Na) > 3, or if (Ti + Zr) > 2, or if (Si + H_4) > 3. To be noted that the chemical formula of andradite reported in Table 4.15 does not comprise Ti, in contrast with the stoichiometry of andradite adopted by other authors (e.g., Deer et al. 1982 and references therein).

The Microsoft Excel spreadsheet provided by Locock (2008) was used in this work to compute the mole fractions of endmember garnets and the mole fractions of cations on the dodecahedral, octahedral, and tetrahedral sites. Cations mole fractions were then used to calculate the activities of andradite and grossular in garnet solid solutions by means of the following relations (Bird and Norton 1981):

$$a_{\mathrm{Grs}} = \mathrm{k_{Grs}} \cdot \mathrm{X}^{3}_{\mathrm{Ca}^{2+}_{\mathrm{X}}} \cdot \mathrm{X}^{2}_{\mathrm{Al}^{3+}_{\mathrm{Y}}} \cdot \mathrm{X}^{3}_{\mathrm{Si}^{4+}_{\mathrm{Z}}} \tag{4.54}$$

$$a_{\mathrm{Adr}} = \mathrm{k_{Adr}} \cdot \mathrm{X}^{3}_{\mathrm{Ca}^{2+}_{\mathrm{X}}} \cdot \mathrm{X}^{2}_{\mathrm{Fe}^{3+}_{\mathrm{Y}}} \cdot \mathrm{X}^{3}_{\mathrm{Si}^{4+}_{\mathrm{Z}}} \tag{4.55}$$

where $k_{Grs} = k_{Adr} = 1$ are the constants relating the inter- and intra-crystalline standard states. Equations (4.54) and (4.55) are based on the hypothesis of random mixing of atoms on energetically equivalent sites (Helgeson et al. 1978; Helgeson and Aagaard 1985).

4.8.2 The Composition of Hydrothermal Garnet Solid Solutions

A total of 201 chemical analyses of garnet solid solutions collected in deep geothermal wells at different depths and temperatures were compiled. The majority of these samples, for a total of 137, come from the geothermal systems of Darajat (N = 83; measured temperature 137–235 °C; Herdianita 2012) and Reykjanes, Iceland (N = 54; measured temperature 176–321 °C; Libbey and William-Jones 2016). Of the remaining 64 chemical analyses, 21 are from Latera, Italy (measured temperatures 220–343 °C; Cavarretta et al. 1985), 9 are from Larderello, Italy (present day temperatures 175–375 °C; Cavarretta et al. 1982; Gianelli and Ruggieri 2002), 9 are from

Table 4.15 Endmembers considered in the procedure proposed by Locock (2008) to recalculate garnet analyses

Order	Endmembers	Cation site			
		Dodecahedral	Octahedral	Tetrahedral	Anion
1	Henritermierite	Ca_3	Mn_2^{3+}	$Si_2(H_4)$	O_{12}
2	*Blythite*	Mn_3^{2+}	Mn_2^{3+}	Si_3	O_{12}
3	Katoite	Ca_3	Al_2	$(H_4)_3$	O_{12}
4	*F-Ca garnet*	Ca_3	Al_2	$(\square)_3$	F_{12}
5	*F-Mn garnet*	Mn_3	Al_2	$(\square)_3$	F_{12}
6	*Yttrogarnet (YAG)*	Y_3	Al_2	Al_3	O_{12}
7	Kimzeyite	Ca_3	Zr_2	$SiAl_2$	O_{12}
8	*Kimzeyite-Fe*	Ca_3	Zr_2	$SiFe_2^{3+}$	O_{12}
9	*Tin garnet*	Ca_3	$SnFe^{2+}$	Si_3	O_{12}
10	Schorlomite	Ca_3	Ti_2	$SiFe_2^{3+}$	O_{12}
11	*Schorlomite-Al*	Ca_3	Ti_2	$SiAl_2$	O_{12}
12	Morimotoite	Ca_3	$TiFe^{2+}$	Si_3	O_{12}
13	*Na–Ti garnet*	Na_2Ca	Ti_2	Si_3	O_{12}
14	*Morimotoite-Mg*	Ca_3	TiMg	Si_3	O_{12}
15	*Morimotoite-Fe*	Fe_3^{2+}	$TiFe^{2+}$	Si_3	O_{12}
16	Majorite	Mg_3	MgSi	Si_3	O_{12}
17	*Sc-garnet*	Ca_3	Sc_2	Si_3	O_{12}
18	Goldmanite	Ca_3	V_2	Si_3	O_{12}
19	*Yamatoite*	Mn_3^{2+}	V_2	Si_3	O_{12}
20	Uvarovite	Ca_3	Cr_2	Si_3	O_{12}
21	Knorringite	Mg_3	Cr_2	Si_3	O_{12}
22	Spessartine	Mn_3^{2+}	Al_2	Si_3	O_{12}
23	Pyrope	Mg_3	Al_2	Si_3	O_{12}
24	Almandine	Fe_3^{2+}	Al_2	Si_3	O_{12}
25	Grossular	Ca_3	Al_2	Si_3	O_{12}
26	Andradite	Ca_3	Fe_2^{3+}	Si_3	O_{12}
27	Calderite	Mn_3^{2+}	Fe_2^{3+}	Si_3	O_{12}
28	*Skiagite*	Fe_3^{2+}	Fe_2^{3+}	Si_3	O_{12}
29	*Khoharite*	Mg_3	Fe_2^{3+}	Si_3	O_{12}

Mineral species names are in regular font, but hypothetical endmembers are in italics

Reydarfjordur, Iceland (inferred temperature of garnet formation 300–360 °C; Exley 1982; Mehegan et al. 1982), 8 are from Los Humeros, Mexico (measured temperatures of 300–325 °C; Martinez Serrano 2002), 6 are from Sabatini, Italy (measured temperatures 165–290 °C; Cavarretta and Tecce 1987), 5 are from Kilauea, Hawaii (present-day temperature 322 °C; Bargar et al. 1996), 4 are from Miravalles, Costa Rica, (measured temperature 255 °C; Milodowski et al. 1989), and 1 each are from Cerro Prieto, Mexico (present-day temperature 325 °C; Schiffman et al. 1985) and Mofete, Italy (measured temperature 324 °C; Balducci and Chelini 1992).

The sum of the mole fractions of endmember garnets calculated adopting the Locock's method and using the Microsoft Excel spreadsheet provided by Locock (2008) is higher than 0.9 in 192 cases, between 0.87 and 0.90 in 5 cases (2 from Reydarfjordur and 1 each from Reykjanes, Los Humeros, and Darajat), close to 0.81 in 2 cases (1 from Reykjanes and 1 from Darajat) and 0.53–0.58 in 2 cases from Darajat. These few samples with values of the sum of the mole fractions of endmember garnets significantly lower than 1 and correspondingly very high remainders might be affected by analytical problems but were not rejected to avoid loss of information.

Andradite and grossular are the most frequent and important endmembers of the considered hydrothermal garnets, with 195 and 139 concentrations $\neq 0$, varying from 0.02 to 99.39 mol% and from 0.07 to 81.59 mol%, respectively. Pyrope and spessartine are also common endmembers but less important, with 105 and 94 contents $\neq 0$, ranging from 0.04 to 13.92 mol% and from 0.03 to 10.80 mol%, respectively. Almandine is not so common, with 37 concentrations $\neq 0$, but varying from 0.01 to 84.69 mol%. The highest almandine concentrations (58.05–84.69 mol%) are found in eight garnets from Larderello rocks affected by contact metamorphism (Gianelli and Ruggieri 2002). Titanium is mainly accommodated in schorlomite-Al and morimotoite, with 77 and 49 contents $\neq 0$, ranging from 0.01 to 7.76 mol% and from 0.02 to 9.98 mol%, respectively, and subordinately in morimotoite-Mg and Na–Ti garnet, with 28 and 24 contents $\neq 0$, ranging from 0.06 to 5.00 mol% and from 0.02 to 1.83 mol%, respectively.

Moreover, the sum of the andradite and grossular mole fractions is relatively close to unity in most of the considered hydrothermal garnets. In fact, they are situated close to the dashed line corresponding to the equation $X_{Adr} = 1 - X_{Grs}$ in the binary diagram of Fig. 4.16a. The only exceptions are the eight almandine-rich garnets from Larderello (see above), which are situated relatively close to the origin in the binary diagram of Fig. 4.16a, having small contents of grossular and especially andradite. Authors of previous studies (e.g., Cavarretta et al. 1982, 1985; Exley 1982; Mehegan et al. 1982; Bird et al. 1984; McDowell and Elders 1983; Schiffman et al. 1985; Cavarretta and Tecce 1987; Milodowski et al. 1989; Balducci and Chelini 1992; Gianelli et al. 1998; Martinez-Serrano 2002; Marks et al. 2010; Herdianita 2012; Libbey and Williams-Jones 2016) already recognized the prevalence of andradite and grossular in most hydrothermal garnets from active geothermal systems, which are therefore called grandites.

Moreover, disregarding the eight almandine-rich garnets from Larderello, andradite prevails over grossular in 145 grandites, i.e., 75% of the 193 cases, whereas

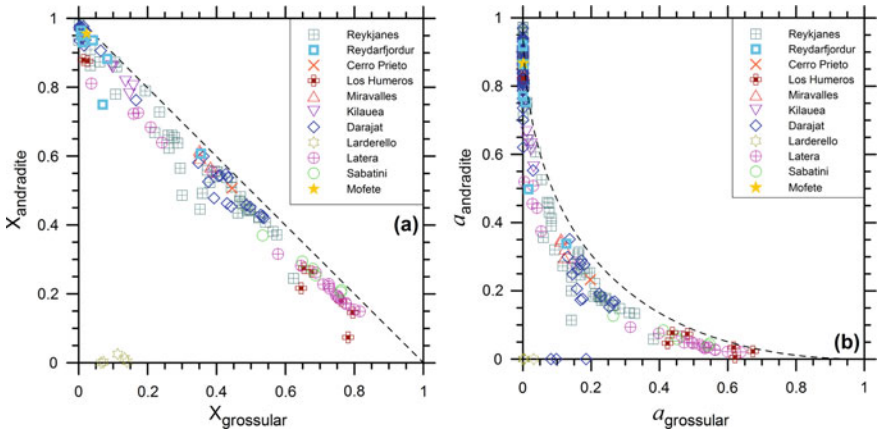

Fig. 4.16 Correlation diagrams between **a** the mole fractions of grossular and andradite and **b** the activities of grossular and andradite for the 173 garnet solid solutions coming from different geothermal systems (see legend). The dashed lines refer to the equations $X_{Adr} = 1 - X_{Grs}$ in **a** and $a_{Adr} = 1 + a_{Grs} - 2 \cdot \sqrt{a_{Grs}}$ in **b**

grossular dominates over andradite in the other 48 grandites, i.e., 25% of the 193 cases (Fig. 4.16a). Of these 48 grossular-rich garnets, 15 are from Latera, 13 are from Reykjanes, 8 are from Darajat, and 6 each are from Sabatini and Los Humeros. It should be noted that garnets are often zoned and exhibit wide intra-crystal compositional variations, with grossular-rich core and andradite-rich rim in some cases, and vice versa in other samples, that were attributed to changes in fluid chemistry in some previous studies. Contact metamorphism and metasomatic processes were also invoked to explain garnet compositions.

4.8.3 The Activity of Grossular and Andradite in the Hydrothermal Garnet Solid Solutions

Excluding the eight almandine-rich garnets from Larderello and the three samples from Darajat with very high remainders, the other 190 garnet solid solutions have andradite activity varying from 0.00539 to 0.972, with mean of 0.541, median of 0.625, and standard deviation of 0.340, whereas grossular activity ranges from $<2.27 \times 10^{-7}$ (in 22 cases) to 0.674, with average of 0.127, median of 0.0142, and standard deviation of 0.179.

The correlation plot of Fig. 4.16b shows that andradite and grossular activities of most garnets approximate the relation $a_{Adr} = 1 + a_{Grs} - 2 \cdot \sqrt{a_{Grs}}$ (dashed line), apart from the eight almandine-rich garnets from Larderello and the three samples from Darajat with very high remainders (see above).

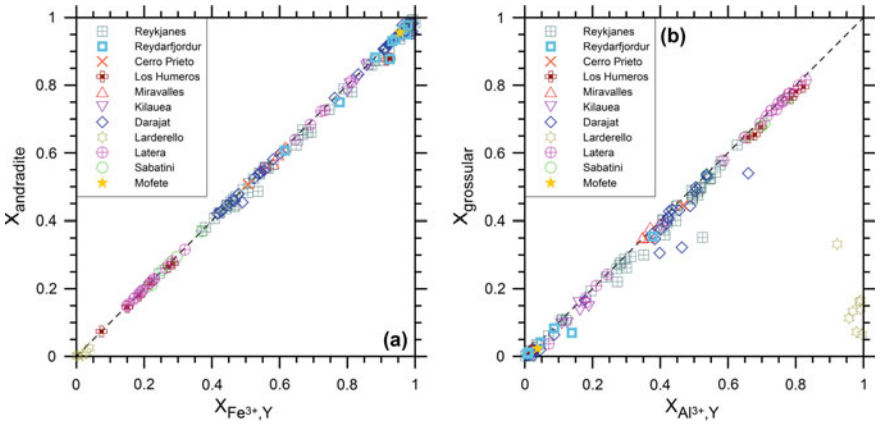

Fig. 4.17 Correlation diagrams between **a** the mole fraction of andradite and the mole fraction of trivalent iron on the octahedral sites and **b** the mole fraction of grossular and the mole fraction of aluminum on the octahedral sites for the 173 garnet solid solutions coming from different geothermal systems (see legend). The dashed lines refer to the equations $X_{Adr} = X_{Fe_Y^{3+}}$ in **a** and $X_{Grs} = X_{Al_Y^{3+}}$ in **b**

This relationships is obtained considering that $X_{Adr} \approx X_{Fe_Y^{3+}}$ and $X_{Grs} \approx X_{Al_Y^{3+}}$, which are reasonable approximations in most cases, as indicated by Fig. 4.17a, b, respectively. Consequently, Eqs. (4.54) and (4.55) simplify to $a_{Grs} \approx X^2_{Al_Y^{3+}} \approx X^2_{Grs}$ and $a_{Adr} \approx X^2_{Fe_Y^{3+}} \approx X^2_{Adr}$, respectively. Considering that $X_{Adr} \approx 1 - X_{Grs}$ (see above), it is a simple matter to obtain, by substitution and rearrangement, the relation written above linking andradite and grossular activities.

4.8.4 The Thermodynamic Properties of Grossular and Andradite

Helgeson et al. (1978) report the thermodynamic properties of grossular and andradite only, whereas almandine, pyrope, and spessartine are also included in the dataset of Holland and Powell (1998), and almandine, knorringite, majorite, pyrope, and spessartine are also comprised in the database of Holland and Powell (2011). The standard state molal thermodynamic properties, at 25 °C, 1 bar of grossular $[Ca_3Al_2Si_3O_{12}]$ and andradite $\left[Ca_3Fe_2^{3+}Si_3O_{12}\right]$ listed in these three compilations are shown in Table 4.16.

For grossular, the $\Delta G°_f$ and $\Delta H°_f$ of Holland and Powell (1998) differ from those of Helgeson et al. (1978) by 4214 and 4574 cal mol^{-1}, respectively, whereas the $\Delta G°_f$ and $\Delta H°_f$ listed by Holland and Powell (2011) differ from those of Helgeson et al. (1978) by 3946 and 4306 cal mol^{-1}, respectively.

Table 4.16 Standard state molal thermodynamic properties, at 25 °C, 1 bar of grossular and andradite from H78 = Helgeson et al. (1978), HP98 = Holland and Powell (1998), and HP11 = Holland and Powell (2011)

Name	$\Delta G°_f$	$\Delta H°_f$	S°	V°	a	b ($\times 10^3$)	c ($\times 10^{-5}$)	d	References
	cal mol^{-1}	cal mol^{-1}	cal K^{-1} mol^{-1}	cm^3 mol^{-1}	cal K^{-1} mol^{-1}	cal K^{-2} mol^{-1}	cal K mol^{-1}	cal $K^{-0.5}$ mol^{-1}	
Grossular	−1,496,967	−1,583,397	60.87	125.30	104.017	17.013	−27.318		H78
Grossular	−1,501,181	−1,587,971	60.95	125.35	149.62	0	−13.813	−956.7	HP98
Grossular	−1,500,913	−1,587,703	60.95	125.35	149.62	0	−13.813	−956.7	HP11
Andradite	−1,297,479	−1,381,005	70.13	131.85	113.532	15.636	−30.889		H78
Andradite	−1,296,446	−1,378,607	76.00	132.04	152.63	0	−11.843	−953.4	HP98
Andradite	−1,296,569	−1,378,843	75.62	132.04	152.63	0	−11.843	−953.4	HP11

For andradite, the $\Delta G°_f$ and $\Delta H°_f$ of Holland and Powell (1998) differ from those of Helgeson et al. (1978) by 1033 and 2398 cal mol^{-1}, respectively, whereas the $\Delta G°_f$ and $\Delta H°_f$ listed by Holland and Powell (2011) differ from those of Helgeson et al. (1978) by 910 and 2162 cal mol^{-1}, respectively.

More recently, Dachs and Geiger (2019) investigated the thermodynamics of three grossular-rich natural solid solutions and three synthetic andradite-grossular solid solutions of composition $Ca_3\left(Al_{0.5}Fe^{3+}_{1.5}\right)Si_3O_{12}$, $Ca_3\left(AlFe^{3+}\right)Si_3O_{12}$, and $Ca_3\left(Al_{1.5}Fe^{3+}_{0.5}\right)Si_3O_{12}$. Using the S° calorimetric value of 325.0 ± 2.0 J K^{-1} mol^{-1} (corresponding to 77.68 ± 0.48 cal K^{-1} mol^{-1}) for andradite (Geiger et al. 2018) and published phase-equilibrium results on three andradite-bearing reactions, they obtained the value of −5763.3 ± 1.5 kJ mol^{-1} (corresponding to −1377.462 ± 0.359 kcal mol^{-1}) for the standard enthalpy of formation of andradite. This $\Delta H°_f$ value is lower than those of Helgeson et al. (1978), Holland and Powell (1998), and Holland and Powell (2011) by 3543, 1145, and 1381 cal mol^{-1}, respectively.

Following the approach outlined in Sect. 2.2.1, it is advisable to consider the grossular/andradite solid solution with average activity of grossular, $a_{Grs} = 0.127$, and to calculate the Gibbs free energy and the thermodynamic equilibrium constant of its dissolution reaction. The results obtained considering the grossular thermodynamic data of Helgeson et al. (1978) are listed in Table 4.17 as a function of temperature together with the standard molal Gibbs free energies and the natural and decimal logarithms of the thermodynamic equilibrium constant of the dissolution reaction of pure grossular:

$$Ca_3Al_2Si_3O_{12} + 12\ H^+ = 2\ Al^{3+} + 3\ Ca^{2+} + 3\ SiO_{2(aq)} + 6\ H_2O. \qquad (4.56)$$

Table 4.17 Standard molal Gibbs free energies and natural and decimal logarithms of the thermodynamic equilibrium constant of the dissolution reactions of both pure grossular and the grossular/andradite solid solution with average activity of grossular as a function of temperature

T(°C)	$\Delta_r G°_{Grs}$	$\Delta_r G°_{Grs,aa}$	ln K_{Grs}	ln $K_{Grs,aa}$	log K_{Grs}	log $K_{Grs,aa}$
	cal mol^{-1}	cal mol^{-1}				
0	−73,115	−71,995	134.6984	132.6348	58.4988	57.6026
25	−70,836	−69,613	119.5573	117.4938	51.9231	51.0269
60	−66,627	−65,261	100.6393	98.5757	43.7071	42.8109
100	−61,295	−59,765	82.6606	80.5970	35.8990	35.0029
150	−54,197	−52,462	64.4522	62.3887	27.9912	27.0950
200	−46,554	−44,614	49.5125	47.4490	21.5030	20.6068
250	−38,059	−35,914	36.6090	34.5455	15.8991	15.0029
300	−28,211	−25,861	24.7689	22.7054	10.7570	9.8608

4.9 Calcite

Anhydrous calcium carbonate occurs as three distinct polymorphs, i.e., calcite, aragonite, and vaterite, whose crystals have trigonal, orthorhombic, and hexagonal symmetry, respectively. Calcite is the thermodynamically stable polymorph at low pressures, aragonite is stable at high pressures (e.g., >3 kbar at 0 °C and >4.4 kbar at 100 °C; Crawford and Hoersch 1972 and references therein), whereas vaterite is unstable and is quickly converted into aragonite or calcite through dissolution and growth (Ogino et al. 1987).

Aragonite is a member of the isomorphous group of orthorhombic carbonates comprising strontianite [$SrCO_3$], witherite [$BaCO_3$], and cerussite [$PbCO_3$], in which Ca^{2+}, Sr^{2+}, Ba^{2+}, and Pb^{2+} have nine-fold coordination. Orthorhombic $BaCO_3$ and $SrCO_3$ invert to the trigonal calcite-type structure at temperatures of 806 and 912 °C, respectively, which are much higher than the range of geothermal interest (Chang 1965).

Calcite belongs to the isomorphous group of trigonal carbonates including magnesite [$MgCO_3$], siderite [$FeCO_3$], rhodochrosite [$MnCO_3$], smithsonite [$ZnCO_3$], sphaerocobaltite [$CoCO_3$], gaspeite [$NiCO_3$], and otavite [$CdCO_3$]. As required by the electroneutrality condition, these trigonal carbonates host divalent cations, the largest of which is Ca^{2+}, whose size represents the uppermost value for six-fold octahedral coordination (Reeder 1990). Complete miscibility occurs between calcite and otavite, whereas limited miscibility occurs between calcite and the trigonal carbonates of Mg, Fe, Mn, Co, and Ni. Nevertheless, significant amounts of Mg, Fe, Mn, Zn, Co, Ni, and Cd are likely to be scavenged from the aqueous solution by calcite precipitation (e.g., McIntire 1963; Marini et al. 2001). Similar considerations hold true for Sr, Ba, and Pb although their carbonates are expected to mix with aragonite instead of calcite.

4.9.1 The Composition of Calcite-Rich Trigonal Carbonates from Active Geothermal Systems

A total of 313 chemical analyses of solid solutions of calcite-rich trigonal carbonates sampled from deep geothermal wells at different depths and temperatures were compiled in this work. The weight percentages of relevant oxides (CaO, MgO, MnO, FeO, ZnO, SrO, BaO, and PbO) were converted into the corresponding moles and their sum was computed. A number of moles of CO_2 equal to the sum of the moles of the relevant oxides was assumed to be present in the mineral and the corresponding CO_2 weight percentage was computed accordingly. The chemical analyses with sum of weight percentages, including CO_2, between 92 and 104% were accepted, whereas the few analyses with sum of oxides <92 wt% were rejected.

Most of the accepted chemical analyses of calcite-rich trigonal carbonates, namely 251, are representative of the two geothermal systems of Darajat, Indonesia (N =

175, temperature 110–300 °C; Herdianita 2012) and Reykjanes, Iceland (N = 76; temperature 19–289 °C; Libbey and Williams-Jones 2016). Of the other 62 chemical analyses, 25 are from Milos, Greece (temperature 190 °C; Liakopoulos 1987), 16 are from Onikobe, Japan (temperature 110–225 °C; Seki et al. 1983), 10 are from Broadlands, New Zealand (temperature 230–290 °C; Lonker et al. 1990), 5 are from Cerro Prieto, Mexico (temperature 185–335 °C; Schiffman et al. 1985), 4 are from Pantelleria, Italy (temperature 85–120 °C; Fulignati et al. 1997), and 2 are from Newberry Caldera, Oregon (temperature 35–130 °C; Keith and Bargar 1988). The main statistical parameters for the mole fractions of calcite, magnesite, siderite, rhodochrosite, $SrCO_3$, $BaCO_3$, smithsonite, and $PbCO_3$ in the considered solid solutions of calcite-rich trigonal carbonates are listed in Table 4.18.

As expected, calcite is by far the main component of the solid solutions of interest, with mole fractions ranging between 0.705 and 1.000, average of 0.972, median of 0.988, and standard deviation of 0.043. Based on the average values, the second major component is rhodochrosite, with mole fractions ranging between 0.0000570 and 0.130, average of 0.0139, median of 0.00522, and standard deviation of 0.0214, and is followed by magnesite, siderite, $SrCO_3$, $PbCO_3$, smithsonite, and $BaCO_3$, in order of decreasing importance. To be noted that the number of available data, N, decreases in the following order: $CaCO_3 > MgCO_3 > MnCO_3 > FeCO_3 > SrCO_3 > PbCO_3 > BaCO_3 > ZnCO_3$.

4.9.2 The Carbonate Minerals Other Than Calcite from Active Geothermal Systems

Calcite is not the only carbonate mineral present in active geothermal systems. Although calcite is a common and important mineral at Ohaaki-Broadlands, occurring in all boreholes, siderite is also present (Browne and Ellis 1970). Siderite is uncommon, but it occurs in quantities of up to 10% in some Broadlands wells, at temperatures between 37 and 130 °C. At Salton Sea, siderite occurs at weakly higher temperatures, close to 135 °C, but it is absent at the depths/temperatures where base metal sulfides are found (Muffler and White 1969). At Wairakei, siderite is reported to be present at depth of only 27 m and low temperatures (Steiner 1953). At Newberry, siderite is abundant and is locally associated with magnesite and solid solutions of ankerite [$CaFe(CO_3)_2$] and dolomite [$CaMg(CO_3)_2$] at depths of 320 to 697 m, where measured temperature varies from 35 to 100 °C. It was probably precipitated after the emplacement of a sill, during a thermal event that caused alteration of Fe-sulfides (Keith and Bargar 1988). Both siderite and ankerite occur also at Darajat, where calcite is the most common hydrothermal mineral (Herdianita 2012).

Table 4.18 Main statistical parameters for the mole fractions of calcite, magnesite, siderite, rhodochrosite, $SrCO_3$, $BaCO_3$, smithsonite, and $PbCO_3$ in the solid solutions of calcite−rich trigonal carbonates from different active geothermal systems

	X $CaCO_3$	X $MgCO_3$	X $FeCO_3$	X $MnCO_3$	X $SrCO_3$	X $BaCO_3$	X $ZnCO_3$	X $PbCO_3$
N	313	292	252	279	68	34	12	57
Minimum	0.705	5.01E−05	1.42E−05	5.70E−05	9.93E−06	6.66E−06	2.39E−04	4.57E−06
Maximum	1.000	0.102	0.109	0.130	1.15E−02	9.90E−03	1.23E−03	1.21E−02
Mean	0.972	9.82E−03	7.86E−03	1.39E−02	1.60E−03	4.31E−04	7.50E−04	9.49E−04
Median	0.988	3.11E−03	2.97E−03	5.22E−03	9.20E−04	2.05E−04	7.23E−04	1.25E−04
Std. Dev.	0.043	1.69E−02	1.41E−02	2.14E−02	2.28E−03	1.30E−03	3.22E−04	2.50E−03

4.9.3 The Thermodynamic Properties of Calcite

Helgeson et al. (1978), Holland and Powell (1998), and Holland and Powell (2011) report the thermodynamic properties of calcite and aragonite of chemical formula $CaCO_3$ (Table 4.19). For calcite, the $\Delta G°_f$ and $\Delta H°_f$ of Holland and Powell (1998) differ from those of Helgeson et al. (1978) by 308 and 163 cal mol^{-1}, respectively, whereas the $\Delta G°_f$ and $\Delta H°_f$ listed by Holland and Powell (2011) differ from those of Helgeson et al. (1978) by 227 and 82 cal mol^{-1}, respectively.

For aragonite, the $\Delta G°_f$ and $\Delta H°_f$ of Holland and Powell (1998) differ from those of Helgeson et al. (1978) by 269 and 88 cal mol^{-1}, respectively, whereas the $\Delta G°_f$ and $\Delta H°_f$ listed by Holland and Powell (2011) differ from those of Helgeson et al. (1978) by 207 and 47 cal mol^{-1}, respectively.

These differences are much smaller than those generally observed for Al-silicates. Nevertheless, they determine some differences in the Gibbs free energy of calcite-aragonite conversion. For instance, this $\Delta G°_r$ value, at 25°C, 1 bar, is 225 cal mol^{-1} based on the data of Helgeson et al. (1978), 186 cal mol^{-1} according to Holland and Powell (1998), and 205 cal mol^{-1} based on the data of Holland and Powell (2011).

Since calcite generally occurs as a virtually pure phase (see Sect. 4.9.1), its activity can be assumed to be equal to one. Therefore, there is no need to correct the Gibbs free energy and the thermodynamic equilibrium constant of its dissolution reaction.

4.10 Quartz and Other Silica Minerals

The main crystalline polymorphs of silica stable at low pressures are quartz, cristobalite, and tridymite. Quartz and chalcedony (i.e., microcrystalline quartz with submicroscopic pores) are the most common hydrothermal minerals in most geothermal fields, if not all, and distribute in a wide temperature range, from 120 to 350 °C according to Henley and Ellis (1983). Above ~180 °C, aqueous solutions are saturated with respect to quartz, whereas at lower temperatures, silica activity is controlled by chalcedony solubility (e.g., Arnórsson et al. 1983a; Fournier 1991). Cristobalite and tridymite also occur as hydrothermal minerals, especially at relatively low temperatures, but are by far less common than quartz and chalcedony.

The crystal structure of all these silica polymorphs consists of a three-dimensional framework of SiO_4 tetraedra, which are linked together by sharing the corners with other tetraedra. In these lattices, therefore, each oxygen atom has two silicon atoms as nearest neighbors and each silicon atom is surrounded by four oxygen atoms (Deer et al. 2004). In spite of these similarities, each silica polymorph has its own crystal structure: α-quartz and β-quartz crystals have trigonal and hexagonal symmetry, respectively; α-cristobalite and β-cristobalite crystals have tetragonal and cubic symmetry, respectively, whereas tridymite occurs in seven distinct crystalline forms indicated by the symbols HP, LHP, OC, OS, OP, MC, and MX-1 (Pryde and Dove 1998).

Table 4.19 Standard state molal thermodynamic properties, at 25°C, 1 bar of calcite and aragonite from H78 = Helgeson et al. (1978), HP98 = Holland and Powell (1998), and HP11 = Holland and Powell (2011)

Name	$\Delta G°_f$	$\Delta H°_f$	S°	V°	a	b ($\times 10^3$)	c ($\times 10^{-5}$)	d	References
	cal mol^{-1}	cal mol^{-1}	cal K^{-1} mol^{-1}	cm^3 mol^{-1}	cal K^{-1} mol^{-1}	cal K^{-2} mol^{-1}	cal K mol^{-1}	cal $K^{-0.5}$ mol^{-1}	
Calcite	−270100	−288772	22.15	36.934	24.98	5.24	−6.2	–	H78
Calcite	−269792	−288609	22.11	36.890	33.68	1.202	−2.272	−205.2	HP98
Calcite	−269873	−288690	22.11	36.890	33.68	1.202	−2.272	−205.2	HP11
Aragonite	−269875	−288723	21.56	34.150	20.13	10.24	−3.340	–	H78
Aragonite	−269606	−288635	21.39	34.150	45.96	−0.729	2.748	−506.3	HP98
Aragonite	−269668	−288676	21.46	34.150	45.96	−0.729	2.748	−506.3	HP11

4.10.1 The Activity of Endmember Quartz in Hydrothermal Quartz

A total of 209 chemical analyses of quartz were compiled in this work. All these analyses are representative of quartz samples collected in the deep wells of the Reykjanes geothermal field, Iceland at different depths, from 150 to 2846 m, and temperatures, from 19 to 342 °C (Libbey and Williams-Jones 2016).

As expected, SiO_2 is by far the main component of these quartz samples, with mole fractions varying between 0.967 and 0.999, average of 0.993, median of 0.994, and standard deviation of 0.005. These statistical parameters indicate that hydrothermal quartz is a pure phase and its activity can be assumed to be equal to one. Strictly speaking this finding concerns the Reykjanes geothermal system only, but it may be considered a general conclusion, in spite of the lack of data for hydrothermal quartz from other geothermal systems.

4.10.2 The Thermodynamic Properties of the Quartz/Chalcedony Mechanical Mixture

Helgeson et al. (1978) report the thermodynamic properties of α- and β-quartz, α- and β-cristobalite, chalcedony, amorphous silica, and coesite. The latter mineral is disregarded in Table 4.20 being stable at very high pressures, outside the range of interest of geothermal systems. Holland and Powell (1998) and Holland and Powell (2011) report instead the thermodynamic properties of quartz, cristobalite, and tridymite (Table 4.20).

For quartz, the $\Delta G°_f$ and $\Delta H°_f$ of Holland and Powell (1998) differ from those of Helgeson et al. (1978) by 53 and 56 cal mol^{-1}, respectively, whereas the $\Delta G°_f$ and $\Delta H°_f$ listed by Holland and Powell (2011) are closer to those of Helgeson et al. (1978), with differences of 5 and 13 cal mol^{-1}, respectively. The opposite is true for cristobalite. In fact, the $\Delta G°_f$ and $\Delta H°_f$ of Holland and Powell (1998) deviate from those of Helgeson et al. (1978) by 6 and 206 cal mol^{-1}, respectively, whereas the $\Delta G°_f$ and $\Delta H°_f$ reported by Holland and Powell (2011) exhibit larger deviations from those of Helgeson et al. (1978), 114 and 636 cal mol^{-1}, respectively.

The methodological approach of Helgeson et al. (1978) for treating quartz is different from that adopted by Holland and Powell (1998) and Holland and Powell (2011). In fact, Helgeson et al. (1978) report the thermodynamic properties of α-quartz at 25 °C, 1 bar, the enthalpy, entropy, and volume of the α-β quartz transition at 575 °C, 1 bar (which are listed in the column $\Delta H°_f$, S°, and V° in Table 4.20 to avoid inserting three more columns), and the heat capacity coefficients of β-quartz. These are the data stored in SUPCRT92, which are used to compute the thermodynamic properties of quartz up to 2000 K. The same applies to other minerals that undergo phase transitions, such as high-albite, 7Å-clinochlore, and prehnite, among those of interest to us.

Table 4.20 Standard state molal thermodynamic properties, at 25 °C, 1 bar of silica polymorphs from H78 = Helgeson et al. (1978), HP98 = Holland and Powell (1998), and HP11 = Holland and Powell (2011)

Name	$\Delta G°_f$	$\Delta H°_f$	S°	V°	a	b ($\times 10^3$)	c ($\times 10^{-5}$)	d	References
	cal mol^{-1}	cal mol^{-1}	cal K^{-1} mol^{-1}	cm^3 mol^{-1}	cal K^{-1} mol^{-1}	cal K^{-2} mol^{-1}	cal K mol^{-1}	cal $K^{-0.5}$ mol^{-1}	
α-Quartz	−204,646	−217,650	9.88	22.688	11.22	8.20	−2.70	–	H78
Transition	–	290	0.342	0.372	–	–	–	–	H78
β-Quartz	–	–	–	–	14.41	1.94	0.00	–	H78
Chalcedony	−204,276	−217,282	9.88	22.688	11.22	8.20	−2.70	–	H78
α-Cristobalite	−203,895	−216,755	10.372	25.74	13.98	3.34	−3.81	–	H78
β-Cristobalite	−203,290	−215,675	11.963	27.38	17.39	0.31	−9.89	–	H78
Am. Silica	−202,892	−214,568	14.34	29.00	5.93	47.2	−22.78	–	H78
Quartz	−204,699	−217,706	9.92	22.690	26.46	−1.240	0.000	−269.7	HP98
Quartz	−204,651	−217,663	9.90	22.690	22.20	−0.153	−1.709	−171.2	HP11
Cristobalite	−203,901	−216,549	11.11	26.100	23.40	−0.801	−1.521	−185.0	HP98
Cristobalite	−203,781	−216,119	12.16	27.450	17.38	0.312	−9.869	0.0	HP11
Tridymite	−204,037	−216,714	11.02	27.000	23.40	−0.801	−1.521	−185.0	HP98
Tridymite	−203,978	−216,797	10.54	28.000	17.90	0.741	−2.806	−56.6	HP11

In contrast, quartz is treated adopting a pressure-dependent Landau tricritical model by Holland and Powell (1998) and Holland and Powell (2011). In this way, there is no need to give separate thermodynamic data for α- and β-quartz. However, it is necessary to consider the pressure-dependent critical temperature and the excess volume, entropies, and energies. The properties given in the Holland and Powell data sets are the Landau critical temperature at 1 bar, $T_c^\circ = 847$ K (i.e., the α-β quartz transition within 1 K); the thermal expansion parameter $a^\circ = 0.65\ K^{-1}\ mol^{-1}$; the bulk modulus at 298 K, $\kappa_{298} = 750$ kbar mol^{-1}; the maximum entropy of disorder, $S_{max} = 4.95\ J\ K^{-1}\ mol^{-1}$ (=1.183 cal $K^{-1}\ mol^{-1}$); and the maximum volume of disorder $V_{max} = 0.1188\ J\ bar^{-1}\ mol^{-1}$ (=1.188 $cm^3\ mol^{-1}$). The approach of Holland and Powell allows calculation of mineral-fluids equilibria up to a pressure of at least 100 kbar, a value exceeding the maximum pressures present in geothermal systems by about three orders of magnitude.

Unlike quartz, α- and β-cristobalite are treated by Helgeson et al. (1978) as two distinct minerals. This different approach was probably adopted because the transition temperature of cristobalite is poorly defined.

The thermodynamic data of chalcedony, cristobalite, and amorphous silica reported by Helgeson et al. (1978) are consistent with those of quartz and were retrieved from solubility measurements at high temperatures by Walther and Helgeson (1977) in their study on the thermodynamic properties of aqueous silica as a function of temperature and pressure.

As shown in Sect. 5.2.2, the solubilities of quartz and chalcedony, at saturation temperatures and pressures, computed using the thermodynamic data of quartz and chalcedony from Helgeson et al. (1978) and those of aqueous SiO_2 from Shock et al. (1989), bracket the functions describing quartz solubilities according to different studies. Therefore, a mechanical mixture constituted by 50% chalcedony and 50% quartz was added to the SUPCRT92 database. At 25 °C, 1 bar, α-quartz and chalcedony have the same entropy, volume, and heat capacity coefficients, whereas the ΔG°_f and ΔH°_f values differ by 370 and 368 cal mol^{-1}, respectively, due to the distinct grain size of these two silica minerals. Therefore, the quartz/chalcedony mechanical mixture has the same entropy, volume, and heat capacity coefficients of the two endmember minerals, whereas its Gibbs free energy and enthalpy are different, with $\Delta G^\circ_f = -204{,}461$ cal mol^{-1} and $\Delta H^\circ_f = -217{,}466$ cal mol^{-1}.

Interpolation of the undissociated SiO_2 concentration data fixed by the quartz/chalcedony mechanical mixture leads to the following polynomial equation (c_{SiO_2} in mg/kg):

$$T(^\circ C) = 2.7195E-12 \cdot c_{SiO_2}^5 - 6.6268E-9 \cdot c_{SiO_2}^4 + 6.4341E-6 \cdot c_{SiO_2}^3 - 3.2559E-3 \cdot c_{SiO_2}^2 + 1.1233 \cdot c_{SiO_2} + 39.790 \quad (4.57)$$

which is valid from 100 to 350 °C, at water saturation pressures, and reproduces the equilibrium temperatures within 0.5 °C below 325 °C and within 5.5 °C above 325 °C.

4.11 Conclusive Considerations on Hydrothermal Minerals

Over 2200 chemical analyses of hydrothermal minerals collected at depth in different active geothermal systems were compiled, processed, and discussed in the previous sections of this chapter. In agreement with the outcomes of previous studies, it turned out that hydrothermal quartz, calcite, adularia, albite, anorthite, and laumontite are virtually pure solid phases and their activities can be assumed to be equal to one. In contrast, the other hydrothermal minerals of interest, i.e., white mica, chlorite, epidote, prehnite, wairakite, and garnet, are solid solutions of variable composition. Therefore, the activities of pertinent endmembers were computed, under the assumption of random mixing of atoms on energetically equivalent sites, obtaining the following results:

(i) In the considered 75 hydrothermal white mica solid solutions, muscovite activity varies from 0.007 to 0.875, but it is higher than 0.40 in most cases. Accordingly, average muscovite activity is 0.654, the median value is 0.688 and the standard deviation is relatively small, 0.156.

(ii) The selected 181 hydrothermal chlorites have highly different $Fe^{2+}/(Fe^{2+} + Mg)$ ratio, from 0.23 to 0.94, with compositions varying from Mg-rich values, relatively similar to clinochlore or sheridanite, to Fe^{2+}-rich values, close to ripidolite. The activity of the clinochlore endmember spans a very wide interval, from 4.39×10^{-7} to 0.250, with an average of 0.0553, a median of 0.0451 and a relatively large standard deviation of 0.0484.

(iii) Clinozoisite is the main component of the 436 hydrothermal epidote solid solutions of interest. Its activity varies from 0.523 to 0.888, with a mean of 0.703, a median of 0.706, and a small standard deviation of 0.057. According to the equilibrium model of Bird and Helgeson (1980), these hydrothermal epidote samples appear to be relatively ordered, but deviations from the equilibrium distribution are possible, due to occurrence of metastable states of substitutional order/disorder on the octahedral sites.

(iv) Prehnite prevails in most of the 127 selected prehnite/ferri-prehnite solid solutions. Its activity ranges from 0.373 to 0.998, with average of 0.763, median of 0.779, and a relatively small standard deviation of 0.154.

(v) Wairakite is the main endmember component of the 136 wairakite/analcime solid solutions under consideration. Its activity varies from 0.573 to 0.999, with mean of 0.891, median of 0.920, and a comparatively small standard deviation of 0.090.

(vi) The sum of the andradite and grossular mole fractions is relatively close to unity in most of the considered 201 hydrothermal garnets, which can be classified as grandites, apart from eight almandine-rich garnets from Larderello. Grossular is the main component in 25% of the cases only. Its activity ranges from $<2.27 \times 10^{-7}$ (in 22 cases) to 0.674, with average of 0.127, median of 0.0142, and relatively large standard deviation of 0.179.

The solid solutions with average activity of muscovite, 7Å-clinochlore, clinozoisite, prehnite, wairakite, and grossular were considered as points of reference.

The ΔG°_f and the log K of their dissolution reactions were computed and compared with the ΔG°_f and the log K of the dissolution reactions of the corresponding pure minerals.

The dilution of the endmember component of interest in a given solid phase increases its stability with respect to that of the pure mineral. An overall view of this effect is provided by the diagram of CO_2 fugacity versus temperature for the system SiO_2–Al_2O_3–CaO–H_2O–CO_2 (Fig. 4.18, modified from Giggenbach 1997), which was constructed assuming saturation with calcite and quartz/chalcedony at any f_{CO_2} and temperature.

In this diagram, the red lines depict the stability fields of the pure hydrothermal minerals, but the blue lines describe the stability fields of the garnet, epidote, wairakite/analcime and prehnite/ferri-prehnite solid solutions with average activities of the relevant endmembers, that is grossular, clinozoisite, wairakite, and prehnite, respectively. Both grids were prepared assuming that laumontite, kaolinite and pyrophyllite are pure phases. The comparison of the two grids shows what follows:

(i) The stability field of the garnet solid solution expands considerably with respect to that of pure grossular, at the expense of the stability field of prehnite. This significant effect is due to the substantial difference between the average activity

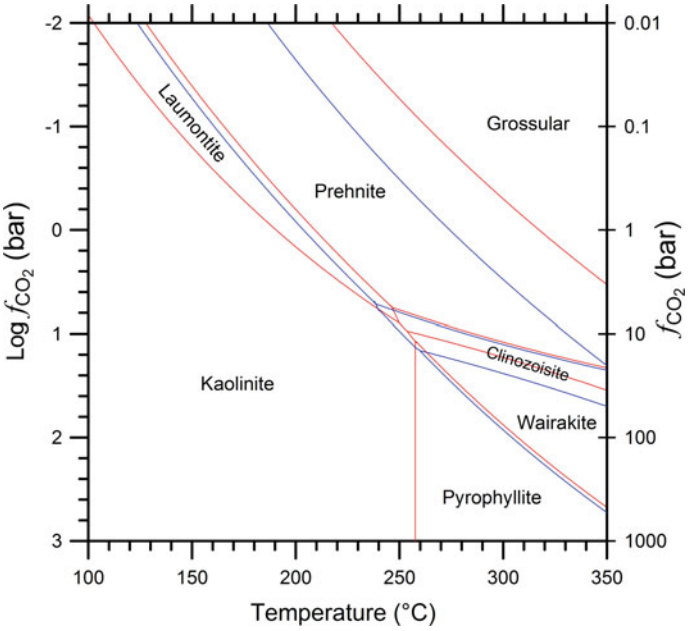

Fig. 4.18 Diagram of CO_2 fugacity versus temperature for the system SiO_2–Al_2O_3–CaO–H_2O–CO_2 (modified from Giggenbach 1997), prepared assuming saturation with quartz/chalcedony and calcite at any f_{CO_2} and temperature

of prehnite, 0.763, and the average activity of grossular, 0.127. To be noted that the following relation:

$$\log\ f_{CO_2,Prh-Grs} = \log\ K_{Cal} + \log\ K_{Prh} - \log\ K_{Grs}, \tag{4.58}$$

links the logarithm of CO_2 fugacity to the log K of the dissolution reactions of calcite, prehnite, and grossular, which are as follows:

$$Cal + 2\ H^+ = Ca^{2+} + CO_{2(g)} + H_2O \tag{4.59}$$

$$Prh + 3\ Qtz/Chc + 10\ H^+ = 2\ Ca^{2+} + 2\ Al^{3+} + 6\ H_2O \tag{4.60}$$

$$Grs + 3\ Qtz/Chc + 12\ H^+ = 3\ Ca^{2+} + 2\ Al^{3+} + 6\ H_2O \tag{4.61}$$

(ii) Also the stability field of the epidote solid solution exhibits a certain expansion in comparison to that of pure clinozoisite, especially to disadvantage of the stability field of wairakite and laumontite, whereas the clinozoisite-prehnite boundary experiences a small shift. This behavior is partly attributable to the fact that the average activity of clinozoisite, 0.703, is similar to that of prehnite, 0.763, but is significantly lower than those of wairakite, 0.891, and laumontite, which is assumed to be equal to 1. However, the differential expansion of the stability field of clinozoisite is also controlled, in part, by the stoichiometry of relevant reactions, as pointed out by the following relations:

$$\log\ f_{CO_2,Czo\text{-}Prh} = \log\ K_{Cal} + \log\ K_{Czo} - 1.5 \cdot \log\ K_{Prh} \tag{4.62}$$

$$\log\ f_{CO_2,Wrk\text{-}Czo} = \log\ K_{Cal} + 3 \cdot \log\ K_{Wrk} - 2 \cdot \log\ K_{Czo} \tag{4.63}$$

$$\log\ f_{CO_2,Lmt\text{-}Czo} = \log\ K_{Cal} + 3 \cdot \log\ K_{Lmt} - 2 \cdot \log\ K_{Czo} \tag{4.64}$$

linking the logarithm of CO_2 fugacity to the log K of the dissolution reactions of clinozoisite, wairakite, and laumontite, which are as follows:

$$Czo + 3\ Qtz/Chc + 13\ H^+ = 2\ Ca^{2+} + 3\ Al^{3+} + 7\ H_2O \tag{4.65}$$

$$Wrk + 4\ Qtz/Chc + 8\ H^+ = Ca^{2+} + 2\ Al^{3+} + 6\ H_2O \tag{4.66}$$

$$Lmt + 4\ Qtz/Chc + 8\ H^+ = Ca^{2+} + 2\ Al^{3+} + 8\ H_2O. \tag{4.67}$$

as well as by the log K of the dissolution reactions of calcite, Eq. (4.59), and prehnite, Eq. (4.60).

Since hydrothermal quartz, calcite, adularia, albite, anorthite, and laumontite occur as virtually pure solid phases, they can be involved without any particular worries and precautions in the theoretical, activity-based geothermometers and f_{CO_2}-indicators representing the aim of this work.

Also the use of white mica, epidote, prehnite, and wairakite for theoretical geothermometry and f_{CO_2} evaluation does not pose particular problems because these minerals exhibit limited compositional variations and, consequently, minor deviations are generally expected from their average activities.

The involvement of chlorite and garnet in theoretical geothermometers and f_{CO_2}-indicators is instead a risky business because these minerals show considerable compositional variations and, therefore, large deviations may occur from their average activities.

Moreover, it must be recalled that (i) hydrothermal feldspars present in active geothermal systems are most likely triclinic, fully ordered, albite and variably ordered adularia, from fully ordered microcline to completely disordered sanidine, with either triclinic or monoclinic symmetry (see Sect. 4.2.3) and (ii) microcline and sanidine have different thermodynamic properties (see Sect. 4.2.5).

The thermodynamic data of Helgeson et al. (1978) are used in this book because they resulted to be consistent with the monoclinic/triclinic transition temperatures of alkali feldspars whereas the thermodynamic data of Holland and Powell (1998) and Arnórsson and Stefánsson (1999) did not, as discussed in Sect. 4.2.4. Unfortunately, as shown in previous sections, there are large differences between the thermodynamic data of Helgeson et al. (1978) and those of Holland and Powell (1998, 2011), for most relevant solid phases, although these three databases are internally consistent. Owing to these large differences, it is meaningless to select data from distinct databases because it would be like mixing apples and oranges, as already recalled above.

In principle, the preparation of a common thermodynamic database for the whole scientific community would be highly desirable. In practice, it is a prohibitive challenge that is probably doomed to remain a chimera for a certain lapse of time, hopefully not too long.

References

Aagaard P, Helgeson HC (1983) Activity/composition relations among silicates and aqueous solutions: II. Chemical and thermodynamic consequences of ideal mixing of atoms on homological sites in montmorillonites, illites, and mixed-layer clays. Clay Clay Miner 31:207–217

Aagaard P, Jahren JS (1992) Diagenetic illite-chlorite assemblages in arenites. II. Thermodynamic relations. Clay Clay Miner 40:547

Akasaka M, Hashimoto H, Makino K, Hino R (2003) 57Fe Mössbauer and X-ray Rietveld studies of ferrian prehnite from Kouragahana, Shimane Peninsula, Japan. J Minerol Petrol Sci 98:31–40

Akizuki M (1987) Al, Si order and the internal texture of prehnite. Can Mineral 25:707–716

Albee AL (1962) Relationships between the mineral association, chemical composition and physical properties of the chlorite series. Am Mineral 47:851–870
Armbruster T, Gunter ME (2001) Crystal structures of natural zeolites. In: Bish DL, Ming DW (eds) Natural zeolites: occurrence, properties, applications. Reviews in mineralogy and geochemistry, vol 45, pp 1–67
Arnórsson S (1978) Major element chemistry of the geothermal sea-water at Reykjanes and Svartsengi. Iceland. Mineral. Mag. 42:209–220
Arnórsson S (1995) Geothermal systems in Iceland: structure and conceptual models—I. High-temperature areas. Geothermics 24:561–602
Arnórsson S, Gunnlaugsson E (1985) New gas geothermometers for geothermal exploration—calibration and application. Geochim Cosmochim Acta 49:1307–1325
Arnórsson S, Stefánsson A (1999) Assessment of feldspar solubility constants in water in the range of 0° to 350°C at vapor saturation pressures. Am J Sci 299:173–209
Arnórsson S, Gunnlaugsson E, Svavarsson H (1983a) The chemistry of geothermal waters in Iceland. III. Chemical geothermometry in geothermal investigations. Geochim Cosmochim Acta 47:567–577
Arnórsson S, Gunnlaugsson E, Svavarsson H (1983b) The chemistry of geothermal waters in Iceland. II. Mineral equilibria and independent variables controlling water compositions. Geochim Cosmochim Acta 47:547–566
Artioli G, Quartieri S, Deriu A (1995) Spectroscopic data on coexisting prehnite-pumpellyite and epidote-pumpellyite. Can Mineral 33:67–75
Badaut D, Decarreau A, Besson G (1992) Ferripyrophyllite and related Fe^{3+}-rich 2:1 clays in recent deposits of Atlantis II Deep, Red Sea. Clay Miner 27:227–244
Bailey SW (1988) Chlorites: structures and crystal chemistry. In: Bailey SW (ed) Hydrous Phyllosilicates (Exclusive of Micas). Reviews Mineralogy, vol 19, pp 347–403
Balducci S, Chelini W (1992) Hydrothermal equilibria in the active Mofete geothermal system, Phlegraean Fields, Naples, Italy. Acta Vulcanologica Marinelli 2:17–34
Ballantyne JM (1978) Hydrothermal alteration at the roosevelt hot springs thermal area, Utah: modal mineralogy, and geochemistry of sericite, chlorite, and feldspar from altered rocks. Thermal Power Company well Utah State 14-2. Topical Report, Dept. of Geology and Geophysics, Utah Univ., Salt Lake City, USA, 42 pp
Bargar KE, Beeson MH (1981) Hydrothermal alteration in research drill hole Y-2, Lower Geyser Basin, Yellowstone National Park, Wyoming. Am Mineral 66:473–490
Bargar KE, Beeson MH (1985) Hydrothermal alteration in research drill hole Y-3, Lower Geyser Basin, Yellowstone National Park, Wyoming. U.S. Geological Survey Professional Paper 1054-C, 23 pp
Bargar KE, Keith TEC, Trusdell FA, Evans SR, Sykes ML (1996) Hydrothermal alteration mineralogy of SOH drill holes, Kilauea East Rift Zone geothermal area, Hawaii. U.S. Geological Survey Open-File Report No. 96-0010, 75 pp
Baur WH, Joswig W, Kassner D, Hofmeister W (1990) Prehnite: structural similarity of the monoclinic and orthorhombic polymorphs and their Si/Al ordering. J Solid State Chem 86:330–333
Bird DK, Helgeson HC (1980) Chemical interaction of aqueous solutions with epidote-feldspar mineral assemblages in geologic systems—I. Thermodynamic analysis of phase relations in the system $CaO\text{-}FeO\text{-}Fe_2O_3\text{-}Al_2O_3\text{-}SiO_2\text{-}H_2O\text{-}CO_2$. Am J Sci 280:907–941
Bird DK, Norton DL (1981) Theoretical prediction of phase relations among aqueous solutions and minerals: Salton Sea geothermal system. Geochim Cosmochim Ac 45:1479–1494
Bird DK, Spieler AR (2004) Epidote in geothermal systems. In: Liebscher A, Franz G (eds) Epidotes, Reviews in Mineralogy and Geochemistry, vol 56, pp 235–300
Bird DK, Schiffman P, Elders WA, Williams AE, McDowell SD (1984) Calc-silicate mineralization in active geothermal systems. Econ Geol 79:671–695

Bird DK, Cho M, Janik CJ, Liou JG, Caruso LJ (1988) Compositional, order-disorder, and stable isotope characteristics of Al-Fe epidote, State 2-14 drill hole, Salton Sea geothermal system. J Geophys Res Sol Earth 93:13135–13144

Bish DL, Boak JM (2001) Cinoptilolite-heulandite nomenclature. In: Bish DL, Ming DW (eds) Natural zeolites: occurrence, properties, applications. Reviews in mineralogy and geochemistry, vol 45, pp 207–216

Bishop BP, Bird DK (1987) Variation in sericite compositions from fracture zones within the Coso Hot Springs geothermal system. Geochim Cosmochim Acta 51:1245–1256

Bourdelle F, Parra T, Chopin C, Beyssac O (2013) A new chlorite geothermometer for diagenetic to low-grade metamorphic conditions. Contrib Mineral Petrol 165:723–735

Boyce AJ, Fulignati P, Sbrana A (2003) Deep hydrothermal circulation in a granite intrusion beneath Larderello geothermal area (Italy): constraints from mineralogy, fluid inclusions and stable isotopes. J Volcanol Geoth Res 126:243–262

Brigatti MF, Guggenheim S (2002) Mica crystal chemistry and the influence of pressure, temperature, and solid solution on atomistic models. Rev Mineral Geochem 46:1–97

Browne PRL (1970) Hydrothermal alteration as an aid in investigating geothermal fields. Geothermics 2:564–570

Browne PRL (1977) Occurrence and hydrothermal alteration of diabase, Heber geothermal field, Imperial Valley, California. UCR/IGPP-77/9 Report, 61 pp

Browne PRL (1978) Hydrothermal alteration in active geothermal fields. Annu. Rev. Earth Pl. Sc. 6:229–248

Browne PRL, Ellis AJ (1970) The Ohaaki-Broadlands hydrothermal area, New Zealand: mineralogy and related geochemistry. Am J Sci 269:97–131

Capuano RM, Cole DR (1982) Fluid-mineral equilibria in a hydrothermal system, Roosevelt Hot Springs, Utah. Geochim Cosmochim Acta 46:1353–1364

Carpenter MA, Putnis A (1985) Cation order and disorder during crystal growth: some implications for natural mineral assemblages. In: Thompson AB, Rubie DC (eds) Metamorphic reactions: kinetics, textures, and deformation. Springer, New York, pp 1–26

Cathelineau M (1988) Cation site occupancy in chlorites and illites as function of temperature. Clay Miner 23:471–485

Cathelineau M, Izquierdo G (1988) Temperature-composition relationships of authigenic micaceous minerals in the Los Azufres geothermal system. Contrib Mineral Petr 100:418–428

Cathelineau M, Nieva D (1985) A chlorite solid solution geothermometer—the Los Azufres (Mexico) geothermal system. Contrib Mineral Petr 91:235–244

Cavarretta G, Tecce F (1987) Contact metasomatic and hydrothermal minerals in the SH2 deep well, Sabatini volcanic district, Latium, Italy. Geothermics 16:127–145

Cavarretta G, Gianelli G, Puxeddu M (1980) Hydrothermal metamorphism in the Larderello geothermal field. Geothermics 9:297–314

Cavarretta G, Gianelli G, Puxeddu M (1982) Formation of authigenic minerals and their use as indicators of the physicochemical parameters of the fluid in the Larderello-Travale geothermal field. Econ Geol 77:1071–1084

Cavarretta G, Gianelli G, Scandiffio G, Tecce F (1985) Evolution of the Latera geothermal system II: metamorphic, hydrothermal mineral assemblages and fluid chemistry. J Volcanol Geoth Res 26:337–364

Černý P, Chapman R (1986) Adularia from hydrothermal vein deposits: extremes in structural state. Can Mineral 24:717–728

Chang LLY (1965) Subsolidus phase relations in the systems $BaCO_3$-$SrCO_3$, $SrCO_3$-$CaCO_3$, and $BaCO_3$-$CaCO_3$. J Geol 73:346–368

Chiodini G, Cioni R, Guidi M, Marini L (1991) Chemical geothermometry and geobarometry in hydrothermal aqueous solutions: a theoretical investigation based on a mineral-solution equilibrium model. Geochim Cosmochim Acta 55:2709–2727

Chipera SJ, Apps JA (2001) Geochemical stability of natural zeolites. Rev Mineral Geochem 45:117–161

Cho M, Maruyama S, Liou JG (1987) An experimental investigation of heulandite-laumontite equilibrium at 1000 to 2000 bar P fluid. Contrib Mineral Petrol 97:43–50
Cho M, Liou JG, Bird DK (1988) Prograde phase relations in the State 2-14 Well metasandstones, Salton Sea geothermal field, California. J Geophys Res Sol Earth 93:13081–13103
Coombs DS (1952) Cell size, optical properties and chemical composition of laumontite and leonhardite. Am Mineral 37:812–830
Coombs DS (1955) X-ray observations of wairakite and non-cubic analcime. Mineral Mag 30:699–708
Crawford WA, Hoersch LA (1972) Calcite-aragonite equilibrium from 50°C to 150°C. Am Mineral 57:995–998
Dachs E, Geiger CA (2019) Thermodynamic behaviour of grossular–andradite, $Ca_3(Al_xFe^{3+}_{1-x})_2Si_3O_{12}$, garnets: a calorimetric study. Eur J Mineral 31:443–451
De Caritat P, Hutcheon I, Walshe JL (1993) Chlorite geothermometry: a review. Clay Clay Miner 41:219–239
Deer WA, Howie RA, Zussman J (1982) Rock forming minerals. Orthosilicates, vol 1A, 2nd edn. Geological Society of London, 919 pp
Deer WA, Howie RA, Zussman J (2001) Rock-forming minerals. Framework silicates: Feldspars, vol 4A, 2nd edn. Geological Society of London, 972 pp
Deer WA, Howie RA, Wise WS, Zussman J (2004) Rock-forming minerals. Framework silicates: silica minerals, feldspathoids, and the zeolites, vol 4B, 2nd edn. Geological Society of London, 982 pp
Droop GTR (1987) A general equation for estimating Fe^{3+} concentrations in ferromagnesian silicates and oxides from microprobe analyses, using stoichiometric criteria. Mineral Mag 51:431–435
Ellis AJ (1970) Quantitative interpretation of chemical characteristics of hydrothermal systems. Geothermics 2:516–528
Ellis AJ, Mahon WAJ (1977) Chemistry and geothermal systems. Academic Press, 392 pp
Ernst WG (1963) Significance of phengitic micas from low-grade schists. Am Mineral 48:1357–1373
Exley RA (1982) Electron microprobe studies of Iceland Research Drilling Project high-temperature hydrothermal mineral geochemistry. J Geophys Res Sol Earth 87(B8):6547–6557
Fishman NS, Turner CE, Brownfield IK (1995) Authigenic albite in a Jurassic alkaline, saline lake deposit, Colorado Plateau. Evidence for early diagenetic origin. U.S. Geological Survey Bulletin 1808, Evolution of sedimentary basins—San Juan Basin, P1-P13
Flehmig W (1977) The synthesis of feldspars at temperatures between 0–80°C, their ordering behaviour and twinning. Contrib Mineral Petr 65:1–9
Foster MD (1962) Interpretation of the composition and a classification of the chlorites: U.S. Geological Survey Professional Paper 414-A, 33 pp
Fournier RO (1991) Water geothermometers applied to geothermal energy. In: D'Amore F (co-ordinator) Application of geochemistry in geothermal reservoir development. UNITAR, pp 37–69
Fowler AP, Zierenberg RA, Schiffman P, Marks N, Friðleifsson GÓ (2015) Evolution of fluid–rock interaction in the Reykjanes geothermal system, Iceland: evidence from Iceland Deep Drilling Project core RN-17B. J Volcanol Geoth Res 302:47–63
Franz G, Liebscher A (2004) Physical and chemical properties of the epidote minerals. An introduction. In: Liebscher A, Franz G (eds) Epidotes. Reviews in mineral and geochemistry, vol 56, pp 1–82
Fulignati P, Malfitano G, Sbrana A (1997) The Pantelleria caldera geothermal system: data from the hydrothermal minerals. J Volcanol Geoth Res 75:251–270
Geiger CA, Dachs E, Vielreicher NM, Rossman GR (2018) Heat capacity and entropy behavior of andradite: a multi-sample and—methodological investigation. Eur J Mineral 30:681–694
Gianelli G, Ruggieri G (2002) Evidence of a contact metamorphic aureole with high-temperature metasomatism in the deepest part of the active geothermal field of Larderello, Italy. Geothermics 31:443–474

Gianelli G, Mekuria N, Battaglia S, Chersicla A, Garofalo P, Ruggieri G, Manganelli M, Gebregziabher Z (1998) Water–rock interaction and hydrothermal mineral equilibria in the Tendaho geothermal system. J Volcanol Geoth Res 86:253–276

Giggenbach WF (1980) Geothermal gas equilibria. Geochim Cosmochim Acta 44:2021–2032

Giggenbach WF (1984) Mass transfer in hydrothermal alterations systems. Geochim Cosmochim Acta 48:2693–2711

Giggenbach WF (1988) Geothermal solute equilibria. derivation of Na-K-Mg-Ca geoindicators. Geochim Cosmochim Acta 52:2749–2765

Giggenbach WF (1997) The origin and evolution of fluids in magmatic-hydrothermal systems. In: Barnes HL (ed) Geochemistry of hydrothermal ore deposits, 3rd edn. Wiley, New York, pp 737–796

Gottschalk M (2004) Thermodynamic properties of zoisite, clinozoisite and epidote. In: Liebscher A, Franz G (eds) Epidotes, reviews in mineralogy and geochemistry, vol 56, pp 83–124

Guidi M, Marini L, Scandiffio G, Cioni R (1990) Chemical geothermometry in hydrothermal aqueous solutions: the influence of ion complexing. Geothermics 19:415–441

Guidotti CV, Sassi FP (2002) Constraints on studies of metamorphic K-Na white micas. Rev Mineral Geochem 46:413–448

Hedenquist JW, Browne PR (1989) The evolution of the Waiotapu geothermal system, New Zealand, based on the chemical and isotopic composition of its fluids, minerals and rocks. Geochim Cosmochim Acta 53:2235–2257

Helgeson HC, Aagaard P (1985) Activity/composition relations among silicates and aqueous solutions; I, Thermodynamics of intrasite mixing and substitutional order/disorder in minerals. Am J Sci 285:769–844

Helgeson HC, Delany JM, Nesbitt HW, Bird DK (1978) Summary and critique of the thermodynamic properties of rock-forming minerals. Am J Sci 278A, 229 p

Henley RW, Ellis AJ (1983) Geothermal systems ancient and modern: a geochemical review. Earth-Sci Rev 19:1–50

Herdianita NR (2012) The evolution of the Darajat geothermal system, West Java—Indonesia. Ph.D. Thesis, University of Auckland, New Zealand, 264 pp

Holland TJ (1989) Dependence of entropy on volume for silicate and oxide minerals: A review and predictive model. Am Mineral 74:5–13

Holland TJB, Powell R (1998) An internally consistent thermodynamic data set for phases of petrological interest. J Metamorph Geol 16:309–343

Holland TJB, Powell R (2011) An improved and extended internally consistent thermodynamic dataset for phases of petrological interest, involving a new equation of state for solids. J Metamorp Geol 29:333–383

Inoue A, Meunier A, Beaufort D (2004) Illite-smectite mixed-layer minerals in felsic volcaniclastic rocks from drill cores, Kakkonda, Japan. Clays Clay Miner 52:66–84

Inoue A, Kurokawa K, Hatta T (2010) Application of chlorite geothermometry to hydrothermal alteration in Toyoha geothermal system, southwestern Hokkaido, Japan. Resour Geol 60:52–70

Jahren JS, Aagaard P (1992) Diagenetic illite-chlorite assemblages in arenites. I. Chemical evolution. Clay Clay Miner 40:540

Kastner M, Siever R (1979) Low temperature feldspars in sedimentary rocks. Am J Sci 279:435–479

Kastner M, Waldbaum DR (1968) Authigenic albite from Rhodes. Am Mineral 53:1579–1602

Keith TE, Bargar KE (1988) Petrology and hydrothermal mineralogy of U.S. Geological Survey Newberry 2 drill core from Newberry Caldera, Oregon. J Geophys Res Sol Earth 93(B9):10174–10190

Keith TE, Muffler LP, Cremer M (1968) Hydrothermal epidote formed in the Salton Sea geothermal system, California. Am Mineral 53:1635–1644

Kiseleva I, Navrotsky A, Belitsky IA, Fursenko BA (1996) Thermochemistry and phase equilibria in calcium zeolites. Am Mineral 81:658–667

Kristmannsdóttir H (1979) Alteration of basaltic rocks by hydrothermal activity at 100–300°C. In: Mortland MM, Farmer VC (eds) International clay conference 1978. Developments in sedimentology, vol. 27. Elsevier, Amsterdam, pp 359–367

Kristmannsdóttir H, Tomasson J (1976) Zeolite zones in geothermal areas in Iceland. Orkustofnun Report OS-JHD-7649, 11 pp

Li G, Peacor DR, Coombs DS, Kawachi Y (1997) Solid solution in the celadonite family: The new minerals ferroceladonite, $K_2Fe_2^{2+}Fe_2^{3+}Si_8O_{20}(OH)_4$, and ferroaluminoceladonite, $K_2Fe_2^{2+}Al_2Si_8O_{20}(OH)_4$. Am Mineral 82:503–511

Liakopoulos A (1987) Hydrothermalisme et minéralisations métallifères de l'île de Milos (Cyclades, Grèce). Ph.D. Thesis Université de Paris VI, 276 pp

Libbey RB, Williams-Jones AE (2016) Compositions of hydrothermal silicates and carbonates as indicators of physicochemical conditions in the Reykjanes geothermal system, Iceland. Geothermics 64:15–27

Liebscher A (2004) Spectroscopy of epidote minerals. In: Liebscher A, Franz G (eds) Epidotes, Reviews in mineralogy and geochemistry, vol 56, pp 125–170

Liou JG (1970) Synthesis and stability relations of wairakite, CaAl2Si4O12 & #x22C5; 2H2O. Contrib Mineral Petrol 27:259–282

Liou JG (1971a) P-T stabilities of laumontite, wairakite, lawsonite, and related minerals in the system $CaAl_2Si_2O_8$-SiO_2-H_2O. J Petrol 12:379–411

Liou JG (1971b) Stilbite-laumontite equilibrium. Contrib Mineral Petr 31:171–177

Locock AJ (2008) An excel spreadsheet to recast analyses of garnet into end-member components, and a synopsis of the crystal chemistry of natural silicate garnets. Comput Geosci 34:1769–1780. Code available from server at http://www.iamg.org/CGEditor/index.htm

Lonker SW, Gerald JDF (1990) Formation of coexisting 1 M and 2 M polytypes in illite from an active hydrothermal system. Am Mineral 75:1282–1289

Lonker SW, Gerald JDF, Hedenquist JW, Walshe JL (1990) Mineral-fluid interactions in the Broadlands-Ohaaki geothermal system, New Zealand. Am J Sci 290:995–1068

Marini L, Canepa M, Cipolli F, Ottonello G, Vetuschi Zuccolini M (2001) Use of stream sediment chemistry to predict trace element chemistry of groundwater. A case study from the Bisagno valley (Genoa, Italy). J Hydrol 241:194–220

Marks N, Schiffman P, Zierenberg RA, Franzson H, Fridleifsson GÓ (2010) Hydrothermal alteration in the Reykjanes geothermal system: Insights from Iceland deep drilling program well RN-17. J Volcanol Geoth Res 189:172–190

Martin RF (1969) The hydrothermal synthesis of low albite. Contrib Mineral Petrol 23:323–339

Martinez-Serrano RG (2002) Chemical variations in hydrothermal minerals of the Los Humeros geothermal system, Mexico. Geothermics 31:579–612

Martinez-Serrano RG, Dubois M (1998) Chemical variations in chlorite at the Los Humeros geothermal system, Mexico. Clay Clay Miner 46:615–628

Mas A, Guisseau D, Mas PP, Beaufort D, Genter A, Sanjuan B, Girard JP (2006) Clay minerals related to the hydrothermal activity of the Bouillante geothermal field (Guadeloupe). J Volcanol Geoth Res 158:380–400

McCulloh TH, Frizzell VA, Stewart RJ, Barnes I (1981) Precipitation of laumontite with quartz, thenardite, and gypsum at Sespe Hot Springs, western Transverse Ranges, California. Clays Clay Miner 29:353–364

McDowell SD (1986) Composition and structural state of coexisting feldspars, Salton Sea geothermal field. Mineral Mag 50:75–84

McDowell SD, Elders WA (1980) Authigenic layer silicate minerals in borehole Elmore 1, Salton Sea geothermal field, California, USA. Contrib Mineral Petrol 74:293–310

McDowell SD, Elders WA (1983) Allogenic layer silicate minerals in borehole Elmore 1, Salton Sea geothermal field, California. Am Mineral 68:1146–1159

McIntire W (1963) Trace element partition coefficients- a review of theory and applications to geology. Geochim Cosmochim Acta 27:1209–1264

Mehegan JM, Robinson PT, Delaney JR (1982) Secondary mineralization and hydrothermal alteration in the Reydarfjordur drill core, eastern Iceland. J Geophys Res Sol Earth 87(B8):6511–6524
Milodowski AE, Savage D, Bath AH, Fortey NJ, Nancarrow PHA, Shepherd TJ (1989) Hydrothermal mineralogy in geothermal assessment: studies of Miravalles field, Costa Rica and experimental simulations of hydrothermal alteration. British Geological Survey Technical Report WE/89/63, 128 pp
Morad S (1978) Feldspars in sedimentary rocks. In: Sedimentology. Encyclopedia of earth science. Springer, Berlin
Muffler PLJ, White DE (1969) Active metamorphism of Upper Cenozoic sediments in the Salton Sea geothermal field and the Salton Trough, Southeastern California. Bull Geol Soc Am 80:157–182
Muramatsu Y, Doi N (2000) Prehnite as an indicator of productive fractures in the shallow reservoir, Kakkonda geothermal system, northeast Japan. J Miner Petrol Sci 95:32–42
Novak GA, Gibbs GV (1971) The crystal chemistry of the silicate garnets. Am Mineral 56:791–825
Ogino T, Suzuki T, Sawada K (1987) The formation and transformation mechanism of calcium carbonate in water. Geochim Cosmochim Acta 51:2757–2767
Openshaw RE, Hemingway BS, Robie RA, Waldbaum DR, Krupka KM (1976) The heat capacities at low temperatures and entropies at 298.15 K of low albite, analbite, microcline, and high sanidine. US Geol Surv J Res 4:195–204
Oscarson RL, Bargar KE (1996) Electron microprobe analyses of zeolite minerals from Neogene volcanic rocks in the Breitenbush-Austin Hot Springs area, Oregon. U.S. Geological Survey Open-File Report 96–41, 61 pp
Ottolini LP, Raffone N, Fridleifsson GÓ, Tonarini S, D'Orazio M, Gianelli G (2012) A geochemical investigation of trace elements in well RN-17 at Reykjanes geothermal system, SW-Iceland. In: IOP conference series: materials science and engineering, vol 32. IOP Publishing, pp 012020
Papike JJ, Zoltai T (1967) Ordering of tetrahedral aluminum in prehnite, Ca_2(Al, Fe+3)[Si3AlO10](OH)2. Am Mineral 52:974–984
Parsons I (2010) Feldspars defined and described: a pair of posters published by the Mineralogical Society.Sources and supporting information. Mineral Mag 74:529–551
Passaglia E, Sheppard RA (2001) The crystal chemistry of zeolites. In: Bish DL, Ming DW (eds) Natural zeolites: occurrence, properties, applications. Reviews in mineralogy and geochemistry, vol 45, pp 69–116
Patrier P, Beaufort D, Meunier A, Eymery JP, Petit S (1991) Determination of nonequilibrium ordering state in epidote from the ancient geothermal field of Saint Martin: application of Mössbauer spectroscopy. Am Mineral 76:602–610
Petrova VV (1970) Zeolites of the Paratunskii formation. In: Naboko SI (ed) Mineralogy of the hydrothermal systems of Kamchatka and the Kurile Islands. Academy of Sciences USSR, Siberian Branch, pp 97–116 (in Russian)
Pirajino F (2009) Hydrothermal processes and mineral systems. Springer, Berlin, p 1250
Preisinger A (1965) Prehnit-ein neuer Schichtsilikattyp. Tscher Miner Petrog 10:491–504
Pryde AKA, Dove MT (1998) On the sequence of phase transitions in tridymite. Phys Chem Miner 26:171–179
Reeder R.J. (1990) Crystal chemistry of the rhombohedral carbonates. In: R. J. Reeder (Ed.), Carbonates: Mineralogy and chemistry. Rev. Mineral. Geochem., 11, 1–47
Reyes AG (1990) Petrology of Philippine geothermal systems and the application of alteration mineralogy to their assessment. J Volcanol Geoth Res 43:279–309
Ribbe PH (ed) (1983) Feldspar mineralogy. Mineralogical Society of America, Washington D.C. Reviews in mineralogy, vol 2, 362 pp
Rickwood PC (1968) On recasting analyses of garnet into end-member molecules. Contrib Mineral Petrol 18:175–198
Ruggieri G, Petrone CM, Gianelli G, Arias A, Henriquez ET (2006) Hydrothermal alteration in the Berlin geothermal field (El Salvador): new data and discussion on the natural state of the system. Period Mineral 75:293–312

Sanjuan B., Brach M., Lasne E. (2001) Bouillante geothermal fluid: mixing and water/rock interaction processes at 250°C. In: Cidu R. (Ed.), Water-Rock Interaction, WRI-10, International Symposium on Water-Rock Interaction, Jun 2001, Villasimius, Italy. A.A. Balkema, 2, 911–914

Sawaki T, Sasaki M, Fujimoto K, Takeno N (2001) Zinc-bearing actinolite from the Kakkonda geothermal system, Iwate Prefecture, northeastern Japan. Bull. Geol. Surv. Jpn 52:315–320

Schiffman P, Bird DK, Elders WA (1985) Hydrothermal mineralogy of calcareous sandstones from the Colorado River delta in the Cerro Prieto geothermal system, Baja California, Mexico. Mineral Mag 49:435–449

Seki Y, Onuki H, Okumura K, Takashima I (1969) Zeolite distribution in the Katayama geothermal area, Onikobe, Japan. Jpn J Geol Geogr 40:63–79

Seki Y, Liou JG, Guillemette R, Sakai H, Oki Y, Hirano T, Onuki H (1983) Investigation of geothermal systems in Japan I. Onikobe geothermal area. Hydroscience and Geotechnology Laboratory, Saitama University, Memoir No. 3, 206 pp

Shearer CK, Papike JJ, Simon SB, Davis BL, Laul JC (1988) Mineral reactions in altered sediments from the California State 2-14 well: Variations in the modal mineralogy, mineral chemistry and bulk composition of the Salton Sea Scientific Drilling Project core. J Geophys Res Sol Earth 93(B11):13104–13122

Shimazu M, Yajima J (1973) Epidote and wairakite in drill cores at the Hachimantai geothermal area, northeastern Japan. J Miner Petrol Sci 68:363–371

Shock EL, Helgeson HC, Sverjensky DA (1989) Calculation of the thermodynamic and transport properties of aqueous species at high pressures and temperatures: standard partial molal properties of inorganic neutral species. Geochim Cosmochim Acta 53:2157–2183

Smith JV, Brown WL (1988) Feldspar minerals. 1. Crystal structure, physical, chemical, and microtextural properties, 2nd edn. Springer, Berlin, 828 pp

Stefánsson A, Arnórsson S (2000) Feldspar saturation state in natural waters. Geochim Cosmochim Acta 64:2567–2584

Steiner A (1953) Hydrothermal rock alteration at Wairakei, New Zealand. Econ Geol 48:1–13

Steiner A (1955) Wairakite, the calcium analogue of analcime, a new zeolite mineral. Mineral Mag 30:691–698

Steiner A (1970) Genesis of hydrothermal K-feldspar (adularia) in an active geothermal environment at Wairakei, New Zealand. Mineral Mag 37:916–922

Sverjensky DA, Hemley JJ, D'Angelo WM (1991) Thermodynamic assessment of hydrothermal alkali feldspar-mica-aluminosilicate equilibria. Geochim Cosmochim Ac 55:989–1004

Teklemariam M, Battaglia S, Gianelli G, Ruggieri G (1996) Hydrothermal alteration in the Aluto-Langano geothermal field, Ethiopia. Geothermics 25:679–702

Thompson JB Jr (1969) Chemical reactions in crystals. Am Mineral 54:341–375

Thompson AB (1970) Laumontite equilibria and the zeolite facies. Am J Sci 269:267–275

Turekian KK, Wedepohl KH (1961) Distribution of the elements in some major units of the earth's crust. Geol Soc Am Bull 72:175–192

Velde B (1977) Clays and clay minerals in natural and synthetic systems. Developments in Sedimentology, vol 21. Elsevier, Amsterdam, p 217

Viereck LG, Griffin BJ, Schmincke HU, Pritchard RG (1982) Volcaniclastic rocks of the Reydarfjordur drill hole, eastern Iceland: 2. Alteration. J Geophys Res Sol Earth 87(B8):6459–6476

Walther JV, Helgeson HC (1977) Calculation of the thermodynamic properties of aqueous silica and the solubility of quartz and its polymorphs at high pressures and temperatures. Am J Sci 277:1315–1351

Weaver CE, Pollard LD (1973) The chemistry of clay minerals. Developments in sedimentology, vol 15. Elsevier, Amsterdam

Weissberg BG, Browne PR, Seward TM (1979) Ore metals in active geothermal systems. In: Barnes HL (ed) Geochemistry of hydrothermal ore deposits, 2nd edn. Wiley, New York, pp 738–780

Wheeler RS, Browne PRL, Rodgers KA (2001) Iron-rich and iron-poor prehnites from the Way Linggo epithermal Au-Ag deposit, southwest Sumatra, and the Heber geothermal field, California. Mineral Mag 65:397–406

Wiewióra A, Weiss Z (1990) Crystallochemical classifications of phyllosilicates based on the unified system of projection of chemical composition: II. The chlorite group. Clay Miner 25:83–92
Winchell AN (1933) Elements of optical mineralogy: an introduction to microscopic petrography. Part 2. Descriptions of minerals, with special reference to their optical and microscopic characters, 3rd edn. Wiley, New York, p 459
Zunić TB, Šćavničar S, Molin G (1990) Crystal structure of prehnite from Komiža. Eur J Mineral 2:731–734